IDŐJÁRÁS

QUARTERLY JOURNAL OF THE HUNGAROMET
HUNGARIAN METEOROLOGICAL SERVICE

CONTENTS

VOL. 129 * NO. 4 * OCTOBER – DECEMBER 2025

IDŐJÁRÁS

Quarterly Journal of the HungaroMet Hungarian Meteorological Service

Editorial Office: Kitaibel P.u. 1, H-1024 Budapest, Hungary
P.O. Box 38, H-1525 Budapest, Hungary
E-mail: journal.idojaras@met.hu

Indexed and abstracted in Science Citation Index Expanded™ and Journal Citation Reports/Science Edition
Covered in the abstract and citation database SCOPUS®
Included in EBSCO's database

Subscription by mail:
IDŐJÁRÁS, P.O. Box 38, H-1525 Budapest, Hungary
E-mail: journal.idojaras@met.hu

DOI:10.28974/idojaras.2025.4.1

IDŐJÁRÁS

Quarterly Journal of the HungaroMet Hungarian Meteorological Service
Vol. 129, No. 4, October – December, 2025, pp. 373–391

Analysis of the long rainfall data series of Mosonmagyaróvár with special regard to the water demand of the vegetation period of winter wheat

Zoltán Varga[1,*], **Tímea Kocsis**[2], **Ottilia Vámos**[1], **Dávid Vasas**[1], and **Norbert Magyar**[2]

[1] *Albert Kázmér Faculty of Agricultural and Food Sciences of Széchenyi István University in Mosonmagyaróvár, Department of Water Management and Natural Ecosystems, Vár Square 2, Mosonmagyaróvár, H-9200, Hungary*

[2] *Budapest University of Economics and Business, Faculty of Commerce, Hospitality and Tourism, Department of Methodology for Business Analysis, Alkotmány street 9-11, Budapest, H-1054, Hungary*

** Corresponding author E-mail: varga.zoltan@sze.hu*

(Manuscript received in final form January 28, 2025)

Abstract— The present study analyzes the long-term (1871–2020) precipitation time series of Mosonmagyaróvár (Hungary) and investigates the precipitation trends affecting winter wheat production. Understanding precipitation trends is important for agriculture due to the increasing frequency and intensity of droughts caused by climate change.

In this study, parametric and non-parametric trend tests (linear and Mann-Kendall trend test) were applied, which showed a significant decrease in April and October. A significant downward shift of the mean can be demonstrated in spring by Pettitt's test. This decrease has a negative impact on key growing periods for winter wheat, which poses a serious challenge to conventional wheat production in the region. The research highlights the importance of different agrotechnical solutions to reduce yield losses due to climate change. The results obtained are in line with trends observed in Keszthely (Hungary), which confirms the regional changes.

These climatic changes can have a significant impact on the cultivation of our most important domestic food crop, winter wheat, so it is worth preparing for adaptation from this point of view as well.

Key-words: climate change, rainfall, vegetation period, water, winter wheat

1. Introduction and literature review

The global climate is changing, with temperatures rising globally, and this rise in global temperature is expected to cause a modification in the annual mean precipitation (*IPCC,* 2021). Simulation results from global climate models (GCMs) have indicated that the intensity, duration, and frequency of future extreme rainfalls are projected to change in many regions around the world (*Lee et al.,* 2011; *Asadieh* and *Krakauer,* 2015; *Wen et al.,* 2016).

Reported analyses of observed extreme precipitation show that there is some evidence of a general increase in extreme precipitation. The review of likely future changes based on climate projections indicates a general increase in extreme precipitation under a future climate, which is consistent with the observed trends. Only a few countries have developed guidelines that incorporate a consideration of climate change impacts (*Madsen et al.,* 2014).

Significant increases in extreme precipitation and drought events have been detected in Europe in the past few decades. In a study by *Berényi et al.* (2023), 16 selected climate indices were used for the analysis of the temporal changes and spatial distribution of precipitation patterns in European plain regions during 1950–2022. Their results suggest a general intensification of precipitation events over the continent, as many regions show a significant increase in the indices related to the intensity of extreme precipitation, and also the frequency of these events increased in a lot of regions. Extreme indices related to dry periods changed significantly in only a few cases. An increase may only be observed in the southern part of the continent, while a significant decrease can be seen in three regions in northern Europe.

Spinoni et al. (2015) reported that in Central Europe and the Balkans, drought variables show a moderate increase. Concerning changes under a future climate, climate modeling studies have shown that an increase in heavy precipitation is likely in most parts of the world in the 21st century (*IPCC,* 2012).

The expected increase in the intensity and frequency of extreme precipitation under climate change has already been experienced in different parts of the world (*Janssen et al.,* 2014; *Wang et al.,* 2017; *Tabari* and *Willems,* 2018; *Zobel et al.,* 2018). While an increase in extreme precipitation events can be detected worldwide (*Donat et al.,* 2016), the pattern of increase is less spatially coherent and often non-significant (*Groisman et* al., 2005) compared to the increase in temperature.

Increasing trends in European extreme precipitations have been discussed in several studies. These studies concluded that a general intensification of extreme events may be observed (*Sun et al.,* 2021). However, the actual rate of the precipitation trends may vary across the continent, for instance, the trends of heavy precipitation events in northern Europe are similar to the trend of total precipitation, but this is not true in southern Europe where heavy precipitation

tends to increase while total precipitation is decreasing (*van den Besselaar et al.,* 2012).

The climate became wetter in several regions in Europe through the increase in extreme and total precipitation (*Ntegeka* and *Willems,* 2008; *Madsen et al.,* 2014). Opposite trends may be observed in some of the southern countries where the decrease in total precipitation coincided with the increase of extreme events resulting in an intensification of precipitation events (*Bartholy* and *Pongrácz,* 2007) or an overall decrease in extreme precipitation events (*Norrant* and *Douguédroit,* 2005).

Between 1901 and 2009, the highest precipitation declines over the territory of Hungary occurred in the spring, nearly 20% of them (*Lakatos* and *Bihari,* 2011).

Bartholy and *Pongrácz* (2007) examined several precipitation extreme indices and suggested that regional intensity and frequency of extreme precipitation increased in the Carpathian Basin in the second half of the last century, while the total precipitation decreased. A 20–33% decrease in precipitation in Hungary is predicted for the summer half-year, and there is high uncertainty for the rainfall for the winter half-year (*Bartholy et al.,* 2007). *Bartholy et al.* (2015) projected that the frequency of extreme precipitation will increase in Central Europe, except in summer, when decreasing tendency is very likely.

Future climate change would further amplify the effects of precipitation variations (*Liu et al.,* 2023). Improved knowledge of the likely future risk profiles also plays an important role in decision-making when considering, for example, societal adaptation to future climate change (*Hall et al.,* 2012; *Bormann et al.,* 2012).

Changes in precipitation have serious effects on human society and are the focus of investigation in many scientific fields, e.g. hydrology, agriculture, and environmental sciences (*Zhao et al.,* 2018).

Water scarcity has become an increasing threat to humans and ecosystem sustainability and is expected to be more serious under future climate change conditions (*Hoekstra,* 2012). Agriculture is the world's largest water user and is prominently impacted by climate change and population growth (*Ward* and *Pulido-Velazquez,* 2008; *Zhang et al.,* 2020).

Agriculture is one of the most vulnerable sectors to climate change and associated extreme weather events (*Pachauri et al.,* 2014). Shifts in precipitation, temperature, and other weather patterns may change the suitability of crop varieties to their present agro-ecosystems, change the need for pest and disease management, and increase the turnover of soil organic matter and the associated risk of nutrient loss (*Olesen et al.,* 2011). Extreme weather events (such as droughts) may also lead to reductions in areas suitable for agriculture, damage to infrastructure, and higher yield variability (*Olesen* and *Bindi,* 2002).

One of the main objectives of the research by *Bartholy* and *Pongrácz* (2010) was to analyze the possible tendency of future precipitation conditions for this century for the Carpathian Basin. Their results suggest that regional intensity and frequency of extreme precipitation increased in the Carpathian Basin during the second half of the 20th century, while the total precipitation decreased, and the mean climate became slightly drier during the whole 20th century. Furthermore, the climate simulations suggest that the climate of this region may become drier in summer and wetter in winter, which highlights the importance of hydrological and agricultural planning in Hungary.

Parametric methods (linear trend, t-test for slope) for analyzing time series are the simplest methods to get insight into the changes in a variable over time. These methods require normal distribution of the residuals that can be a limit for application. Non-parametric methods are distribution-free methods, and investigators can have a more sophisticated view of the variable tendencies in time series. Historical climate (precipitation) data covering the past almost one and a half centuries measured at the meteorological station in Keszthely, Hungary were analyzed by *Kocsis et al.* (2017) and *Kocsis* and *Anda* (2018) for detecting tendencies in the time series. The parametric method proved significant decreasing tendencies for spring, April, and October. Non-parametric tests show significant declining tendencies for spring, autumn, and October.

Kocsis et al. (2020) also tried to detect change points in the time series of monthly, seasonal, and annual precipitation records of Keszthely. Change points and monotonic trends were analyzed separately in annual, seasonal, and monthly time series. While no breakpoints could be detected in the annual precipitation series, a significant decreasing trend of 0.2–0.7 mm/year was highlighted statistically. Significant change points were found in those time series in which significant tendencies had been detected in previous studies. These points fell in spring and winter for the seasonal series, and October for the monthly series. The question, therefore, was raised that these trends were the result of a shift in the mean. The downward and upward shifts in the mean seasonal amounts in spring and winter led to a suspicion that changes in precipitation were also in progress in these seasons. The study concluded that homogeneity tests are of great importance in such analyses, because they may help to avoid false trend detections.

Wheat is one of the most valuable and widely grown cereal crops worldwide, with a cultivation area of around 245–250 million hectares. Its importance for food security is only rivalled by rice. The widespread distribution of wheat is made possible by the diverse climatic requirements of wheat species and varieties and their strong adaptability. It can be found from near the Equator to the 60°N and 40°S latitudes. As a result of its wide adaptation, wheat is grown at such diverse geographical latitudes that harvests occur year-round, but it is primarily a crop of continental climates.

In Hungary, wheat is also the most important cereal crop, cultivated on approximately 1 million hectares annually (Hungarian Statistical Office's website). In years with average weather conditions, with appropriate agrotechnics, and considering the varieties currently grown, the water demand of winter wheat in Hungary is estimated at 350–410 mm. This water amount is mostly not covered by natural precipitation. Of the 390–480 mm (50-year average) of precipitation falling from sowing to harvest, only 40–60% is effectively utilized, depending on the water management properties of the soil. Since wheat requires an average of 280–340 mm of water from late March to early July, and the precipitation during this period only partially covers this need, the available soil water at the end of winter is of fundamental importance for the water supply of winter wheat (*Harmati,* 1987).

Wheat needs water throughout its entire growth period, but there are certain stages during which water scarcity can cause significant yield reduction (*Araus et al.,* 2008). In the early stages of the growing season, drought can have severe consequences, as it reduces plant growth (*Jaleel* and *Llorente,* 2009). Early spring drought negatively affects the development of the secondary root system and tillering (*Harmati,* 1987; *Araus et al.,* 2008). Water deficiency also delays the appearance of side shoots and fertilization, leading to yield loss (*Mosaad et al.,* 1995).

In our study, we aimed to study the trends in the precipitation data from Mosonmagyaróvár between 1871 and 2020 and to draw conclusions about how these trends might impact winter wheat cultivation conditions in the Moson-plain.

2. Material and methods

2.1. Dataset

Monthly precipitation amount measured at Mosonmagyaróvár (northwestern edge of Hungary, of 47° 53' 23" N and 17° 16' 02" E, *Fig. 1*) was used for the analysis of tendencies for the period of 1871–2020. The dataset was collected in around a circle of a diameter of 5 kilometers in plain ground, and the original data were used. To gain coherent precipitation data over flat terrain in the mid-latitudes, even interpolation should yield acceptable results on scales smaller than 10 km (*Dingman,* 2015). The dataset was controlled but not homogenized by the MASH method (*Szentimrey*, 1999) that is usually used for homogenization of meteorological datasets in Hungary. In purpose of testing homogeneity of the time series, Pettitt's test (*Pettitt,* 1979) was applied. This test detects shifts in the average and calculates their significance (*Liu et al.,* 2012) in a hypothesis test. The 5% significance level was used as threshold.

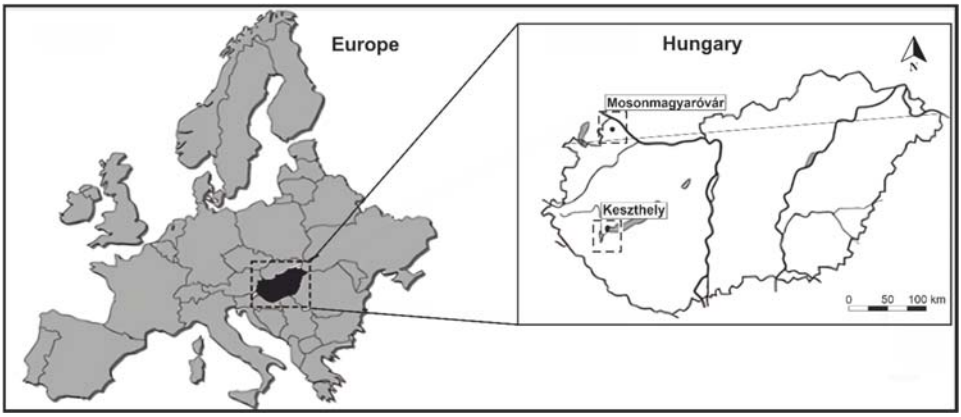

Fig. 1. Location of Mosonmagyaróvár (Hungary; 47°53′N, 17°16′E, elevation 121.5 m above Baltic Sea level) and Keszthely (Hungary; 46°44′N, 17°14′E, elevation 114.2 m above Baltic Sea level), redrawn from *Kocsis et al*. (2020, 2024)

The location of the meteorological station, which provides representative measurements of the region's climate, changed six times during the century and a half, but these relocations took place within a very narrow area. The time series of yearly, seasonal, and monthly amounts of precipitation were examined, and an analysis was conducted to detect linear or monotonic trends. Each time series used contained 150 data. The dataset was complete, without missing data.

2.2. Statistical methods

First, the tendency of the time series was estimated by a linear trend using the ordinary least squares method

$$\hat{y}_t = b_0 + b_1 * t \,, \tag{1}$$

where t is the serial number of the time step, $t = 1, 2, 3, \ldots, n$, where n is the number of the data, $\hat{y}_t$ is the estimated value of precipitation amount for a certain time step, b_0 is the intercept of the trendline, and b_1 is the slope coefficient on the trendline.

In the diagnostic stage of a linear trend, the normal distribution of the residuals was tested by the Kolmogorov-Smirnov test. In this case, the residuals' distribution could be accepted to be normal, the slope coefficient of the linear trend was tested in a parametric *t*-test for significance. Otherwise, when the distribution of the residuals could not be accepted to be normal according to the Kolmogorov-Smirnov test, the Mann-Kendall trend test was used. The Mann-Kendall trend test is based upon the work of *Mann* (1945) and *Kendall* (1975), and it is closely related to the Kendall's rank correlation coefficient. This test is

suitable to detect monotonic trends in the time series. The Mann-Kendall trend test is widespread in climatological and hydrological analyses for time series, because it is simple and robust, it can cope with missing values and values under detection limit (*Gavrilov et al.,* 2016). This non-parametric test is commonly used to detect monotonic tendencies in a series of environmental data, too (*Pohlert,* 2016). This method has no requirement for the distribution, as the regression method requires normal distribution. No assumption of the normality is required (*Helsel* and *Hirsh,* 2002). The Mann-Kendall test statistic is given as (*Singh et al.,* 2024):

$$S = \sum_{i=1}^{n-1} \sum_{j=i+1}^{n} sgn(x_j - x_i) \ , \tag{2}$$

where $j > i$ and $i = 1, 2, \ldots, n\text{-}1$; $j = 2, 3, \ldots, n$, and n is the number of the data.

S serves for the hypothesis test, where the null hypothesis is that there is not a significant trend, and the alternative hypothesis is that a significant monotonic trend over time is present. $Sgn(x_j\text{-}x_i)$ is calculated as (*Hipel* and *McLeod,* 1994; *Hu et al.,* 2020):

$$sgn(x_j - x_i) = \begin{cases} +1 \ \ if \ \ x_j - x_i > 0 \\ 0 \ \ if \ \ x_j - x_i = 0 \\ -1 \ \ if \ \ x_j - x_i < 0 \end{cases} \ . \tag{3}$$

Decisions were made based on the p-value in the hypothesis tests, at 5% significance level as a threshold. After determining the presence of the trend, the Sen's slope estimator (*Sen,* 1968) was applied. It is a non-parametric method that can calculate the change per time unit (direction and volume) and is commonly used in hydro-meteorological time series to calculate the magnitude of a trend (*Lone et al.,* 2022).

Calculations were carried out using IBM SPSS and R softwares.

3. Results

3.1. Descriptive statistics of the annual, seasonal, and monthly precipitation sums

The average annual precipitation amount at Mosonmagyaróvár was 593.32 mm between 1871 and 2020 with a standard deviation of 104.13 mm. The median of the dataset is 586.25 mm. Based on the relation of the average and the median (average > median), the ratio of those values that are less than the mean is supposed to be more than 50%, but the boxplot of the annual data does not represent this skewness, probably for the reason that two data have been considered as outliers (*Fig. 2*).

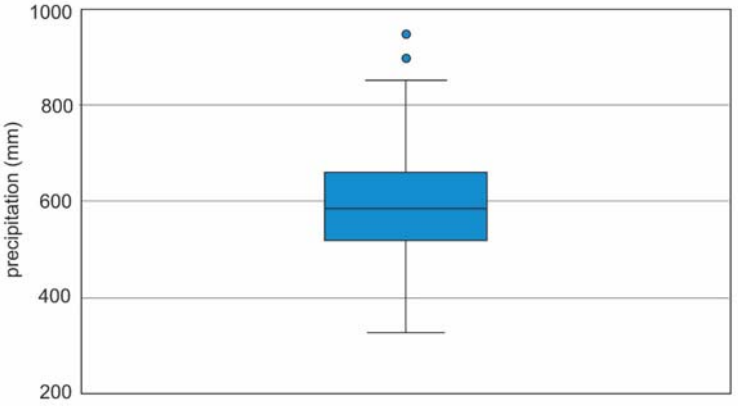

Fig. 2. Boxplot of the annual precipitation amount (mm).
The box indicates the interquartile range, the black line in it is the median.

Table 1 summarizes the descriptive statistics of the seasonal precipitation sums. It can be observed that the order of the mean, median, and mode is the same for all seasons, as the mean is greater than the median, and the median is greater than the mode. When the mode is the lowest one, a positively skewed distribution should be supposed, where the values of lower than the average are overrepresented. This can also be observed in *Fig. 3.* The same type of skewness can be seen in the case of the monthly precipitation sums, as well. A skewness can be observed towards the values lower than the average of the dataset (*Table 2, Fig. 4*). The highest monthly amounts can be expected in June and July, so the maximum of the yearly course is in summer. Usually, a peak can be observed in May and a secondary maximum in September. This yearly course seems to be rearranged at Mosonmagyaróvár.

Table 1. Main descriptive statistics of the seasonal precipitation sums

	Descriptive statistics (mm)			
Season	Mean	Median	Mode	Standard deviation
Spring	142.28	138.50	77.0	51.12
Summer	190.53	185.05	121.0	65.34
Fall	149.29	148.50	126.0	52.72
Winter	111.33	102.50	87.0	41.91

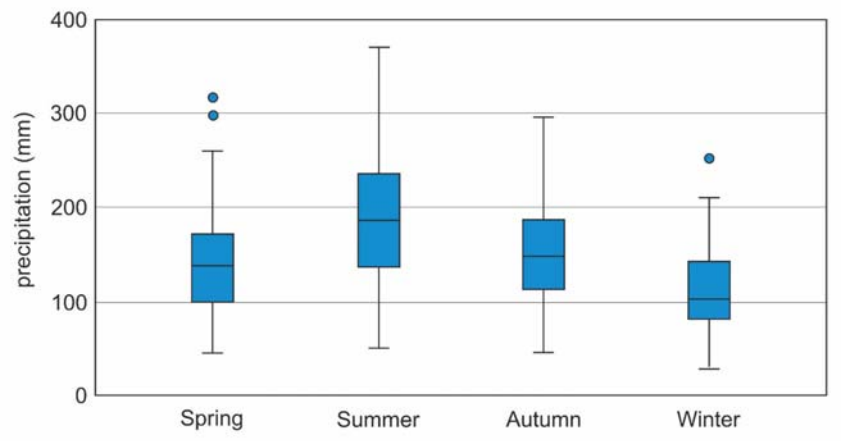

Fig. 3. Boxplots of the seasonal precipitation amount (mm).
The boxes indicate the interquartile range, the black line in it is the median.

Table 2. Main descriptive statistics of the monthly precipitation sums

	Descriptive statistics (mm)			
Month	Mean	Median	Mode	Standard deviation
Jan	34.53	32.00	28.0	19.31
Feb	32.32	27.00	16.0	22.25
Mar	37.77	34.50	39.0	23.78
Apr	42.46	37.50	19.0	26.72
May	62.05	54.50	39.0	37.40
Jun	65.36	59.25	53.0	34.68
Jul	65.56	58.30	49.0	39.25
Aug	59.62	51.50	57.0	36.08
Sept	50.03	43.35	31.0	33.39
Oct	49.64	46.00	60.0	33.00
Nov	49.61	40.90	31.0	31.94
Dec	44.38	42.40	37.0	24.29

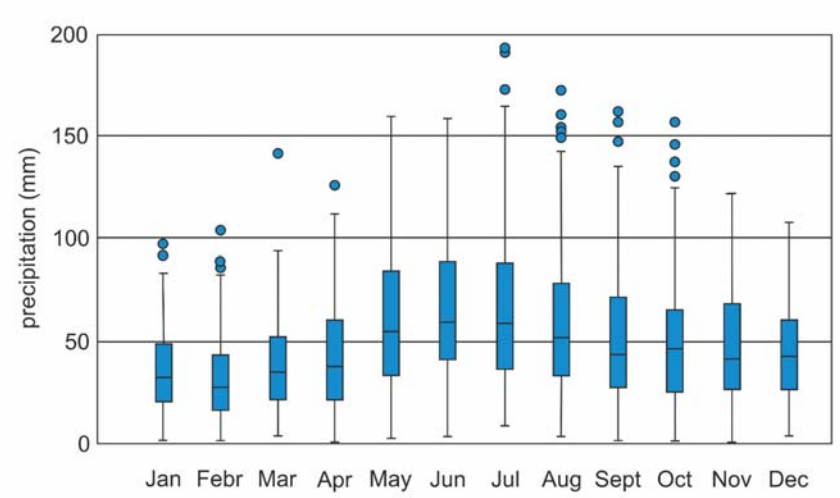

Fig. 4. Boxplots of the monthly precipitation amount (mm).
The boxes indicate the interquartile range, while the black line in the middle is the median.

3.2. Trends of the examined time series

Following the steps of time series analysis written about in Section 2.2, a significant linear trend can be detected in spring ($\alpha = 0.05$, *Table 3, Fig. 5.*). Regarding the homogeneity of the time series, it should be noted that in case of only one time series, a change point could be detected by the Pettitt's test. This one is spring (p-value = 0.032). The change point took place in 1945, and no other change point could be found. Therefore, to be sure to detect a real trend, the time series was divided into two parts, but no significant trends could be seen in the separated parts. The Pettitt's test suggests a significant downward shift of the mean (*Fig. 5*), that can be the same proof of the changes, as the precipitation decrease can be realized not only as a gradual change, but also as an abrupt shift of the mean.

When analyzing the trends of the monthly precipitation sums, significant monotonic trends can be determined for April and October (*Table 4*). In April, 9.1 mm per 100 years declining trend could be found, and in October the average decrease was 11.08 mm per 100 years. These results are in good coincidence with the findings of *Kocsis* and *Anda* (2018) and *Kocsis et al.* (2020) at Keszthely (western Hungary). It should be highlighted that Keszthely and Mosonmagyaróvár are about 150 km far from each other, and there is the Bakony Hills region as a barrier for the vapour flows that can modify the direction of the

air movements. Keszthely's microclimate is affected by the Balaton Lake. As a similarity, the proximity of the Mosoni-Danube River can be mentioned in the case of Mosonmagyaróvár.

Table 3. Results of the time series analysis

	Linear slope coefficient	***p*-value of *t*-test**	**Kolmogorov-Smirnov *p*-value**	**Kendall tau**	***p*-value of MK test**
Annual	-0.353	0.072	0.2		
Spring	**-0.213**	0.026*	0.2		
Summer	0.014	0.908	0.2		
Fall	-0.115	0.249	0.2		
Winter	-0.043	0.591	0.002*	-0.035	0.522

** significant at the 5% significance level*

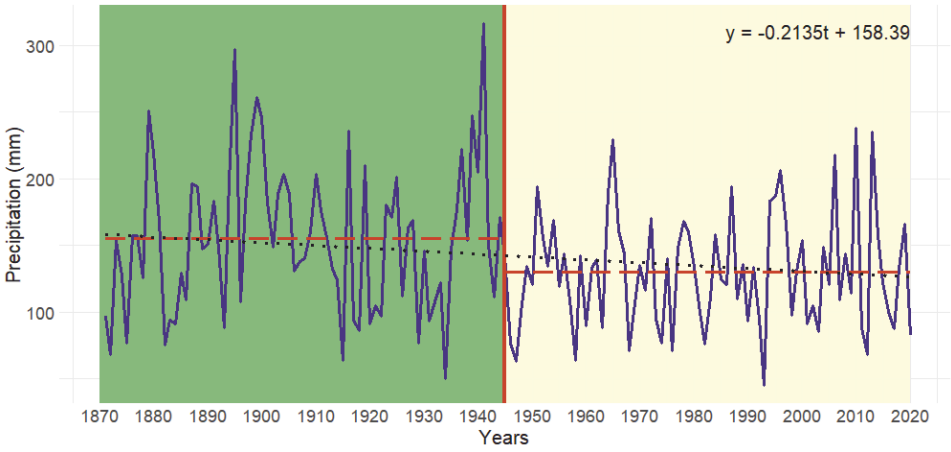

Fig. 5. Time series of the precipitation amount measured at Mosonmagyaróvár in spring (1871–2020). The blue line represents the observed data, while the black dotted line shows the significant decreasing linear trend. The red vertical line indicates the breakpoint obtained by the Pettitt's test and the red dashed lines show the means of the precipitation data in the separated time intervals.

Table 4. Results of the time series analysis of the monthly precipitation amounts

Month	Linear slope coefficient	*p*-value of *t*-test	Kolmogorov-Smirnov *p*-value	Kendall tau	*p*-value of MK test	Sen's slope
Jan	0.009	0.798	0.013*	0.015	0.791	0.005
Feb	0.014	0.744	0.002*	0.037	0.501	0.024
Mar	-0.049	0.274	0.001*	-0.071	0.199	-0.048
Apr	-0.104	0.038*	0.001*	-0.107	0.048*	**-0.092**
May	-0.060	0.397	0.001*	-0.035	0.521	-0.042
Jun	-0.007	0.918	0.021*	0.001	0.979	0.000
Jul	0.034	0.652	0.001*	0.017	0.753	0.019
Aug	-0.013	0.854	0.001*	0.021	0.71	0.023
Sept	0.018	0.771	0.001*	-0.013	0.81	-0.013
Oct	-0.132	0.033*	0.032*	-0.11	0.046*	**-0.112**
Nov	-0.002	0.980	0.001*	0.028	0.619	0.026
Dec	-0.062	0.178	0.02*	-0.057	0.305	-0.045

** significant at the 5% significance level*

3.3. Trends of the vegetation period of winter wheat

The precipitation conditions of the vegetation period of winter wheat were also studied, and the precipitation sums between September and the consecutive June were analyzed. The requirement for normality of the residuals of the linear trend was fulfilled (*p*-value of the Kolmogorov-Smirnov test was 0.087), therefore its slope can be interpreted as it was significant at the 5% significance level (*p*-value = 0.022). There was no significant change point in the time series (*p*-value = 0.108). A declining tendency could be detected by 0.411 mm per year on average. This means 40.89 mm less precipitation in a 100-year period.

4. Discussion

During the last years, Europe has been exposed to a continuous period of dry conditions, leading to increasingly frequent agricultural, meteorological, and hydrological droughts across the continent. The years 2021 and 2022 caused one of the most severe water shortages in Europe and Hungary in the past decades. Because of the historic drought of 2022, the yields of autumn and summer crops fell below the average of previous years.

Wheat, by origin, is a plant that generally prefers drier conditions, as its gene center is located in the Fertile Crescent of the Middle East. During centuries of

breeding in Central Europe, the goal was to make the plant thrive under the local continental-type climate as much as possible, but even this essentially means drier conditions.

Wheat is a moderately water-demanding crop, requiring approximately 350–410 mm of precipitation in growing seasons with average weather conditions, when proper agrotechnics are applied. Its transpiration coefficient is 300–350 l/kg of dry matter (*Harmati,* 1987).

Our studies found that there has been a tendency to the reorganization of precipitation amounts in Mosonmagyaróvár between 1871 and 2020. Analysis of the data shows that both the spring and autumn periods have experienced a decrease, which was significant in the case of some months, in precipitation. This is particularly harmful for winter wheat, as these periods correspond to the phenological phases that greatly determine the quantity and quality of the yield.

The sowing time of winter wheat must be chosen so that the wheat can establish itself before the onset of winter. The crop's response to sowing time is specific and genetically determined, it generally occurs between September 20 and October 30, but it can be extended until early November.

From the perspective of water supply, the autumn period is critical in Hungary, as it is often dry, which can result in poor germination and uneven wheat stands. Our study results also indicate a significant decreasing trend in precipitation in October. The accompanying extreme weather conditions are generally unfavorable for wheat development and yield. Extremely dry autumn weather makes the proper germination, early development, establishment of a strong plant stand, and successful overwintering impossible. Germination can begin, only if the sown seeds receive sufficient water and the temperature is appropriate (*Varga-Haszonits et al.,* 2006).

The tillering phase lasts from December to the end of March, during which the formation of the secondary root system occurs. If there is a significant drought during this period, tillering may be delayed or fail. The more developed the secondary root system is the more resilient the wheat becomes.

The heading phase in our region lasts from mid-April to the end of May, which is the period of intense growth. The amount of precipitation during this period has a decisive impact on the maximum height of the varieties. During heading, wheat requires an uninterrupted water supply, as this phase - which lasts about 30 days - produces the most dry matter, nearly 50% of the total amount. Unfavourable water conditions disrupt plant development. If drought occurs during this developmental stage, the yield can be reduced to half. The vegetative organs become smaller, and assimilation activity decreases, leading to underdeveloped flowering organs in the spikes.

For this reason, it is crucial to ensure optimal soil moisture during this period, from mid-April to the end of May. The water demand closely approaches the evapotranspiration rate during this time, i.e., around 150–160 mm over this approximately 6-week period. The deeper and better water-managed the soil is,

and the more abundant the natural precipitation is, the less irrigation is needed. However, higher production targets require better water availability (*Harmati,* 1987). The significant decrease in April and spring precipitation amounts can therefore be a cause for serious concern.

The heading-flowering phase, which lasts for a relatively short time, is also a critical period (*Varga-Haszonits et al.,* 2006). Due to high temperatures and poor water supply, partial death of the flowering organs occurs, resulting in incomplete fertilization and a significant decrease in yield. If the autumn and winter are wet and the spring is not too dry, the moisture stored in the soil can meet the water requirements of these two phases without irrigation, especially in deep, fertile soils. In a dry year, or shallow soils, irrigation before or during this critical period is essential and effective.

Winter wheat takes up the most water during the flowering and fertilization period (from the middle of May to early June), but the pre-ripening period is also significant in terms of water consumption. Lack of precipitation during the ripening period can result in deformed, shrivelled grains, and the kernels may shrink. In May and June, the average required amount of precipitation is about 115 mm (*Harmati,* 1987). Full maturity in Hungary typically occurs in the first part of July. If the weather is too rainy at this time, the grains may become overripe, and their baking quality can deteriorate.

In the Carpathian Basin and Hungary, extreme weather events have become more frequent, and it is also unfavourable that precipitation shows decreasing tendencies. Such a modification of the main water intake factor, together with unfavourable thermal changes affecting the water loss side of the water balance, may endanger the water supply of winter wheat. Most climate simulations suggest that this trend will continue in the future, and even decade-long extremes may occur in the second half of the century.

5. Conclusions

The main findings of this research are that between 1871 and 2020 decreasing trends were detected in April and October, and a significant downward shift of the mean can be found in spring. For the growing period of winter wheat (September- June), a significant precipitation decline can be demonstrated.

The entire area of Hungary is suitable for the cultivation of winter wheat, but due to climate change, the weather could be extreme sometimes. Unfortunately, dry years and even droughts are becoming more and more frequent. Such problems may also occur in the studied region. Therefore, we considered it important to quantify the trends in precipitation conditions based on the longest data series available. The good agreement with the results of previous, similar research on Keszthely suggests that the conclusions drawn from our investigations may be more general.

Winter wheat yields are expected to decrease by 8% by 2050 and by 21% by 2100 in Hungary (*Kemény et al.,* 2019), but the results may differ significantly by the model used for prognostications. More intensive nutrient management and irrigation cannot even compensate for the negative impact of climate change on average (*Kemény et al.,* 2019). The negative effects of climate change and more frequent dry periods can be mitigated in two ways: with passive and active methods. The passive methods are the right choice of varieties, as well as efficient agrotechnics in terms of water conservation and water use. Active intervention could be achieved through irrigation to reduce the water deficit.

With agrotechnics adapted to the environment and genotypes, we can keep the yield quantity and quality stable, and it is important to use genotypes that are not only capable of achieving high yield and good quality but are also able to keep it stable under different meteorological conditions and on different quality soils, with different agrotechnical levels. These varieties are characterized by good stress tolerance - such as drought tolerance, excellent winter resistance, and better resistance to diseases and pests, as well as good or excellent adaptability and a good reaction to agrotechnics. It is advisable to select successive plants in such a way that plants with lower and higher water consumption follow each other in the crop rotation.

A fundamental consideration for Hungary must be the use of a water-saving soil cultivation system that is minimized as much as possible. Preference should be given to tillage tools without rotation, sealing the soil at the optimal time, and increasing the water absorption and water retention capacity of the soil. In terms of nutrient supply, plant stands in better condition and can withstand drought better. The close interactive relationship between water and nutrient supply in our cultivated plants is well known. It is important to emphasize that the water supply plays a key role in the vegetative and generative development and crop formation of field plants; however, it also affects the effectiveness of various agrotechnical inputs (e.g., soil cultivation, plant protection, etc.).

In the case of sowing technology, the stand density of plants primarily affects the drought tolerance of plants. It is a common misconception that the sowing rate should be increased with the intention of "sowing more so that some will remain". This actually results in the opposite effect. By choosing the right sowing time, we can avoid the coincidence of the phenophase of the given plant species, which is sensitive to water shortage, and the typically dry period of the given area. Plant protection can also contribute to better drought tolerance of plant populations. Adequate weed control is particularly important, as weeds not only consume more water than cultivated plants, but they can take up water much more aggressively.

In these times, we can irrigate only 2% (approximately 100,000 ha) of the domestic arable land in Hungary, which is extremely small. Wheat is a plant that prefers drier conditions since its genetic center is located in the area called the Fertile Crescent of the Middle East. During centuries of breeding in Central Europe, the aim was to make the plant thrive under the local continental climate

as well as possible in the continental-type climate, but even this basically means drier conditions. Under normal weather conditions, there is no need to irrigate winter wheat. In the case of extremely dry months, it is worth watering the plants.

Nowadays, one of the most important questions of arable crop production is how we can ensure optimal water supply for plants under changing and less favorable climatic conditions. In this, it must be taken into account that passive agrotechnical elements play a decisive role, as the irrigated area is extremely limited in Hungary today. This is the key issue for the further development of domestic crop production. We wanted to contribute to this with our work quantifying regional precipitation conditions and trends.

References

Araus, J. L., Slafer, G.A., Royo, C., and *Serret, M.D.,* 2008: Breeding for Yield Potential and Stress Adaptation in Cereals. *Critical Rev.Plant Sc. 27*, 377–412. https://doi.org/10.1080/07352680802467736

Asadieh, B. and *Krakauer, N.Y.*, 2015: Global trends in extreme precipitation: Climate models versus observations. Hydrol. *Earth Syst. Sci. 19*(2), 877–891. https://doi.org/10.5194/hess-19-877-2015

Bartholy, J. and *Pográcz, R*., 2007: Regional analysis of extreme temperature and precipitation indices for the Carpathian Basin from 1946 to 2001. *Glob. Planet. Change 57*(1–2), 83–95. https://doi.org/10.1016/j.gloplacha.2006.11.002

Bartholy, J. and *Pongrácz, R*., 2010: Analysis of precipitation conditions for the Carpathian Basin based on extreme indices in the 20th century and climate simulations for 2050 and 2100. *Phys. Chemist. Earth 35*, 43–51. https://doi.org/10.1016/j.pce.2010.03.011

Bartholy, J., Pongrácz, R., and *Gelybó, Gy*., 2007: Regional climate change in Hungary for 2071–2100. *Appl. Ecol. Environ. Res. 5*, 1–17. https://doi.org/10.15666/aeer/0501_001017

Bartholy, J., Pongrácz, R., and *Kis, A.,* 2015: Projected changes of extreme precipitation using multimodel approach. *Időjárás 119*, 129–142.

Berényi, A., Bartholy, J., and *Pongrácz, R*., 2023: Analysis of precipitation-related climatic conditions in European plain regions. *Weather Climate Extr. 42*, 100610. https://doi.org/10.1016/j.wace.2023.100610

van den Besselaar, E.J.M., Klein Tank, A.M.G., and *Buishand, T.A*., 2012: Trends in European precipitation extremes over 1951-2010. *Int. J. Climatol. 33*, 2682–2689. https://doi.org/10.1002/joc.3619

Bormann, H., Ahlhorn, F., and *Klenke, T*., 2012: Adaptation of water management to regional climate change in a coastal region – hydrological change vs. community perception and strategies. *J. Hydrol. 454–455*, 64–75. https://doi.org/10.1016/j.jhydrol.2012.05.063

Dingman, S.L., 2015: Physical hydrology (3rd ed.). Long Grove, IL: Waveland Press.

Donat, M.G., Lowry, A.L., Alexander, L.V., O'Gorman, P.A., and *Maher, N*., 2016: More extreme precipitation in the world's dry and wet regions. *Nat. Clim. Change 5*, 508–513. https://doi.org/10.1038/nclimate2941

Gavrilov, M. B., Tosic, I., Markovic, S. B., Unkasevic, *M.,* and *Petrovic, P*., 2016: Analysis of annual and seasonal temperature trends using the Mann- Kendall test in Vojvodina, Serbia. *Időjárás 120*, 183–198.

Groisman, P.Y., Knight, R.W., Easterling, D.R., Karl, T.R., Hegerl, G.C., and *Razuvaev, V.N.,* 2005: Trends in intense precipitation in the climate record. *J. Climate 18* (9), 1326–1350. https://doi.org/10.1175/JCLI3339.1

Harmati, I., 1987: A búza vízigénye, vízfogyasztása, és vizhasznositása. (Water requirements, water consumption and water utilisation of wheat.) In (Ed. *Barabas Z.*) Wheat Production Manual. Mezőgazdasági Kiadó, Budapest, pp.: 414-415. (in Hungarian)

Hall, J.W., Brown, S., Nicholls, R.J., Pidgeon, N.F., and *Watson, R.T.*, 2012: Proportionate adaptation. *Nat. Clim. Change 2* (12), 833–834. https://doi.org/10.1038/nclimate1749

Helsel, D. R. and *Hirsh, R. M.*, 2002: Trend analysis. In: Techniques of Water-Resources Investigations of the United States Geological Survey Book 4, Hydrologic Analysis and Interpretation Chapter A3: Statistical Methods in Water Resources. Chapter 12: 327.

Hipel, K.W. and *McLeod, A. I.*, 1994: Time series modelling of water resources and environmental systems. Elsevier, Amsterdam, The Netherlands: 864–866, 924–925.

Hoekstra, A. and *Mekonnen, M.*, 2012: The water footprint of humanity. *Proc. Natl. Acad. Sci. USA 109*, 3232–3237. https://doi.org/10.1073/pnas.1109936109

Hu, Z., Liu, S., Zhong, G., Lin, H., and *Zhou, Z.*, 2020: Modified Mann-Kendall trend test for hydrological time series under the scaling hypothesis and its application. *Hydrol. Sc. J. 65* (14), 2419–2438. https://doi.org/10.1080/02626667.2020.1810253

Hungarian Statistical Office: Major crop's cultivation area. https://www.ksh.hu/s/kiadvanyok/a-fontosabb-novenyek-vetesterulete-2024-junius-1/index.html#:~:text=Haz%C3%A1nkban%20a%20sz%C3%A1nt%C3%B3ter%C3%BClet%20legnagyobb%20r%C3%A9sz%C3%A9n%20gabonaf%C3%A9l%C3%A9ket%20termesztenek.%202024-ben,%C5%91szi%20b%C3%BAz%C3%A1%C3%A9%20%28875%20ezer%20hekt%C3%A1r%29%20a%20legnagyobb%20kiterjed%C3%A9s%C5%B1. (in Hungarian)

IPCC, 2012: Intergovernmental Panel on Climate Change In: *Field, C.B., Barros, V., Stocker, T.F., Qin, D., Dokken, D.J., Ebi, K.L., Mastrandrea, M.D., Mach, K.J., Plattner, G.-K., Allen, S.K., Tignor, M. and Midgley, P.M.* (Eds.), Managing the Risks of Extreme Events and Disasters to Advance Climate Change Adaptation. A Special Report of Working Groups I and II of the Intergovernmental Panel on Climate Change. Cambridge University Press, Cambridge, UK, and New York, NY, USA.

IPCC, 2021: Intergovernmental Panel on Climate Change: Climate Change 2021: The Physical Science Basis. Contribution of Working Group I to the Sixth Assessment Report of the Intergovernmental Panel on Climate Change. Edited by *Masson-Delmotte, V.P., Zhai, A., Pirani, S.L., Connors, C., P´ean, S., Berger, N., Caud, Y., Chen, L., Goldfarb, M.I., Gomis, M., Huang, K., Leitzell, E., Lonnoy, J.B.R., Matthews, T.K., Maycock, T., Waterfield, O., Yelekçi, R. and Yu, B.Z.* Cambridge University Press Cambridge United Kingdom and New York NY USA.

Jaleel, C.A. and *Llorente, B.E.*, 2009: Drought stress in plants: A review on water relations. *Bioscie. Res. 6*(1), 20–27.

Janssen, E., Wuebbles, D.J., Kunkel, K.E., Olsen, S.C., and *Goodman, A.*, 2014: Observational and model-based trends and projections of extreme precipitation over the contiguous United States. *Earth's Future 2* (2), 99–113.

Kemény, G., Molnár, A., and *Fogarasi, J.*, (eds.), 2019: Modeling the impact of climate change for the key cereal crops in Hungary. Agricultural Books. NAIK Agricultural Research Institute, Budapest. ISBN 978-963-491-605-5 (in Hungarian) https://doi.org/10.1002/2013EF000185

Kendall, M.G., 1975. Rank correlation methods. Charles Griffin, London

Kocsis, T. and *Anda, A.*, 2018: Parametric or non-parametric: analysis of rainfall time series at a Hungarian meteorological station. *Időjárás 122*, 203–216. https://doi.org/10.28974/idojaras.2018.2.6

Kocsis, T., Kovács-Székely, I., and *Anda A.*, 2017: Comparison of parametric and non-parametric time-series analysis methods on a long-term meteorological data set. *Cent Eur Geol 60*, 316–332. https://doi.org/10.1556/24.60.2017.011

Kocsis, T., Kovács-Székely, I., and *Anda A.*, 2020: Homogeneity tests and non-parametric analyses of tendencies in precipitation time series in Keszthely, Western Hungary. *Theor. Appl. Climatol. 139*, 849–859. https://doi.org/10.1007/s00704-019-03014-4

Kocsis, T., Pongrácz, R., Hatvani, I. G., Magyar, N., Anda, A., and *Kovács-Székely, I.* 2024: Seasonal trends in the Early Twentieth Century Warming (ETCW) in a centennial instrumental temperature record from Central Europe. *Hungarian Geograph. Bull 73*(1), 3–16. https://doi.org/10.15201/hungeobull.73.1.1

Lakatos, M. and *Bihari, Z.*, 2011: A közelmúlt megfigyelt hőmérsékleti és csapadéktendenciái [Temperature and precipitation tendencies observed in the recent past]. – In: Bartholy, J., Bozó,

L., Haszpra, L. (Eds): Klímaváltozás 2011. Hungarian Meteorological Society, Budapest, 146–169. (in Hungarian)

Lee, T.C., Chan, K.Y., Chan, H.S., and *Kok, M.H.*, 2011: Projections of extreme rainfall in Hong Kong in the 21st century. *Acta. Meteor. Sin. 25* (6), 691–709. https://doi.org/10.1007/s13351-011-0601-y

Liu, J.J., Fu, Z.H., and *Liu, W.F.*, 2023: Impacts of precipitation variations on agricultural water scarcity under historical and future climate change*. J. Hydrol. 617*, 128999. https://doi.org/10.1016/j.jhydrol.2022.128999

Liu,. L, Xu, Z.X., and *Huang, J.X.,* 2012: Spatio-temporal variation and abrupt changes for major climate variables in the Taihu Basin, China. Stoch *Environ Res Risk Assess 26*(4),777–791. https://doi.org/10.1007/s00477-011-0547-8

Lone, B. A., Qayoom, S., Nazir, A., Ahanger, S. A., Basu, U., Bhat, T. A., Dar, Z. A., Mushtaq, M., El Sabagh, A., Soufan, W., ur Rahman, M. H., and *El-Agamy, R. F.*, 2022. Climatic trends of variable temperature environment: A complete time series analysis during 1980-2020. Atmosphere. 13, 749. https://doi.org/10.3390/atmos13050749

Madsen, H., Lawrence, D., Lang, M., Martinkova, M., and *Kjeldsen, T.R.*, 2014: Review of trend analysis and climate change projections of extreme precipitation and floods in Europe. *J. Hydrol. 519*, 3634–3650. https://doi.org/10.1016/j.jhydrol.2014.11.003

Mann, H. B., 1945. Nonparametric tests against trend. *Econometrica. 13*, 245–259. https://doi.org/10.2307/1907187

Mosaad, M.G., Ortiz-Ferrara,G., and *Mahalaksmi,V.*, 1995: Tiller development and contribution on yield under different moisture regime in two Triticum species. *J. Agronomy Corp Sci. 174* (3), 173–180. https://doi.org/10.1111/j.1439-037X.1995.tb01100.x

Norrant, C. and *Douguédroit, A.*, 2005: Monthly and daily precipitation trends in the Mediterranean (1950–2000). *Theor. Appl. Climatol. 83* (1–4), 89–106. https://doi.org/10.1007/s00704-005-0163-y

Ntegeka, V. and *Willems, P.,* 2008: Trends and multidecadal oscillations in rainfall extremes, based on a more than 100-year time series of 10 min rainfall intensities at Uccle, Belgium. *Water Resour. Res. 44* (7), W07402. https://doi.org/10.1029/2007WR006471

Olesen, J.E. and *Bindi, M.*, 2002: Consequences of climate change for European agricultural productivity, land use and policy. Eur. *J. Agron. 16*, 239–262. https://doi.org/10.1016/S1161-0301(02)00004-7

Olesen, J.E., Trnka, M., Kersebaum, K.C., Skjelvåg, A.O., Seguin, B., Peltonen-Sainio, P., Rossi, F., Kozyra, J., and *Micale, F.,* 2011: Impacts and adaptation of European crop production systems to climate change. Eur. *J. Agron. 34*, 96–112. https://doi.org/10.1016/j.eja.2010.11.003

Pachauri, R.K., Allen, M., Barros, V., Broome, J., Cramer, W., Christ, R., Church, J., Clarke, L., Dahe, Q., and *Dasgupta, P.*, 2014: Climate Change 2014: Synthesis Report. Contribution of Working Groups I, II and III to the Fifth Assessment Report of the Intergovernmental Panel on Climate Change.

Pettitt, A.N. 1979: A Non-parametric Approach to the Change-point Problem. *Appl. Stat. 28*(2), 126–135.

Pohlert, T., 2016: Non-parametric trends and change-point detection. https://doi.org/10.32614/CRAN.package.trend

Sen, P. K., 1968. Estimates of the regression coefficient based on Kendall's tau. *J. Amer. Stat. Assoc. 63*, 1379-1389. https://doi.org/10.1080/01621459.1968.10480934

Singh, S, Singh S. K., Kanga, S., kr Shrivastava, P., Sajan, B., Meraj, G., Kumar, P., Đurin, B., Krajčić, N., and *Dogančić, D.*, 2024: Analysis of hydrological changes in the Banas River: Analysing Bisalpur Dam impact and trends of the water scarcity. *Results Engin. 22*, 101978. https://doi.org/10.1016/j.rineng.2024.101978

Spinoni, J., Naumann, G., Vogt, J.V., and *Barbosa, P.*, 2015: European drought climatologies and trends based on a multi-indicator approach. *Glob. Planet Change. 127*, 50–57. https://doi.org/10.1016/j.gloplacha.2015.01.012

Sun, Q., Zhang, X., Zwiers, F., Westra, S., and *Alexander L.V.*, 2021: A global, continental, and regional analysis of changes in extreme precipitation. *J. Climate 34* (1), 243–258. https://doi.org/10.1175/JCLI-D-19-0892.1

Szentimrey, T., 1999: Multiple Analysis of Series for Homogenization (MASH). Proceedings of the 2nd Seminar for Homogenization of Surface Climatological Data, Budapest, Hungary; WMO, WCDMP 41, 27–46.

Tabari, H. and *Willems, P*., 2018: Seasonally varying footprint of climate change on precipitation in the Middle East. *Sci. Rep. 8*, 4435. https://doi.org/10.1038/s41598-018-22795-8

Varga-Haszonits, Z., Varga, Z., Lantos, Zs., and *Enzsölné, Gerencsér E*., 2006: Az éghajlati változékonyság és az agroökoszisztémák. (Climatic variability and agroecosystems) Monocopy, Mosonmagyaróvár. (in Hungarian)

Wang, G., Wang, D., Trenberth, K.E., Erfanian, A., Yu, M., Bosilovich, M.G., and *Parr, D.T*., 2017: The peak structure and future changes of the relationships between extreme precipitation and temperature. *Nat. Clim. Change 7* (4), 268–275. https://doi.org/10.1038/nclimate3239

Ward, F.A. and *Pulido-Velazquez, M*., 2008: Water conservation in irrigation can increase water use. *Proc. Natl. Acad. Sci. USA 105* (47), 18215–18220. https://doi.org/10.1073/pnas.0805554105

Wen, X., Fang, G., Qi, H., Zhou, L., and *Gao, Y*., 2016: Changes of temperature and precipitation extremes in China: Past and future. *Theor. Appl. Climatol. 126* (1–2), 369–383. https://doi.org/10.1007/s00704-015-1584-x

Zhang, L., Chen, F., and *Lei, Y.D.,* 2020: Climate change and shifts in cropping systems together exacerbate China's water scarcity. *Environ. Res. Lett. 15* (10), 104060. https://doi.org/10.1088/1748-9326/abb1f2

Zhao, N., Yue, T., Li, H., Zhang, L., Yin, X., and *Liu, Y*., 2018: Spatio-temporal changes over Beijing-Tianjin-Hebei region. China. *Atmos Res. 202*, 156–168. https://doi.org/10.1016/j.atmosres.2017.11.029

Zobel, Z., Wang, J., Wuebbles, D.J., and *Kotamarthi, V.R*., 2018: Analyses for high-resolution projections through the end of the 21st century for precipitation extremes over the United States. *Earth's Future 6* (10), 1471–1490.

DOI:10.28974/idojaras.2025.4.2

IDŐJÁRÁS

Quarterly Journal of the HungaroMet Hungarian Meteorological Service
Vol. 129, No. 4, October – December, 2025, pp. 393–417

Statistical structure of the homogenized precipitation time series of Hungary

Part 1: Statistics of dry days and areas in Hungary

Károly Tar[1,*], **Sándor Szegedi**[1], **István Hadnagy**[2], **Tamás Tóth**[1] and **István Lázár**[1]

[1]*University of Debrecen,*
Department of Meteorology,
H-4032 Egyetem tér 1, Debrecen, Hungary

[2]*Ferenc Rákóczi II Transcarpathian Hungarian College of Higher Education,*
Department of Biology and Chemistry,
UA-90200 Kossuth Square, 6, Beherove, Ukraine

**Corresponding Author E-mail: tarko47@gmail.com*

(Manuscript received in final form February 21, 2025)

Abstract— An exact statistical description of present and future climate requires a database representative in space and time. However, observation records – that is raw climatological time series – are loaded with inhomogeneities due to changes in the location of the weather stations and usage of different instruments and observation protocols. Datasets must be homogenized first, which means that previous measurement data must be adjusted to the present observation protocols, while missing data must be supplemented. The data base of the present examination is the homogenized precipitation time series of Hungary, that is diurnal amounts of precipitation for the 1233 grid cells which cover the area of the country over the period of 1971-2022 in the state of the database in 2023. Firstly, the diurnal amount of precipitation over the area of the country, that is the sum of precipitation what falls in each cell of the grid over the area of the country has been chosen as a variable to be analyzed. Its annual and monthly characteristics have been analyzed for different independent variables. Secondly, spatial characteristics of the diurnal amount of precipitation, that is its distribution among the grid cells have been examined as well. In this article, after summarizing the climatic characteristics and the characteristics for the examined period of the total precipitation in Hungary, we analyze the spatial and temporal statistical properties of the daily dry grids and the dry days per grid. Dry days and grid cells are those when and where the daily precipitation amount is under 0.1 mm.

Key-words: nationally dry days, dry days and areas

1. Introduction – General spatial and temporal characteristics of the precipitation in Hungary

The amount of annual mean precipitation ranges between 500 and 800 mm over Hungary during the period between 1991 and 2020 with remarkable spatial differences and year-to-year fluctuations.

The spatial pattern of precipitation is formed by the maritime effect and the relief together (*Fig. 1*). The maximum occurs in the southwestern part of Transdanubia, where the maritime effect is the most emphasized (*Mersich et al.,* 2002, *Kocsis et al.,* 2018, *HungaroMet, 2024d*).

Other regions gaining high annual precipitation over 800 mm are the low-mountain ranges in Transdanubia and Northern Hungary over 700 meters above sea level. The minimum occurs over the low-lying central part of the Carpathian Basin on the Great Hungarian Plain with values between 500 and 550 mm (*Mersich et al.,* 2002, *Kocsis et al.,2018*, *HungaroMet, 2024d*).

Hungarian low-mountain ranges get higher amounts of precipitation than lowland regions due to orographic lift. There is a 35 mm increase in the annual mean precipitation amount with an increase of elevation of 100 meters on average (*Mersich et al.,*2002, *HungaroMet, 2024d*).

This anomaly is not symmetric over the mountain regions of Hungary, since positive anomaly occurs on the western sides of the mountain ranges facing the moist maritime air masses, while the eastern slopes are drier than the lowland areas due to the rain shadow effect of foehn winds.

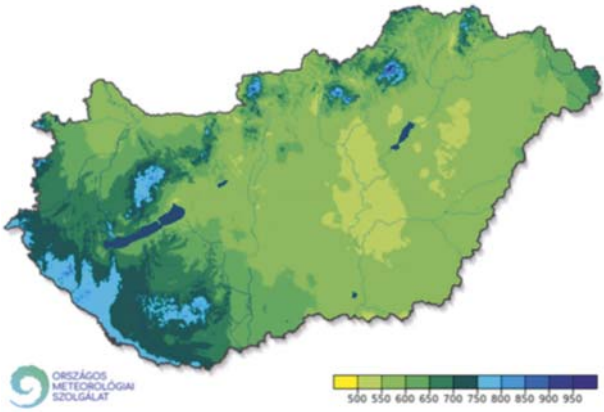

Fig. 1. Spatial pattern of annual mean precipitation during the normal period between 1991 and 2020 (*HungaroMet, 2024d*).

The minimum of the precipitation occurs between January and March due to low water vapor pressure of the cold air and the frequent dry, high pressure air

masses from the Siberian high. The main maximum of the precipitation occurs between May and July due to the high water vapor content of the air, favorable conditions for convection, and the high cyclone activity in that period (*Mersich et al.,*2002, *Kocsis et al.,2018*, *HungaroMet, 2024d*).

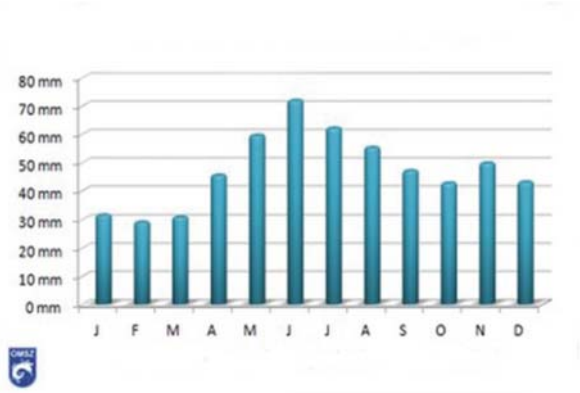

Fig. 2. Monthly mean precipitation during the normal period between 1971 and 2000. Based on homogenized, interpolated data (*HungaroMet, 2024d*).

There is a secondary precipitation maximum in the late autumn in the datasets before 2000 (*Fig. 2*). However, September and October have become considerably wetter since 2000 so the late autumn secondary maximum has disappeared, and there is a more or less gradual decrease of the monthly amounts of precipitation from August to December (*Fig. 3*, *HungaroMet, 2024d*). Autumn precipitation is caused mainly by warm fronts of mid-latitude cyclones formed over the western Mediterranean seas (*Mersich et al.,*2002).

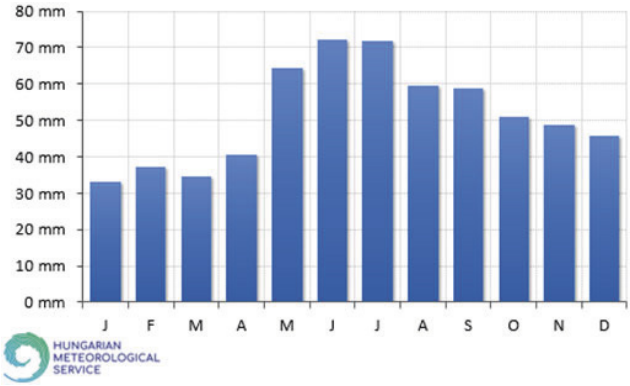

Fig. 3. Monthly mean precipitation during the normal period between 1991 and 2020 (*HungaroMet, 2024d*).

Among the meteorological parameters, precipitation shows the strongest variability on both spatial and temporal scales (*Gaál* and *Becsákné Tornay,* 2023, *Lakatos* and *Bihari,* 2011).

There can be 200% differences in the annual amount of precipitation in two consecutive years (*Fig. 4).* Annual precipitation of the driest years is under 500 mm only, while there is 800–900 mm of precipitation in the rainiest years. There can be an absolute lack of precipitation in any month of the year (*HungaroMet*, 2024d). However, the mean number of rainy days is 120 that is every third day is rainy, theoretically. The length of the longest period without precipitation is 60 days. It is quite frequent to have 200–300 mm precipitation in one month during the summer season (*Bacsó,* 1953).

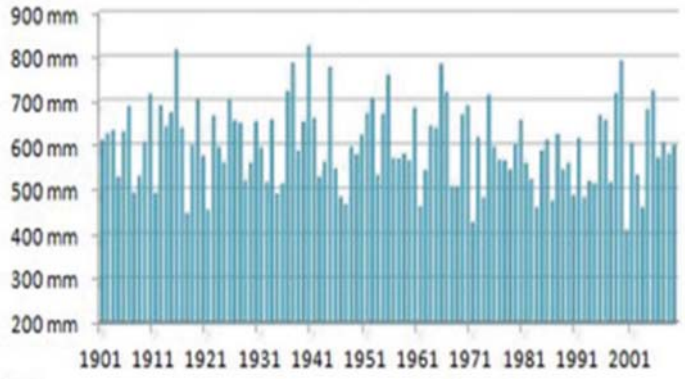

Fig. 4. Fluctuations of annual amounts of precipitation during the period between 1901 and 2009. Based on homogenized interpolated data (*HungaroMet*, 2024a).

Thunderstorms and hailstorms are summer phenomena typically in Hungary since they require high amount of moisture and energy in the atmosphere which is available during the period between the late spring and early autumn over the mid-latitudes. Thunderstorms are most frequent (more than 30 day annually) over the North Hungarian Mountain ranges, and the southeastern and northeastern parts of the Great Hungarian Plain, while the least thunderstorm (less than 20 per a year) occurs over the central part of the country (*Mersich et al.,*2002).

Low intensity rains are dominant by time span in Hungary: 75% of rainy days have intensities under 1 mm/hour. These rains provide only 30% of the total amount of precipitation. Medium intensity rains (1-5mm/hour) fall in 22% of rainy periods and provide 50% of the total amount of precipitation (*Mersich et al.,*2002).

High intensity rains (over 5 mm/hour) count for 2% of rainy periods but provides 20% of the total amount of precipitation. Most extreme precipitation events result in 150-200 mm of rain in 24 hours (*Mersich et al.,*2002).

It is a fundamental feature of the climate of Hungary that there is snow in the winters, although its amount fluctuates in a wide interval year by year. It not necessarily means the development of a snow cover in each year. There are 18–22 snowy days in the great Hungarian Plain, 25–30 snowy days in Transdanubia, and 50-60 snowy days in the hills over 700 meters above sea level on a multidecadal average (*Mersich et al.,*2002).

The least days with a snow cover occurs in the central Great Hungarian plain (30-35), where the amount of snow is the lowest, while the hilly regions have the longest periods of snow cover (*Fig. 5*).

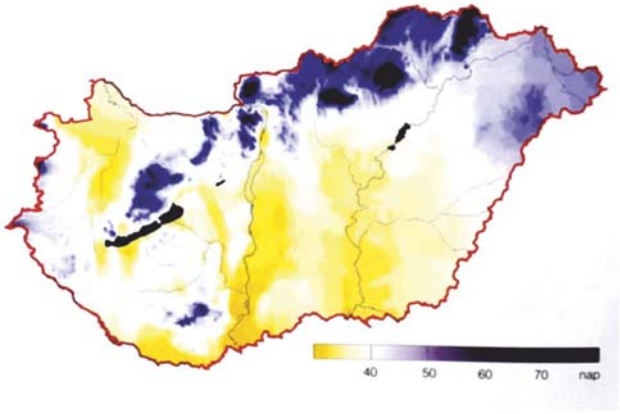

Fig. 5. Annual number of days with a snow cover given in days (*Mersich et al.,* 2002).

There are 40–45 days with a snow cover in most parts of Transdanubia due to the higher amount of snow precipitation despite slightly higher January mean temperatures. The number of days with a snow cover is over 50 in the hilly regions and reaches 100-120 over 700 meters above sea level (*Mersich et al.,*2002).

The great Hungarian Plain has the most extreme climate from the aspect of snow cover: there are winters when there is no snow cover, while there are winters when there are 80–100 days with a snow cover on the other hand (*Mersich et al.,*2002).

Another important climatic parameter is the thickness of the snow cover. It has an increasing tendency from the center of the Carpathian Basin towards its margins as well. It reaches 15–20 cm only over the cold but less snowy Great Hungarian Plain. It is around 25–40 cm over the milder and snowier Transdanubia and is over 50 cm over 500 m above sea level (*Mersich et al.,*2002).

Climate change has a remarkable impact on precipitation conditions in Hungary, however, depending on the time scale and region of focus the changes are different. For the whole country there was a moderate decrease in the annual amount of precipitation during the period between 1901 and 2020 (*Fig. 6*). The strongest decline of 20% occurred in the spring (*Kocsis* and *Anda,* 2018).The decrease is more emphasized over the western part of the country, while there was a slight increase in the eastern half of the country (*HungaroMet,* 2024b). There is a significant decrease of 17 days in the number of precipitation days during the period between 1901 and 2020. However, the number of days with precipitation over 20 mm increased during the same period. Daily intensities increased in the summer season during this period as well, which suggests more intenseprecipitation events (*HungaroMet*, 2024c).

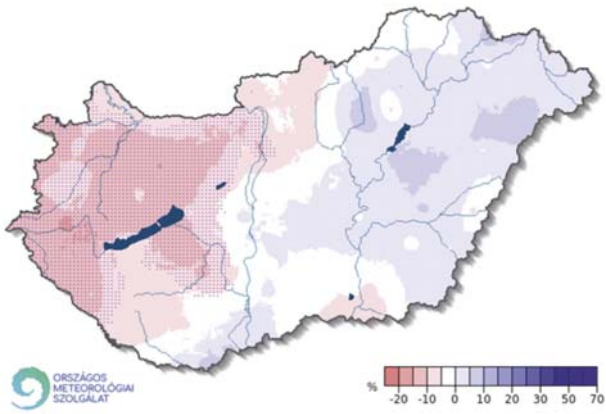

Fig. 6. Changes in the annual amount of precipitation (%) during the period between 1901 and 2020 (*HungaroMet*, 2024b).

Nevertheless, there was an increase in the annual amount of precipitation during the 1881–2020 period over most of the country (*Fig. 7*). The increase is the most remarkable over the central and northern parts of the country, where it can reach an 50% excess (*HungaroMet,* 2024b). The intensity and frequency of extremities has already been increased during the second half of the 20th century (*Barhtoly* and *Pongrácz,* 2007). The year 2010 was the wettest and 2011 the driest since 1901 with annual amount of precipitation of 959 mm and 407 mm, respectively (*Pongrácz et al.,* 2014).

According to climate change scenarios, an increasing tendency of the precipitation is projected for the autumn-winter months and a significant decrease is expected for the summer, while the annual sum is not expected to change considerably along with an increasing frequency of extreme precipitation events

concentrated in the winter half year (*Gaál* and *Becsákné Tornay,* 2023, *Kocsis* and *Anda,* 2017, *Csáki et al.,* 2018, *Kocsis et al*., 2023).

Precipitation extremities are expected to result in increasing frequency of floods and droughts (*Birinyi et al.,*2023, *Gerhátné Kerényi,* 2018).

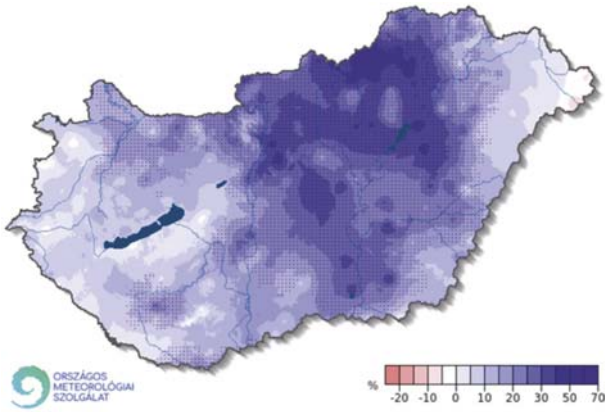

Fig. 7. Changes in the annual amount of precipitation (%) during the period between 1981 and 2020 (*HungaroMet,* 2024).

2. Material and methods

An exact statistical description of present and future climate requires a database representative in space and time. However, observation records – that is raw climatological time series – are loaded with inhomogeneities due to changes in the location of the weather stations and usage of different instruments and observation protocols. Datasets must be homogenized first, which means that previous measurement data must be adjusted to the present observation protocols, while missing data must be supplemented. Homogenization of Hungarian climatological datasets and supplementation of missing data have been carried out using the MASH (Multiple Analysis of Series for Homogenization) and MISH (Meteorological Interpolation based on Surface Homogenized Data Basis) methods (*Szentimrey*, 1999; *Szentimrey* and *Bihari*, 2007) developed at the Climatological department of the HungaroMet what providing homogenized, supplemented, and verified diurnal datasets. Gridded data sets have been produced by the MISH method. The papers of *Izsák et al.* (2021) and *Szentes* (2023) provide a good review on the different phases of the production of the climatological database. Both papers contain numerous references for other studies what deal with theoretical and practical problems of the different phases

of the process. Authors would like to draw attention to the papers of *Izsák et al*. (2022), *Szentes et al*. (2023), and *Izsák et al*. (2024) from the newest literature on homogenization of precipitation time series. Besides a detailed description of the homogenization process of precipitation time series, the articles deal with the application of the method on different data sources.

The database of the present examination is the homogenized precipitation time series of Hungary, that is diurnal amounts of precipitation for the 1,233 grid cells which cover the area of the country over the period of 1971-2022 in the state of the database in 2023 (*HungaroMet*, 2023). According to the method of the homogenization there are 1,233 grid cells defined for the area of Hungary between the coordinates (45,7° N,16,1° E) and (48,6° N, 22,9° E).

Therefore, the data matrix contains 18,628*1,233 pieces of precipitation data. Firstly, the diurnal amount of precipitation over the area of the country, that is the sum of precipitation that falls in each cell of the grid over the area of the country has been chosen as a variable to be analyzed. Its annual and monthly characteristics have been analyzed for different independent variables. Secondly, spatial characteristics of the diurnal amount of precipitation, that is its distribution among the grid cells have been examined as well.

Hereinafter, precipitation over a point of the country or what falls in the point of the country corresponds to these data.

3. Statistical characteristics of the diurnal amount of precipitation over the country

The 51 years long period involved in our study contains 18,628 days, that is *the diurnal amounts of precipitation* for the total 1,233 grid cells *for all days of the period*. These sums determine the diurnal amount of precipitation that falls over the country.

The total amount of precipitation during the study period (the sum of the precipitation of the 18,628 days) equals 37,580,312 mm that is this amount of water in liters/m^2 fell over the area of the country, more exactly over the area covered by the 1,233 grid cells. It is 736,869 mm on annual average on total, and it means 597.6 mm on spatial average (per one grid cell). Therefore, 597.6 mm is the amount of annual mean precipitation of Hungary for the study period.

The sum of rainfall in a day in the 1,233 grid cells is *the daily national precipitation total*. The most important statistical features of this time series (average, standard deviation, coefficient of variation, maximum, mode) are shown in *Table 1*.

Table 1. The most important statistical characteristics of daily national precipitation totals

average* mm	stand. dev. mm	coeff. of var.	median mm	maximum** mm	mode*** mm
2,017.4	3,714.8	*1.84*	354.4	38,666	0.0

* average rainfall in a day in the covered area, ** May 15, 2010, ***see below

26.8% of the elements of the time series is over the average only. The maximum, occurred on May 15, 2010, is 0.1% of the sum of the elements.

98% of the daily national precipitation totals falls into the interval between 0 and 14,000 mm. Most of them (73.2%) is between 0 and 2,000 mm. 52.5% of the values within the interval between 0–2,000 mm is between 0 and 100 mm and 57% of these values is between 0 and 10 mm. *40% of the* latest category *is 0, which are the national dry days* of the time series when the daily national precipitation totals are under 0.1 mm. Therefore, 0 mm is the *mode* of the distribution that is the most probable daily amount of precipitation.

Monthly distribution of the national daily precipitation amount of the studied period is presented in *Fig. 8*. 44% of the total annual precipitation falls during May and the summer months. Average monthly national precipitation amounts are presented in *Fig. 8* as well. Annual courses are similar naturally: there is a maximum in June (12.2%, 72.3 mm) and a minimum in March (5.6%, 33.6 mm). There is an increasing trend between January and June and a decreasing one from June to December. Average monthly precipitation amounts are in accordance with the values derived from observation data of the period of 1991–2020 (see *Fig. 3*).

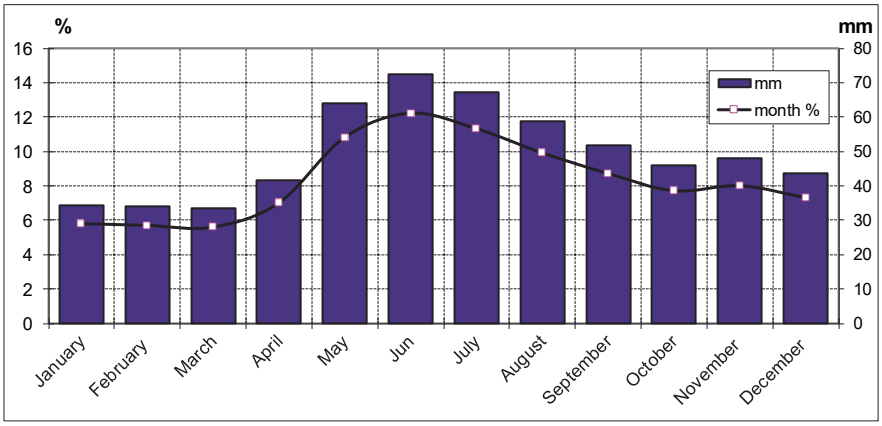

Fig. 8. Monthly distribution of the national daily precipitation amount (%) and the average monthly national precipitation amounts (mm), 1971–2021.

The figure on the temporal characteristics of the annual precipitation amount will be presented in part 2 of this article. According to *Fig. 9a,* the annual precipitation amount (APA) falls into the 740,000–820,000 mm interval in 15 years of the studied period, it is the mode of the distribution this way. The average and the median falls into this class as well, therefore a normal distribution can be assumed.

The values of the annual relative precipitation amount (ARA=annual precipitation / precipitation in the 51 years long period) are between 1.38% (2011) and 3.22% (2010). The secondary maximum was in 1999 with 2.63%, while the secondary minimum was in the following year again with 1.39%! Their average is 1.96%, standard deviation is 0.34%, so the variation coefficient is 0.17, while their median is 1.98%. The mode can be determined from the frequency distribution shown in *Fig. 9b*.

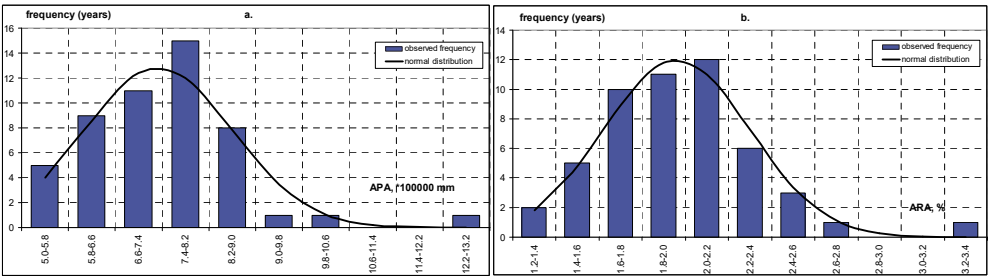

Fig. 9. Frequency distribution of the annual precipitation amount (a) and relative precipitation amount (b) and their approximation to the normal distribution.

On the base of *Fig. 9b,* the mode is about 2%, so we tried to approximate the empirical frequencies with the normal distribution. According to the χ^2 probe, the annual precipitation amount and relative precipitation amount can be approximated by the normal distribution at a high level of probability.

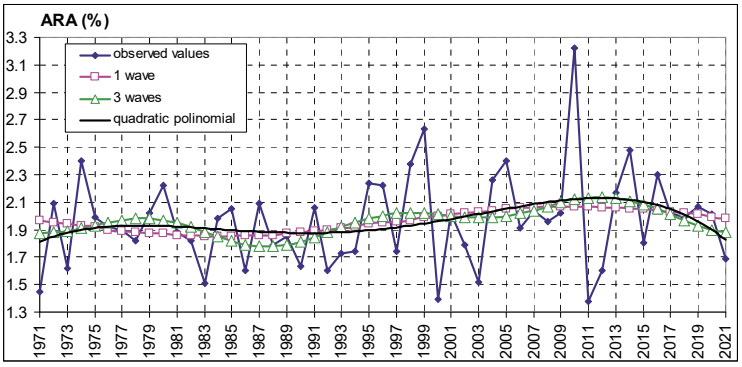

Fig. 10. Observed values of annual relative precipitation sums (ARA, %) and their approximation with quadratic and trigonometric polynomials.

Annual relative precipitation sums of the individual years (*observed data*) of the studied period are presented in *Fig. 10*. Analyzing the tendencies in annual relative precipitation sums during the studied period applying one direction analytic trends (linear, logarithmic, exponential etc.) would be counterproductive naturally, due to the relatively large difference between the extreme values (1.84%). Applying a fourth-degree polynomial results in a two-maximum curve, that is a double wave one can be presumed. Therefore, it is reasonable to carry out a period analysis on the time series.

The presumed periodicity has been examined approximating the observed annual values with trigonometric polynomials. The method is called harmonic analyses as well (see e.g., *Dobosi* and *Felméry*, 1971, *Huzsvai* and *Vincze*, 2012). An improved version of the method has been used in the present study. For detailed description of the method see: *Tar et al.* (2001, 2002), *Tar* and *Kircsi,* (2001), *Tar* (2004*,* 2007, 2014).

If we apply a four-element polynomial (a wave) to the observed values of the annual relative precipitation sums (ARA, %), then the expected value, E, of the amplitudes of the waves is 0.08. Using this method, the amplitudes for each wave, A_m, the A_m/E ratio refering to the suddenness of wave m, the goodness of the approximation, s_{0m}, and the root mean square error parameter, RMSE, have been determined.

The s_{0m} values show that all the four waves provide a rather weak approximation. Based on the amplitudes, the first wave with an amplitude of 51 years is real, what can be considered as obvious. The next is the third wave with a random period of 17 years. However, the periodicity has not been justified according to the nearly equal RMSE values.

The annual sign change (ΔARA) of relative precipitation amounts have been examined also. It is negative in 52% of the years that is the year-by-year decrease is larger by 4% than the increase. The so-called transition/conditional probabilities/relative frequencies have been calculated as well. Results are presented in *Table 2*.

Table 2. Conditional probabilities of the annual sign change (ΔARA) of relative precipitation amounts

		condition	
		ΔARA ≤0	**ΔARA >0**
conditional event	**ΔARA ≤0**	0.3462	*0.7083*
	ΔARA >0	*0.6154*	0.2917

According to the table, the probability of a sign change of the ΔARA difference is about twice as high as the perseverance of the sign.

The above results have been obtained using data for all the days and grid cells' precipitation data involved. In the following examinations, *dry* (no precipitation) and *rainy days and grids* have been distinguished. Dry and rainy days have been divided into two further subsets: *nationally and locally dry* and *nationally and locally rainy days,* respectively.

4. Temporal and spatial characteristics of dry days

Dry days and grid cells are those when and where the daily precipitation amount is under 0.1 mm. Statistical characteristics of daily dry grid cells and dry days by grid cells are dealt with in the following chapter.

4.1. Temporal statistics of nationally dry days

The beforementioned 40% is the ratio of the *nationally dry days,* when there was no more precipitation than 0.1 mm in any grid cells. It is 1645 days in total during the 51 years, that is 8.8% of the studied period. It means that every eleventh day is nationally dry on average. On the base of the abundant database of the study, it can be stated that it is the probability of a nationally dry day in Hungary. Therefore, there are dry and rainy grid cells (areas) within a day in most cases.

There are *locally* or *nationally rainy days* between the nationally dry days. These are the precipitation intervals with time spans from 0 to 199 days. Their length is 10.3 days on the average during the studied period in harmony with the previous estimation. It is 0 in the case, when a nationally dry day is followed by a similar day. The length of the precipitation periods is between 0 and 10 days in 74% of the cases. Most of them have a length of 0 days which is 45% of the nationally dry days. Thus, a nationally dry day is followed by a locally or nationally rainy day with a higher probability (55%) than by a nationally dry day.

The average of the annual number of nationally dry days (DDC) is 32.3, its standard deviation is 10.9, therefore, the variation coefficient is 0.34. The maximum is 61 days in 1992, while the minimum is 10 days in 1999 and 2014, the is median 33 days.

The "observed" values curve shows the annual number of nationally dry days in *Fig. 11*. The maximum is 61 days in 1992 which is 17% of the total length of the year. According to the criteria defined by *Szentes* (2023) for the dry and rainy years, there was a durative dry period in the first half of the 1990s, peaking in 1992. Therefore, in the definition of dry years or the driest year, the annual number of nationally dry days can be a parameter. In our case (1971–2021), during the 1990s, the lowest annual precipitation was not in 1992 but in 2000 at the end of the decade.

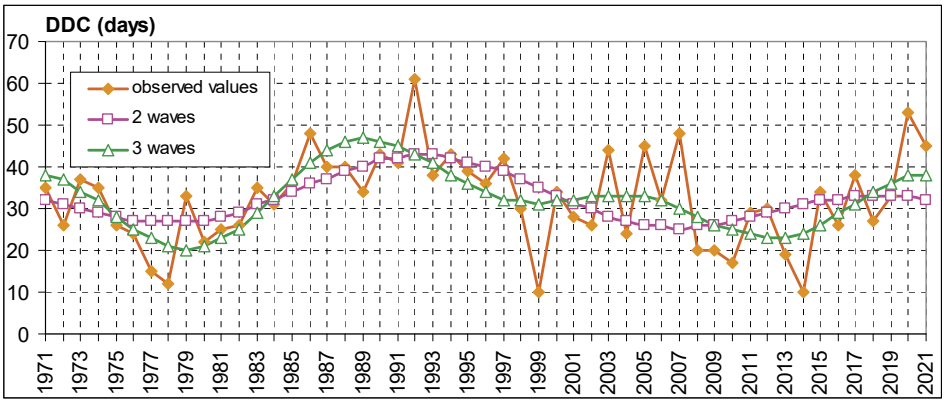

Fig. 11. Annual number of nationally dry days (DDC) and their approximation with trigonometric polynomials.

The 10 least nationally dry days occurred in 1999 and 2014. When examining the tendencies of nationally dry days, the application of one direction analytic trends (linear, logarithmic, exponential, etc.) would be counterproductive obviously, due to the relatively large difference between the extreme values (51 days). Therefore, it is reasonable to carry out a period analysis on the time series.

Carrying out the examinations detailed in the previous chapter, the following results have been achieved. In the case of the approximation with two waves, the 51/2=25.5 years period of the second wave; and in the case of the approximation with three waves, the 51/3=17 years period of the third wave can be considered as realistic. It can be seen in the corresponding curves of *Fig. 11*. In the case of the two waves approximation, the minima occur in the late 1970's and the mid 2000's with a periodicity of 25–28 years. The three waves curve has three local minima with a periodicity of about 18–16 years. Based on the highest A_3/E ratio, the *17 years period has been accepted*.

The *distribution of the number of nationally dry days per year* has been examined as well by a classification into five days long intervals/classes.

As it is visible in *Fig. 12,* the number of nationally dry days per year falls into the 25–30 and 30–35 classes most frequently in 10-10 years. Therefore, in 20 years (about 40%) of the studied period, the annual number of nationally dry days is between 25 and 35 days. On this basis, it can be assumed that the mode of distribution is the middle of this interval, that is 30 days. This way, the mode, the average, and the median are close to each other enough to make the approximation of the empirical distribution with a normal distribution possible. This approximation has been proved to be successful at a significance level of 0.05 according to the χ^2-test.

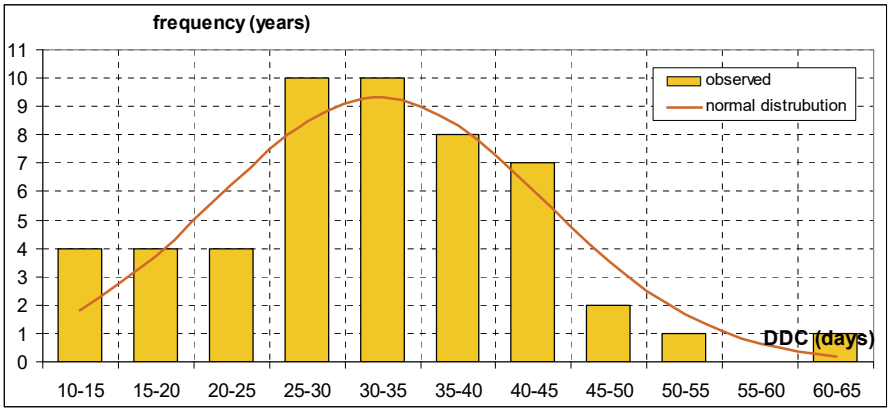

Fig. 12. Observed distribution of the number of nationally dry days (DDC) per year and its approximation to the normal distribution.

The increasing annual number of nationally dry days has a reducing effect on the annual amount of precipitation naturally. This stochastic relationship can be demonstrated most simply via a linear correlation presented in *Fig. 13*. The linear correlation coefficient is -0.4117.

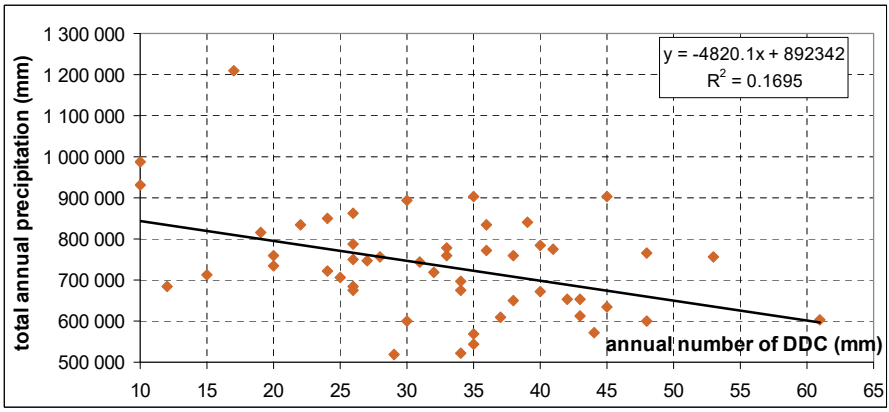

Fig. 13. Linear regression between the national annual precipitation and the number of nationally dry days per year.

To test the significance of the linear correlation coefficient, r, between the variables, the F-test used in variance analyses has been applied according to the interpretation of *Miller* (1997) and *Hadnagy* (2020, 2023).

The result of the test showed that the correlation coefficient r = -0.4117 differs from 0 at a significance level of 0.01. This way there is a weak correlation between the two variables (*Huzsvai* and *Vincze,* 2012). According to the interpretation of the determination coefficient (r^2), the number of nationally dry days per year explains the annual precipitation in about 17% during the studied period only. According to the regression coefficient, an increase of 1 day in the number of nationally dry days per year results in a decrease in the national annual precipitation of 4816 mm.

The monthly distribution of the 1645 nationally dry days per year is presented in the curve of "total DDC days" in *Fig. 14*. The other curve is a comparison between the monthly number of nationally dry days and the total number of days in a month (51*31 or 51*30, and 1441 in February). These ratios give the probability of a given day of a given month being nationally dry. Naturally, there is a strong linear correlation between the two quantities, since their calculation relies on a common mathematical base. It is visible that the *nationally driest month* is September, followed by March, August, and October, respectively. The number of nationally dry days is lower in all the three winter months than in all other months. Seasonally it is 30.9% in autumn, 29.2% in spring, 26.7% in summer and 13.2% in winter.

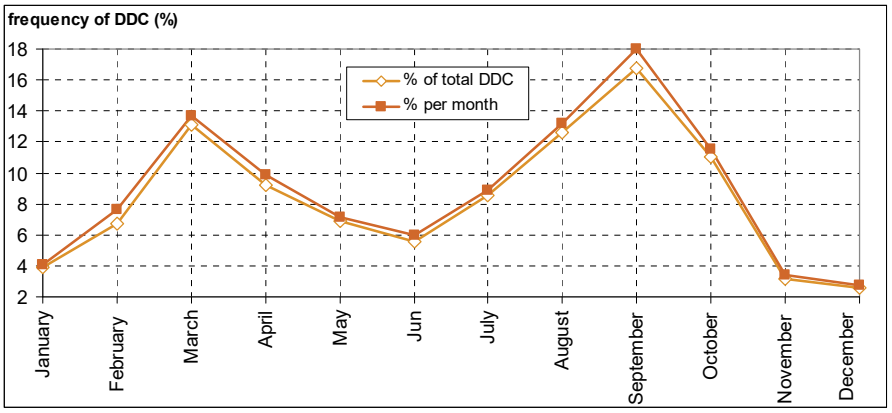

Fig. 14. Monthly distribution of nationally dry days.

4.2. Statistical characteristics of daily dry grids

Statistical characteristics of *daily dry grids* (0 to 1,233) have been studied also. There are 22,968,324 grid data from the 18,628 days of the 51 years of the studied

period. The total number of *dry grids* is 12,051,721, that is more than half (52.5%) of the total number of cases. 16.8% of dry grids are the nationally dry grids (1,645*1,233=2,028,285).

The most important statistical characteristics of daily dry grids are shown in *Table 3*. According to the table, there has been no precipitation in more than half (52.5%) of the grids during the studied period. The value of the median is close to the average. Mode can be determined via examination of the distribution.

Table 3. Statistical characteristics of daily dry grids (pieces, *calculated*).

total	average	stand. dev.	coeff. of var.	median
12,051,721	647	448.3	*0.69*	667

Examining the distribution of the number of daily dry grids the following can be stated. The number of daily dry grids is under 100 in 18.3% of the cases (3,414 days), which is the highest frequency. However, almost as frequent (14.8%) is the case when almost all grids (1,200–1,233) are dry. The lowest frequency case is when the number of daily dry grids falls into the interval which involves the average (600–700).

It is probably a bimodal distribution. To judge this issue, a higher resolution classification of the 0–100 and 1,200–1,300 intervals has been established, shown in *Fig. 15*.

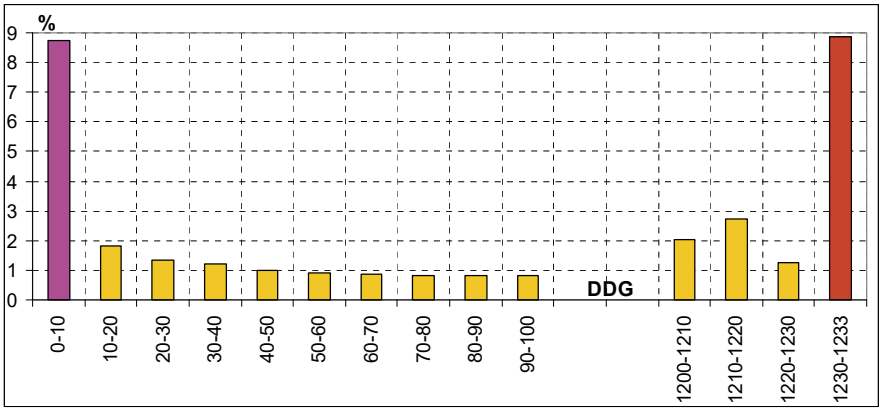

Fig. 15. Distribution of the number of daily dry grids (DDG, %) in the intervals 0–100 and 1200–1233.

The figure shows that the probability of the occurrence of less than 10 daily dry grid cells in a day (a rainy day with a high probability) is lower by 0.2% than the probability of the occurrence of a nearly nationally dry day only.

For the 1,233 grid cells that cover the area of the country, it has nearly equally maximal probability to have precipitation over less than 0.8% of the area of the country and to have no precipitation at all over 99.8% percent of the area of the country in a day according to *Fig. 15.*

The number of the *daily dry grids* (DDG, %) indicates the percentage of the area of the country, where there was no precipitation in a day. This ratio is between 0 % (*nationally rainy days*) and 100% (*nationally dry days*), obviously. There has been no precipitation over more than half of the studied period (52.5%), that is 5% higher than the ratio of the area, where there has been precipitation (47.5%) during the studied period. Further features of DDG_r are its standard deviation is 36.4%, its variation coefficient is 0.69, and the median is 54.1%, respectively.

The distribution of DDG_r is shown in *Fig. 16*. It is a bimodal distribution according to the figure. Having no precipitation over 90–100% of the area of the country in a day has the highest probability (24.8%). The case when this ratio is between 0 and 10% has the second highest probability (20%). The lowest probability case (6.3%) is when 40–50% of the country is dry (about half dry-half rainy).

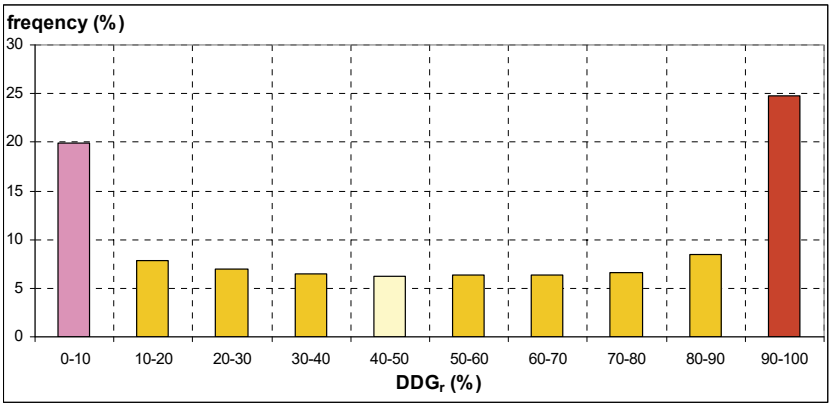

Fig. 16. Distribution of the relative number of dry grids per day (DDG_r, %).

The monthly distribution of dry grids as a percentage of the total number cases *(% of total*) is presented in *Fig. 17*. The driest month is October, followed by August, September, and March, respectively. The percentage is 26.8% in autumn, 25.2% in summer, 24.8% in spring, and 23.2% in winter. The second

curve in the figure shows the total number of dry grids per a day of a month (*1 day per month*). Due to the common base, its annual course is in harmony with the previous one. However, the order is a bit different: October, September, August, and March. The values are higher than the average (647) in those months only. The standard deviation of the monthly data set is 67.2, that is the variation coefficient is 0.10. The spread (October-May), that is a measure of the annual fluctuation is 183, which is about 15% of the total number of grids. The average numbers of dry grids per a day are 607 in winter, 636 in spring, 647 in summer and 697 in autumn.

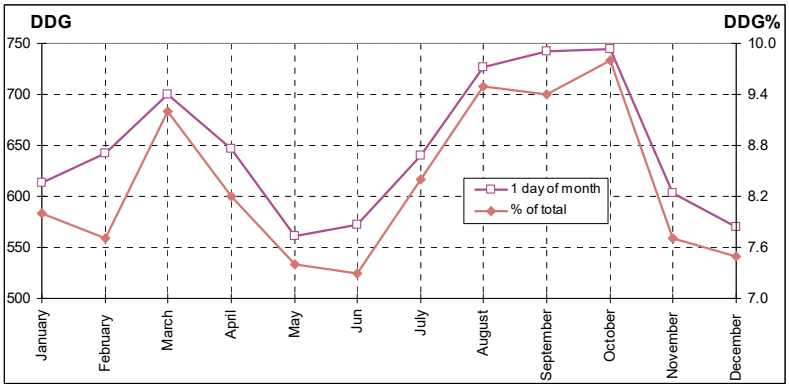

Fig. 17. The number of dry grids per day of the month (DDG, *1 day of month*) and the total number of dry grids per month as a % of their total number (DDG$_{\%}$, *% of total)*.

4.3. Statistics of the dry days per grids

The most important statistical characteristics of the sum of dry days per grid (DNP_g) and their average number per year (DNP_g/year) are summarized in *Table 4*.

Table 4. The most important statistical characteristics of the sum of dry days per grid (DNPg) and their average number per year (DNPg/year).

	DNP_g	**DNP_g/year**
average, days	9,774	195
stand. dev., days	531	11
coeff. of var.	0.05	0.05
minimum, days	8,486	170
maximum, days	13,155	263
median, days	9,750	195
mode, days	9,737	195

There have been 9,774 dry days per grid on average, which is 0.08% of all dry grids (the number of dry days in all grids is 12,051,721). The variation coefficient indicates a relative stability of this variable around the average. The number of values over and under the average are 594 (48%), and 639 (52%), respectively.

(Spatial) distribution of *dry days* per grids have been fluctuating between 13,155 days and 8,486 days during the studied period. Our data show the strongest similarity to the map showing the annual average number of consecutive dry days during the 1991–2000 climatological normal period (*Szentes,* 2023).

The average, median, and mode of average number per year of dry days per grid are practically equal according to *Table 4.* Despite this, the approximation with normal distribution was not successful. It can be explained by that in our case, 74.5% of all cases fall into the average+standard deviation interval instead of 68.2% which is the requirement for the normal distribution (*Dobosi* and *Felméry*, 1971). Otherwise, this 74.5% can explain the value of the variation coefficient, i. e., the relative stability around the average. Attempts for the approximation with the lognormal and square lognormal distribution have not been successful also. According to the χ^2 test, the lognormal distribution provides the best approximation. However, there is a significant difference between the observed and the approximating values, which are higher than the level of acceptance. The opportunity of the approximation with the gamma distribution has been examined as well. The $\Gamma(p)$ function in the density function has shown an overflow due to the high value of the p parameter what made the gamma distribution inapplicable in our case.

As it has been discussed in the beginning of this chapter, it is expedient to examine the relationship between the annual average of dry days per grid (DNP_g/year) and the geographical coordinates (φ latitude and λ longitude) of the grids, that can be carried out most simply via a linear regression.

On the basis of analyses referred in Section 4.1, the relationship between the annual average of dry days per grid and the longitude and latitude of the grids is statistically real. The correlation coefficients are $r_\lambda = -0.4308$ (for longitude), $r_\varphi = -0.3357$ (for latitude), that is the annual average of dry days per grid (its spatial distribution) is in a stronger stochastic relationship with the longitude (within a climate zone). There is a decreasing tendency in the values of DNP_g/year with the increase of both geographical coordinates. It is 2.8 days per 1 degree of longitude and almost twice as much, 5.2 days per 1 degree of latitude (meridionally), according to the steepness of the regression lines.

The realistic stochastic relationship discussed above makes it possible to present the results in a form of a map. Spatial distribution of dry days during the studied period is presented in *Fig. 18.* From the relative homogeneity of the map, the spots over the northeastern part of the Great Hungarian Plain, the Nyírség and Hajdúság emerge, where the annual number of dry days is minimal (160–175). Highest values appear sporadically within the Small Hungarian Plain over the Hanság and Rábaköz.

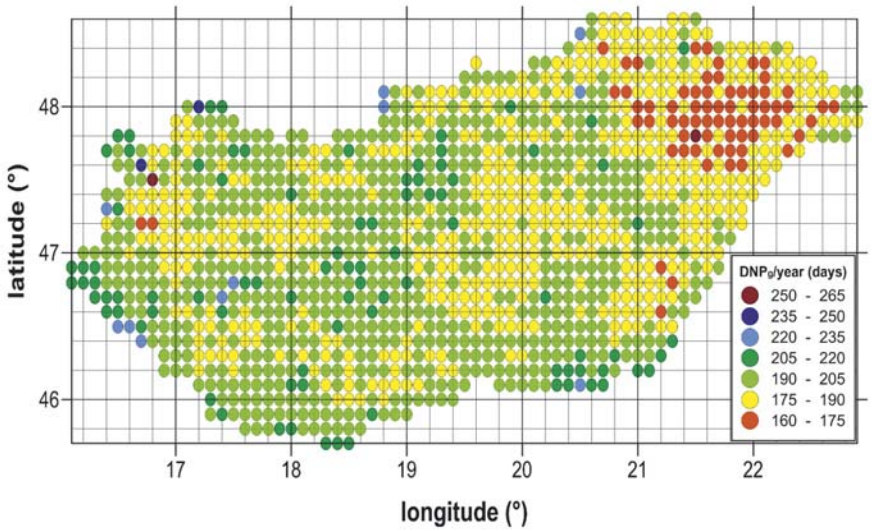

Fig. 18. Distribution of the annual average of dry days per grid (DNP_g/year) in the examined period.

5. Discussion and conclusions

The database of the present study is the homogenized diurnal precipitation time series of Hungary on 1,233 grid cells covering the area of the country for the 1971–2022 period. Diurnal amount of national precipitation that is the sum of diurnal precipitation in all grid cells has been chosen as the studied variable. Firstly, the annual and monthly characteristics of this variable have been analyzed in the case of different independent variables. Secondly, spatial patterns of precipitation, that is its distribution per grid cells has been analyzed as well.

Based on the analyses of the total dataset (1,233 grid cells*18,626 days), the following conclusions have been drawn.

The amount of annual mean precipitation over Hungary is 597.6 mm during the studied period. The average and maximal diurnal amounts of precipitation are 2,017.4 mm and 38,666 mm (May 15, 2010), respectively.

98 % of diurnal precipitation amounts fall into the 0–14,000 mm interval, most of them (73.2%) is in the 0–2,000 mm category. 52.5% of the values is between 0 and 100 mm, and 57% of these values is between 0 and 10 mm. 40% of the latest category *is 0,* which are the national dry days of the time series when the daily national precipitation totals are under 0.1 mm. Therefore, 0 mm is the *mode* of the distribution that is the most probable daily amount of precipitation.

44% of annual precipitation falls in May and in the summer months. The maximum and minimum of the monthly mean national precipitation are in June with 72.3 mm and March with 33.6 mm.

The distribution of the annual amount of precipitation and annual relative amount of precipitation have been examined also. According to the χ^2 test, both parameters have a normal distribution with a high probability.

Trends of the relative amounts of precipitation in the different years has been examined as well. As the application of one direction analytic trends would be counterproductive, supposedly period testing has been carried out on the data. A weak wave has been found with a 17-year accidental periodicity, which means periodicity practically has not been proved the findings supported by other parameters too.

The annual changes in the sign of the distribution of the relative amounts of precipitation have been examined as well. It is negative in 52% of the years that is the year-by-year decrease is larger by 4% than the increase. Conditional probabilities show that the change of the sign year-by-year has about twice as high probability than the perseverance of the sign.

The number of *nationally dry days* is 1,645 days, therefore, every 11th day is nationally dry during the 51 years of the studied period. It is 8.8% of the total length of the period. It is the probability of a nationally dry day in Hungary with a good approximation.

There are *locally* or *nationally rainy days* between the nationally dry days. These are the precipitation intervals with time spans from 0 to 199 days. Their length is 10.3 days on the average during the studied period in harmony with the previous estimation. It is 0 in the case, when a nationally dry day is followed by a similar day. The length of the precipitation periods is between 0 and 10 days in 74% of the cases. Most of them have a length of 0 days which is 45% of the nationally dry days. Thus, a nationally dry day is followed by a locally or nationally rainy day with a higher probability (55%) than a nationally dry day.

The average of the annual number of nationally dry days is 32.3, its standard deviation is 10.9, therefore, the variation coefficient is 0.34. The maximum is 61 days in 1992, while the minimum is 10 days in 1999 and 2014, the median is 33 days.

Annual tendencies of nationally dry days have been examined by period testing again. The 17 years long wave has been accepted as real, since it has 3–3 local minima and maxima like the observed time series, and it is in the best agreement with the statistical requirements.

The distribution of the number of nationally dry days per year has been examined as well. The number of nationally dry days per year falls into the 25–30 and 30–35 classes most frequently in 10–10 years. Therefore, in 20 years (about 40%) of the studied period, the annual number of nationally dry days is between 25 and 35 days. On this basis, it can be assumed that the mode of distribution is the middle of this interval, that is 30 days. This way, the mode, the average, and the median are close to each other enough to make the approximation of the empirical distribution with a normal distribution possible. This

approximation has been proved to be successful at a significance level of 0.05 according to the χ^2-test.

The reducing effect of increasing annual number of nationally dry days on the annual amount of precipitation can be demonstrated most simply via a linear regression. The linear correlation coefficient is r = -0.4117. The result of the F-test showed that the correlation coefficient r = -0.4117 at a significance level of 0.01 differs from 0. This way, there is a weak correlation between the two variables. According to the interpretation of the determination coefficient, the number of nationally dry days per year explains the annual precipitation in about 17% during the studied period only. According to the regression coefficient, an increase of 1 day in the number of nationally dry days per year results in a decrease in the national annual precipitation of 4,816 mm.

The monthly distribution of the 1,645 nationally dry days per year has been studied in two approximations. The monthly ratios give the probability of a given day of a given month being nationally dry. The *nationally driest month* is September, followed by March, August, and October, respectively. According to this the driest season is the autumn, followed by the spring, the summer, and the winter.

Statistical characteristics of *daily dry grids* have been studied also. The total number of *dry grids* is more than half (52.5%) of the total number of cases. 16.8% of dry grids are the nationally dry grids.

The average number of daily dry grid cells is 667, their standard deviation is 448.3, therefore, the variation coefficient is 0.69, and the median is 667 grid cells, respectively. Thus, there has been no precipitation in more than half (52.5%) of the grids during the studied period.

The number of daily dry grids is under 100 in 18.3% of the cases (3,414 days), which is the highest frequency. However, almost as frequent (14.8%) is the case when almost all grids are dry. The lowest frequency case is when the number of daily dry grids falls into the interval which involves the average (600–700). It is probably a bimodal distribution.

To judge this issue, a higher resolution (10 grid cells per class) classification of the 0–100 and 1,200–1,300 intervals has been established. Based on this, for the area of the country measured in grid cells, it has nearly equally maximal probability to have precipitation over less than 0.8% of the area of the country and to have no precipitation at all over 99.8% percent of the area of the country in a day.

Based on the comparison between the monthly numbers of dry grids to the total number cases the driest month is October, followed by August, September, and March, respectively. There are the same four months like in the case of nationally dry days but in a different order. The seasonal order is autumn, summer, spring and winter.

The number of dry grids per a day of a month has been determined also. The order is a bit different: October, September, August, and March. The values are

higher than the annual average in those months only. The annual fluctuation (October-May) is 183, which is about 15% of the total number of grids. The average numbers of dry grids per a day are 697 in autumn, 647 in summer 636 in spring and 607 in winter.

Characteristics of dry days per grid cells (their spatial pattern) have been examined for the total studied period and its years. The average, the minimum and the maximum for the total period are 9,774, 8,486, and 13,155 days, while annually they are 195, 170, and 363 days. To map the spatial distribution, the stochastic relationships between the annual averages of dry days per grid geographical coordinates of the grids have been examined first.

The examination can be carried out most simply via a linear regression. Using the appropriate test it has been proved, that the relationship between the annual average of dry days per grid and the longitude and latitude of the grids is statistically real. The correlation coefficients are $r_\lambda = -0.4308$ (for longitude), $r_\varphi = -0.3357$ (for latitude), that is the annual average of dry days per grid (its spatial distribution) is in a stronger stochastic relationship with the longitude. There is a decreasing tendency in the values with the increase of both geographical coordinates. It is 2.8 days per 1 degree of longitude and almost twice as much, 5.2 days per 1 degree of latitude (meridionally), according to the steepness of the regression lines.

The realistic stochastic relationship discussed above makes it possible to present the results in a form of a map. The most important information from the map are the following: the annual number of dry days is minimal (160–175) over the northeastern part of the Great Hungarian Pain, the Nyírség and Hajdúság. Highest values appear sporadically within the Small Hungarian Plain over the Hanság and Rábaköz.

References

Bacsó N., 1953: Magyarország éghajlata. *OMI, Budapest*. (in Hungarian)

Barhtoly, J. and *Pongrácz, R.,* 2007: Regional analysis of extreme temperature and precipitation indices for the Carpathian Basin from 1946 to 2001. *Glob. Planet. Change 57*, 83–95. https://doi.org/10.1016/j.gloplacha.2006.11.00

Birinyi, E., Lakatos, B. O., Belényesi, M., Krisóf, D., Hetesi, Zs., Mrekva, L. and *Mikus, G.,* 2023: Contribution of data-driven methods to risk reduction and climate change adaptation in Hungary and beyond. *Időjárás 127*, 421–446. https://doi.org/10.28974/idojaras.2023.4.1

Csáki, P., Szinetár, M. M., Herceg, A., Kalicz, P. and *Gribovszki, Z.,* 2018: Climate change impacts onthe water balance - case studies in Hungarian watersheds. *Időjárás 122*, 81–99.

Dobosi Z. and *Felméry L.,* 1971: Klimatológia. *Egyetemi jegyzet,* Tankönyvkiadó, Budapest. (in Hungarian).

Gaál, M. and *Becsákné Tornay, E.,* 2023: Drought events in Hungary and farmers' attitudes towards sustainable irrigation. *Időjárás 127*, 143–165. https://doi.org/10.28974/idojaras.2023.2.1

Gerhátné Kerényi, J., 2018: Application of remote sensing for the determination of water management parameters, Hydrology SAF. *Időjárás 122*, 1–13. https://doi.org/10.28974/idojaras.2018.1.1

Hadnagy I., 2020: A felszín közeli szélmező energetikai jellemzése Kárpátalján. Egyetemi doktori (PhD) értekezés. Debreceni Egyetem, Természettudományi és Informatikai Doktori Tanács, Földtudományok Doktori Iskola. (in Hungarian)

Hadnagy I., 2023: A felszín közeli szélmező energetikai jellemzése Kárpátalján. Monográfia. II. RF KMF-„RIK-U" Kft, Bergszász-Ungvár. (in Hungarian)

HungaroMet, 2023: Meteorológiai Adattár. (in Hungarian) https://odp.met.hu/climate/homogenized_data/gridded_data_series/daily_data_series/from_1971/precipitation_sum/

HungaroMet, 2024a: Elmúlt évszázad éghajlata. (in Hungarian) https://www.met.hu/eghajlat/magyarorszag_eghajlata/eghajlati_visszatekinto/elmult_evszazad_idojarasa/

HungaroMet, 2024b: Éves és évszakos csapadékösszegek változása. (in Hungarian) https://www.met.hu/eghajlat/eghajlatvaltozas/megfigyelt_hazai_valtozasok/homerseklet_es_csapadektrendek/csapadekosszegek/

HungaroMet, 2024c: Csapadék szélsőségek változása. (In Hungarian) https://www.met.hu/eghajlat/eghajlatvaltozas/megfigyelt_hazai_valtozasok/homerseklet_es_csapadektrendek/csapadek_szelsosegek/

HungaroMet, 2024d: Magyarország csapadékviszonyai. (in Hungarian) https://www.met.hu/eghajlat/magyarorszag_eghajlata/altalanos_eghajlati_jellemzes/csapadek/

Huzsvai L. and *Vincze Sz.* (2012): SPSS könyv. Seneca Books, Debrecen. (in Hungarian)

Izsák B., Szentes O., Bihari Z., Bokros K. and *Lakatos M.,* 2024: Reprezentatív meteorológiai adatok biztosítása a múlt és a jelen éghajlatának megismerésére. *Légkör*, 69, különszám. 4–11. (In Hungarian) https://doi.org/10.56474/legkor.2024.K.1

Izsák, B., Szentimrey, T., Lakatos, M., Pongrácz, R. and *Szentes, O.*, 2022: Creation of a representative climatological database for Hungary from 1870 to 2020. *Időjárás 126*, 1–26. https://doi.org/10.28974/idojaras.2022.1.1

Izsáki B., Bihari Z. and *Szentes O.*, 2021: Éghajlatváltozás: Homogenizált vagy nyers adatsorokat vizsgáljak? *Légkör 66*, 12–15. (in Hungarian)

Kocsis, K., Gercsák, G., Horváth, G., Keresztesi, Z. and *Nemerkényi, Zs (Eds.)* 2018: National atlas of Hungary, volume 2. *Geographical Institute, Research Centre for Astronomy and Earth Sciences.* Climate – Precipitation. 62–65.

Kocsis, T. and *Anda, A.*, 2017: Analysis of precipitation time series at Keszthely, Hungary (1871–2014), *Időjárás 121*, 63–78.

Kocsis, T. and *Anda, A.*, 2018: Parametric or non-parametric: analysis of rainfall time series at a Hungarian meteorological station. *Időjárás 122*, 203–216. https://doi.org/10.28974/idojaras.2018.2.6

Kocsis, T., Magyar-Horváth, K., Bihari, Z. and *Kovács-Székely, I.,* 2023: Analysis of the correlation between the incidence of food-borne diseases and climate change in Hungary. *Időjárás 127*, 217–231. https://doi.org/10.28974/idojaras.2023.2.4

Lakatos, M. and *Bihari, Z.,* 2011: Temperature- and precipitation tendencies observed in the recent past. In (Eds.: *Bartholy, J., Bozó, L., Haszpra, L.*): Klímaváltozás 2011. 159–169. (in Hungarian)

Mersich I., Práger T., Ambrózy P., Hunkár M. and *Dunkel Z.,* 2002: Magyarország éghajlati atlasza. OMSZ Budapest, 35–48. (in Hungarian)

Miller, R. G., 1997: Beyond ANOVA: Basics of Applied Statistics. Chapman & Hall/CRC, University of Stanford, California, USA. https://doi.org/10.1201/b15236

Pongrácz, R., Bartholy, J. and *Kis, A.*, 2014: Estimation of future precipitation conditions for Hungary with special focus on dry periods. *Időjárás 118*, 305–321

Szentes O., 2023: Szárazság Magyarországon 2022-ben és a múltban. *Légkör 68,* 9–19. (in Hungarian) https://doi.org/10.56474/legkor.2023.1.2

Szentes, O., Lakatos, M. and *Pongrácz, R.,* 2023: New homogenized precipitation database for Hungary from 1901. *Int. J. Climatol 43*, 4457–4471. https://doi.org/10.1002/joc.8097

Szentimrey, 1999: Multiple Analysis of Series for Homogenization (MASH). Paper presented at the Proceedings of the Second Seminar for Homogenization of Surface Climatological Data, Budapest, Hungary, WMO WCDMP-No. 41: 27–46. Retrieved from https://library.wmo.int/index.php?lvl=notice_display&id=11624#.X48Glu28qUk

Szentimrey and *Bihari,* 2007: Mathematical background of the spatial interpolation methods and the software MISH (Meteorological Interpolation based on Surface Homogeni-zed Data Basis). In: Proceedings from the Conference on Spatial Interpolation in Climatology and Meteorology, Budapest, Hungary, 2004, COST Action 719, COST Office, 17–27.

Tar K., 2004: Becslési módszerek a magyarországi szélenergia potenciál meghatározására. *Magyar Energetika,* XII. 4, 37-48. (in Hungarian)

Tar K. and *Kircsi A.,* 2001: Módszer a napi átlagos fajlagos szélteljesítmény meghatározására. A légköri erőforrások hasznosításának meteorológiai alapjai. Meteorológiai Tudományos Napok, 2001, 129–137. (in Hungarian)

Tar, K., 2007: Diurnal course of potential wind power with respect to the synoptic situation. *Időjárás 111*. 261–279.

Tar, K., 2014: Statistical structure of the surface layer wind field in Hungary. Direction, speed and energy of the wind. Lambert Academic Publishing, ISBN: 978-3-8484-0139-0.

Tar, K., Kircsi, A. and *Szegedi, S.,* 2001: A possible statistical estimation of wind energy. Proceedings of the European Wind Energy Conference, Copenhagen, Denmark, 2-6 July, 886–889.

Tar, K., Kircsi, A. and *Vágvölgyi, S.,* 2002: Temporal changes of wind energy in connection with the climatic change. Proceedings of the Global Windpower Conference and Exhibition, Paris, France, 2-5 April, CD-ROM.

DOI:10.28974/idojaras.2025.4.3

IDŐJÁRÁS

Quarterly Journal of the HungaroMet Hungarian Meteorological Service
Vol. 129, No. 4, October – December, 2025, pp. 419–442

Analysis of lower tropospheric temperature trends in the Northern Hemisphere (1940-2023)

Seyed Hossein Mirmousavi * and **Helaleh Fahimi**

Department of Climatology, Faculty of Human Sciences,
University of Zanjan, Zanjan, Iran

**Corresponding author E-mail: hossein.mirmousavi@znu.ac.ir*

(Manuscript received in final form January 12, 2025)

Abstact— This study analyzes long-term (1940–2023) monthly temperature trends across the Northern Hemisphere, focusing on tropical, temperate, and polar regions, as well as key mountainous areas such as the Rocky Mountains, the Tibetan Plateau, and the Alps. Results show that polar regions experienced the highest seasonal temperature increase, averaging 0.081°C per season during winter, while tropical regions exhibited the lowest increase, with 0.036°C during winter. In temperate regions, seasonal warming trends ranged from 0.05°C in winter to 0.039°C in summer. Monthly trends revealed that February and March exhibited the highest increases, with rates of 0.0195 °C and 0.0194 °C, respectively, while August showed the lowest increase at 0.0116 °C. Furthermore, trend maps indicate that over 92% of the Northern Hemisphere experienced warming across all months except June and January. These findings provide a comprehensive understanding of regional and seasonal temperature variations in the Northern Hemisphere, emphasizing the importance of localized and temporal analyses for a more nuanced perspective on climate change.

Key-words: Northern Hemisphere, temperature trend, lower troposphere, Intertropical Convergence Zone

1. Introduction

Air temperature is a fundamental driver of surface-atmospheric processes, influencing weather, climate, and ecological systems (*Vinniko et al*., 1990). Over recent decades, the rise in global temperatures has been well-documented across all latitudes and seasons (*Simmons et al*., 2017; *Hansen et al.*, 2010; *Al Mutairi et al*., 2023). However, these changes are neither uniform across time and space nor consistent in magnitude, with some regions experiencing accelerated warming

while others exhibit minimal change or even cooling trends (*Luterbacher et al*., 2005; *Siddik* and *Rahman*, 2014).

Since the late 19th century, significant warming has been observed, particularly during the periods of 1920–1944 and post-1975 (*Jones* and *Moberg*, 2003). Research suggests that warming in the Northern Hemisphere has been approximately double that of the Southern Hemisphere, with the most pronounced trends occurring in higher latitudes (*Croitoru et al*., 2012; *Steiner et al*., 2020). This hemispheric disparity can be attributed to factors such as reduced sea ice thickness in polar regions, which intensifies heat conduction to the surface, especially during colder months (*Manabe* and *Stouffer,* 1979, 1980). Conversely, summer warming in Arctic regions is moderated by seasonal sea ice loss (*Manabe* and *Stouffer,* 1979). Seasonal variations in warming trends are further corroborated by studies like *Chapman* and *Walsh* (1993), who identified distinct increases in winter and spring temperatures, while summer trends remained negligible. Although the magnitude of these increases varies across studies due to differences in datasets and methods, there is broad agreement on the accelerated warming since the mid-20th century (*Folland et al*., 2001; IPCC, 2013). Recent findings highlight an average warming of 0.06 °C per decade since 1850, with this rate tripling since 1982 (*Lindsay*, 2005). The primary driver of this warming is the increased concentration of greenhouse gases, predominantly from anthropogenic activities (*Choi et al*., 2009; *Trewin,* 2016). Beyond surface temperatures, tropospheric warming patterns provide additional insights, with observations indicating a warming rate of 0.14 °C per decade since 1958 (*Lindzen et al*., 2002). However, variations in warming rates between the surface and the troposphere, as well as across geographic regions, highlight the complexity of these processes (*Christy et al.*, 2007). The impacts of global warming are profound, including reduced snow and ice cover (*Rosenzweig et al.*, 2008), increased frequency of extreme weather events (*Reidmiller et al*., 2018), and shifts in precipitation patterns leading to more floods and droughts (*Salzmann*, 2016; *Tabari*, 2020). While these phenomena have been extensively studied at global scales, there are notable gaps in regional and long-term analyses. Research has disproportionately focused on short-term trends and neglected the detailed examination of specific geographic regions, such as mountainous areas or distinct latitudinal zones.

This study addresses these gaps by conducting a comprehensive monthly and long-term analysis (1940–2023) of temperature trends in the Northern Hemisphere. It focuses on key mountainous regions, including the Rockies, Appalachians, Himalayas, Alps, and the Tibetan Plateau, while also examining trends across tropical, temperate, and polar zones. By distinguishing trends by geographic region and season, this research aims to provide a detailed understanding of regional and temporal variations, contributing to the broader discourse on climate change and its localized impacts.

2. Data and methodology

Monthly temperature data were extracted from the ERA5 dataset provided by the ECMWF database for the statistical period of 1940–2023. ERA5 data have been available since 1940, which is why the start of the statistical period in this study is set from that year. The temperature trend analysis was conducted at the 850 hPa pressure level. The 850 hPa level is one of the most commonly used atmospheric levels. The 850, 925, and 1000 hPa pressure levels are nearly similar to sea-level pressure maps (Rahimi 2010). Thus, the selection of the 850 hPa level as a lower tropospheric layer can simultaneously provide valuable information regarding both the earth's surface and the 1000 hPa level. Since most of the regions examined in this study have elevations exceeding sea level, it is likely that the 1000 hPa level and sea level data may not be suitable for areas with elevations above 100 meters, and the results might not align with actual conditions. Moreover, at the 850 hPa level, the topography's influence on climatic parameters is better represented. For this reason, the 850 hPa level was deemed more appropriate for analyzing lower tropospheric temperature trends in this research. Given that the primary objective of this study is to examine temperature trends in the Northern Hemisphere, the study area encompasses latitudes from 0 to 90 degrees north and longitudes from 180 degrees west to 180 degrees east. For a more detailed analysis, the tropical region was defined as latitudes from 0 to 30 degrees north, the temperate zone as latitudes from 30 to 60 degrees north, and the polar region as latitudes from 60 to 90 degrees north (*Fig. 1*).

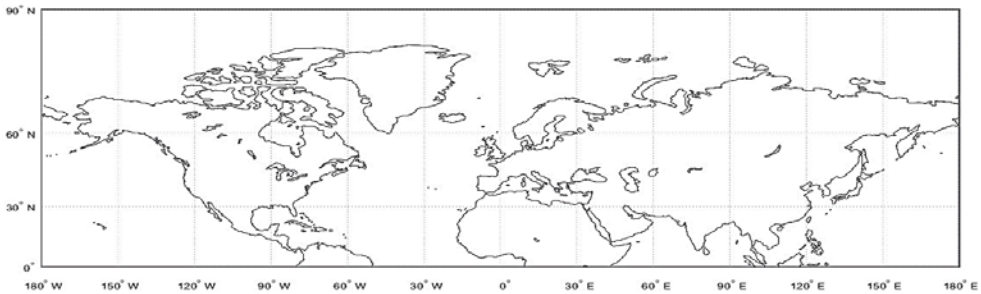

Fig. 1. The study area.

In order to check the normality of data distribution, the Q-Q and P-P graphicalmethods were used. Graphical methods can perform better than quantitative methods due to the fact that they are able to show the location and cause of the lack of goodness of fit in the total data (*Asakereh*, 2011).

2.1. Q-Q plot (quantile-quantile diagram)

The Q-Q plot (quantile-quantile plot) is a graphical tool used to compare the quantiles of observed data with those of a theoretical distribution, such as a normal distribution, to assess data normality. If the points form a straight line, it indicates that the data conforms to the theoretical distribution. The coordinates of the points of this diagram show the position of the points whose coordinates are obtained from real and theoretical estimations and measurements. To draw the Q-Q graph, first, the observations are arranged in ascending order from 1 to n (n is the number of observations) and drawn along the x-axis. On the y-axis, the expected quantile points, which are a function of the rank and length of the statistical period, are plotted. This axis has a cumulative distribution function equal to and less than observation (*Asakereh*, 2011).

2.2. P-P plot (probability-probability diagram)

The P-P plot (Probability-Probability plot) evaluates the cumulative probability of observed data against expected probabilities, providing another method to test normality. In a P-P plot, the cumulative probability of the observed data is plotted against the cumulative probability of the expected values from the assumed distribution. If the points fall on the 45-degree line (the bisector), it suggests that the observations fit the assumed distribution well. In the case of normality, the cumulative probability in a normal distribution is defined by the equation:

$$F_m = \left(Z \leq \frac{x_m - \bar{x}}{s_m}\right) \quad , \tag{1}$$

where F_m is the cumulative probability associated with the m-th ordered observation, x_m denotes the m-th order statistic (the m-th smallest value in the sample), $\bar{x}$ is the sample mean, s_m represents the estimated standard deviation corresponding to the m-th ordered value, Z is a standard normal random variable with distribution N(0,1), P ($Z \leq \cdot$) refers to the cumulative distribution function (CDF) of the standard normal distribution. Plotting the values of Fm against m/n produces the P–P plot. The deviation between Fm and m/n indicates the extent to which the empirical distribution departs from normality. In the P–P plot, the x-axis represents the empirical probability values (m/n), while the y-axis represents the expected probability values from the normal distribution (*Asakereh, 2011*). To further clarify the statistical methodologies employed, we emphasize that the P-P plot assesses the goodness-of-fit of observed data against a theoretical distribution by comparing cumulative probabilities. The Q-Q plot, in contrast, examines whether the distribution of data follows the theoretical quantiles. These graphical methods, combined with the Kolmogorov-Smirnov test, ensure the robustness of the assumption of normality (*Neter et al*., 1988). Additionally, the selection of the least squares regression method was based on its effectiveness in reducing errors

while analyzing long-term trends in climatic datasets *(Asakereh, 2011; Momeni, 2008)*. Further validation was achieved through reanalysis of key datasets such as ERA5 from previous studies (*Simmons et al., 2017*), ensuring consistency with established methodologies.

2.3. Least squares method

The least squares regression line is the one that minimizes the sum of the squared vertical distances between the observations *Y* and the line (*Neter et al*. 1988). In other words, it fits a line to the data in such a way that the sum of squared errors is minimized (*Asakereh*, 2011). The simple linear regression model was estimated using the least-squares method. In this approach, the intercept and slope of the fitted regression line are denoted by b_0 and b_1, respectively. The least-squares criterion requires that b_0 and b_1 minimize the function Q, defined as the sum of the squared deviations between the observed values and the fitted values:

$$Q = \sum_{i=1}^{n}[Y_i - (b_0 + b_1 x_1)]^2 \, . \tag{2}$$

In the simple linear regression model, the least squares estimators for b_0 and b_1 are given by the following formulas:

$$b_1 = \frac{\sum X_1 Y_1 - \frac{(\sum X_1)(\sum Y_1)}{11}}{\sum X_1^2 - \frac{(\sum X_1)^2}{11}} \, , \tag{3}$$

$$b_0 = \frac{1}{n}(\sum Y_1 - b_1 \sum X_1) \, , \tag{4}$$

Therefore, the least squares estimates b_0 and b_1 are obtained by calculating the values of $\sum X_1$, $\sum Y_1$, $\sum X_1 Y_1$, and $\sum X_1^2$ from the sample data and substituting them into Eqs. (3) and (4) (*Neter et al*., 1988).

2.4. Significance level

Significance refers to the probability of making an error when rejecting the null hypothesis H_0. It is also known as the p-value. The smaller the significance value, the easier is to reject the null hypothesis. The critical region probability of the sampling distribution (α) is the level of error that the researcher is willing to accept (*Momeni*, 2007). Thus, in a statistical test, the null hypothesis H0 is either rejected or accepted against the alternative hypothesis H1 with an error probability of alpha (*Asakereh*, 2011). By choosing the significance level, α determines the acceptable probability of error.

$$\text{Sig} \; < \alpha \rightarrow \; H_0 \text{ is rejected} \tag{5}$$

$$\text{Sig} \geq \alpha \rightarrow H_0 \text{ is accepted} \quad (6)$$

In this study, the temperature trend was analyzed with a 95% significance level and an error rate of 0.05.

3. Discussion and conclusion

To select an appropriate method for analyzing temperature trends, the normality of the data was first tested. Although it is generally assumed that long-term data follow a normal distribution, graphical methods such as P-P and Q-Q plots were used to ensure greater accuracy, confirming the normality of the data. Following the confirmation of normality, a parametric linear regression method based on the least squares criterion with a 95% significance level was applied to determine the temperature trends (*Neter et al*., 1988). Temperature trend maps for each month across the Northern Hemisphere were generated, and the interpretation of these maps is presented below. This study analyzed the percentage of areas experiencing increasing and decreasing temperature trends, as well as the magnitude of these trends on a monthly and seasonal basis across three regions: the tropical, temperate, and polar zones. Special attention was given to cold regions and high-altitude areas during the statistical period of 1940 to 2023. The resulting temperature trend maps indicate that increasing temperature trends dominate throughout all months in the Northern Hemisphere. However, regional differences in the magnitude of warming are clearly observed during monthly and seasonal intervals (*Feidas et al*., 2005). Except for the months of June (covering 86% of the area) and January (covering 89% of the area), more than 92% of the Northern Hemisphere experienced increasing temperature trends in the remaining months. One of the most obvious early signs of climate change is the warming of air and oceans, as well as the melting of land ice and polar ice (*Seidel et al.,* 2018). This phenomenon is strongly reflected in the findings of the present study. Cold regions of the Northern Hemisphere, including the polar regions, Greenland, Alaska, Siberia, the Tibetan Plateau, and high-altitude areas such as the Himalayas and the Alps, have experienced significant temperature increases. Some regions, such as Alaska, Siberia, and the Tibetan Plateau, have even emerged as hotspots of warming. This result is consistent with *Huang et al.* (2023) study, which showed that between 1991 and 2019, the spatial extent of cold areas decreased by 7.13% compared to the period of 1901 to 1930.

3.1. Seasonal temperature trends in the Northern Hemisphere

The largest area with a positive temperature trend in the Northern Hemisphere is observed during the autumn season (*Table 1 Fig.2.* B), with an increase of 0.042 °C. Following autumn, the seasons of spring, winter, and summer,

respectively, have the largest areas with increasing temperature trends. Although summer is typically the warmest season, it shows a higher percentage of areas with decreasing trends compared to other seasons. In winter, while the area with an increasing trend is smaller compared to autumn and spring, the highest rate of temperature increase is recorded during this season. These findings align with multiple studies which demonstrated that winter temperature increases are more pronounced than in other seasons. Examples include the works of *Karl et al.* (1993), *Otterman et al.* (2002). This temperature increase has also been observed regionally. For instance, more pronounced warming in winter has been reported in regions such as Saudi Arabia (*Almazroui,* 2020), Korea (*Chung* and *Yoon*, 2000), the mid-latitudes of Asia (IPCC, 2014), and Venezuela and Colombia (*Quintana-Gomez*, 1999). The lowest temperature trend is observed in the summer season (*Table 1, Fig. 2.* A), meaning that summer not only has the smallest area with a positive trend, but also shows the lowest increase in temperature. In terms of decreasing trends, winter exhibits the largest negative trend, while spring shows the smallest (*Table 1* and *Fig. 2.* A).

Table 1. Percentage of the area and the amount of decreasing and increasing trends of the Northern Hemisphere in different seasons of the year during the statistical period of 1940–2023

Seasons	Area with negative trend (%)	Magnitude of negative trend	Area with positive trend (%)	Magnitude of positive trend
Winter	7.41	-0.021	92.57	0.056
Spring	7.20	-0.014	92.79	0.045
Summer	8.26	-0.017	91.73	0.038
Autumn	4.05	-0.016	93.75	0.042

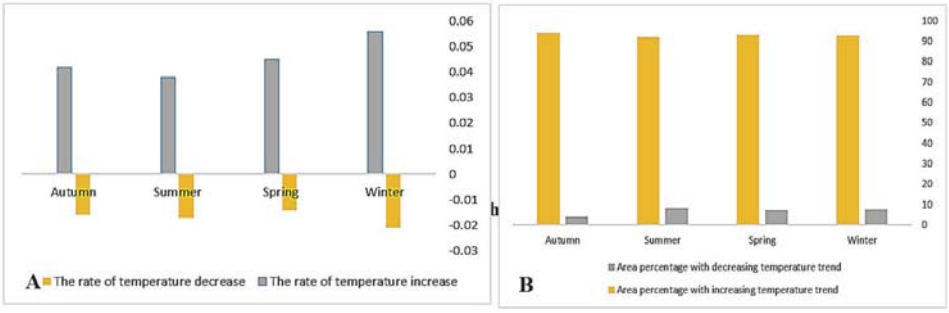

Fig. 2. Seasonal analysis of temperature trends: magnitude and spatial coverage (1940–2023)

3.2. Monthly temperature trends in the Northern Hemisphere

Given the varying results for the negative temperature trends across different months, it is difficult to attribute the decline in negative trends specifically to the warmer or colder months of the year. However, for the positive temperature trends, the opposite is true. The rate of increase in positive trends is higher in the colder months compared to the warmer ones (*Table 2, Fig. 3*). February and March exhibit the highest positive temperature trends and the lowest negative trends (*Figs. 3–5, Table 2*). After February and March, the highest temperature increases occur in December, January, and November (*Figs. 3* and *4, Table 2*).

Table 2. Monthly temperature trends in the Northern Hemisphere (1940–2023): area coverage and magnitude of increasing and decreasing trends

Month	Percentage of area with positive trend (%)	Change per year	Percentage of area with significant positive trend (%)	Percentage of area with negative trend (%)	Change per year	Percentage of area with significant negative trend (%)
December	96.10	0.0175	55.11	3.89	-0.0037	0.0021
January	89.02	0.0193	57.80	10.97	-0.0057	0.0200
February	92.62	0.0195	52.80	7.37	-0.0119	0.5200
March	89.63	0.0194	58.95	10.37	-0.0073	0.9500
April	97.25	0.0140	47.53	2.74	-0.0031	0.0023
May	91.50	0.0120	48.00	8.49	-0.0043	0.8700
June	86.57	0.0130	55.50	13.42	-0.0069	1.5700
July	94.02	0.0140	67.31	5.98	-0.0054	0.4200
August	94.62	0.0116	56.32	5.38	-0.0047	0.6000
September	93.55	0.0130	60.60	6.44	-0.0052	0.2400
October	92.23	0.0120	49.85	7.76	-0.0073	0.0660
November	95.48	0.0170	55.10	4.51	-0.0035	0.0000

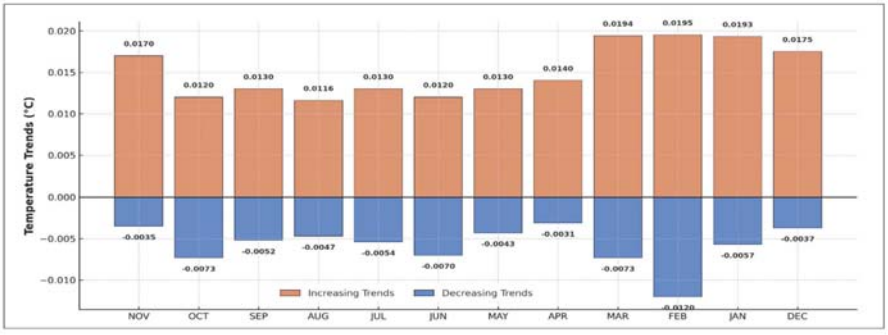

Fig. 3. Increasing and decreasing trends of the monthly temperature of the Northern Hemisphere during the statistical period (1940-2023)

These findings are further detailed in *Table 2* and illustrated in *Figs. 4,5,8,* and *10,* which show the spatial extent and magnitude of temperature trends across the Northern Hemisphere. For example, *Fig. 5* highlights the warming trends in March and April, particularly in temperate regions, while *Fig. 10* provides insights into the variations observed during autumn months such as October and November.

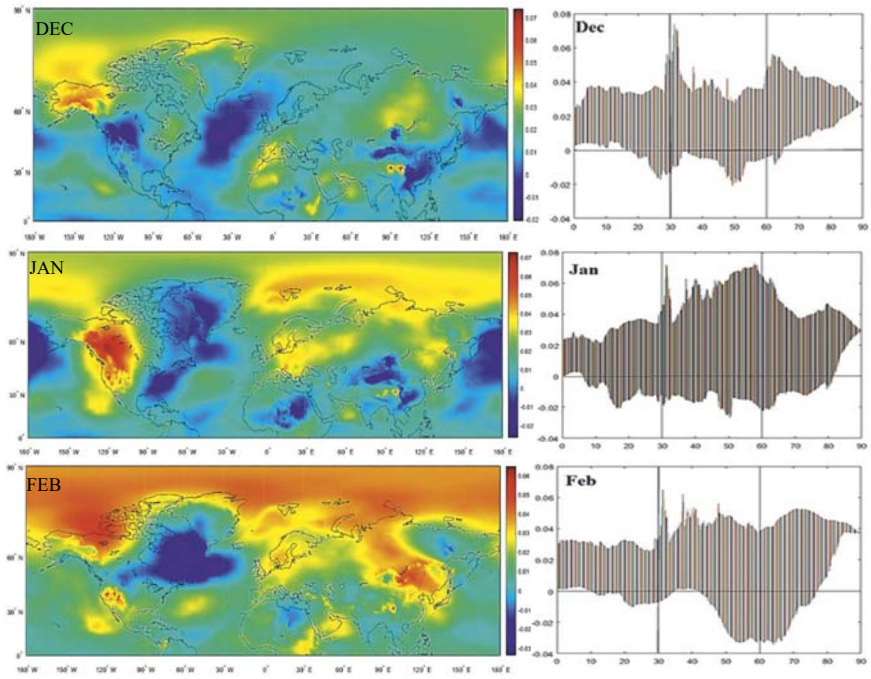

Fig. 4. The temperature trend of the winter months (December, January, February) of the Northern Hemisphere during the statistical period from 1940 to 2023.

The largest temperature increases are observed during the colder months, while the smallest increases are recorded in August, during the summer season. Following August, September and October show similarly small differences in positive temperature trends (*Fig. 10*, A and B), with June and September both exhibiting an increase of 0.013 °C. Furthermore, February and March show the largest temperature decreases in regions with negative trends, with reductions of -0.011 °C and -0.0073 °C, respectively. In terms of area with increasing trends, April covers the largest area, with only 2.74% of the Northern Hemisphere experiencing negative trends in this month. These negative trends are concentrated in regions such as eastern Pakistan, central China in northern Tibet,

the northern Atlantic Ocean, and Canada in North America (*Fig. 5*, B and E). The largest area with negative trends occurs in the warm month of June, covering 13.4% of the Northern Hemisphere, with a temperature decline of -0.0069 °C. Following June, January during the winter season also shows a larger area with negative temperature trends, with a decrease of -0.0057 °C. In June and July, during the summer, more tropical regions experience negative trends (*Fig. 8*, A, B, D, and E). *Table 2* provides the percentage of areas with significant temperature trends.

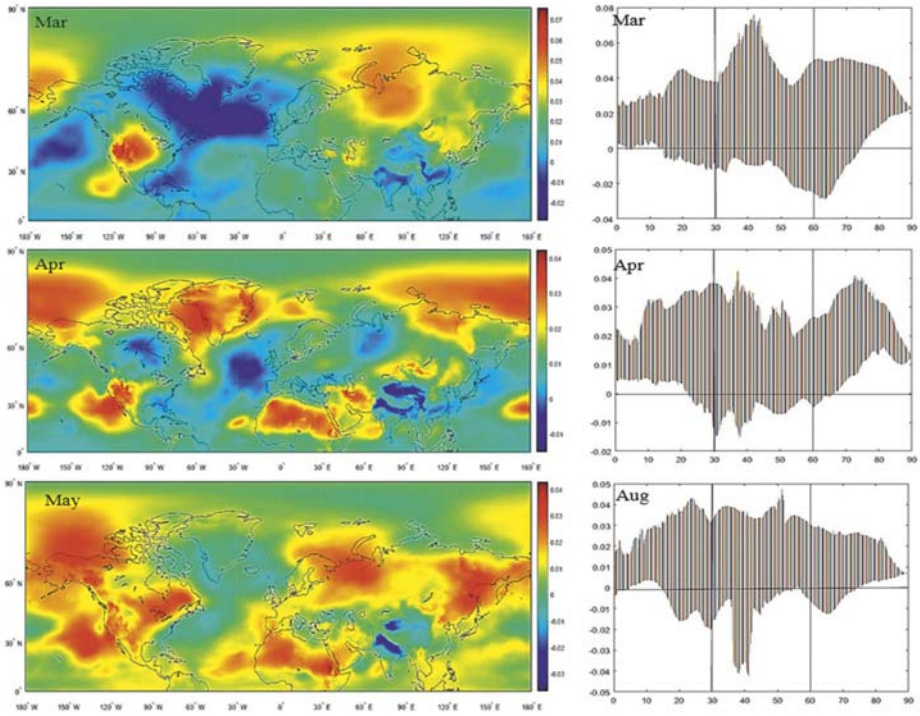

Fig. 5. The temperature trend of the spring months (March, April, May) of the Northern Hemisphere during the statistical period from 1940 to 2023

As shown in *Fig. 5*, the warming trends during March, April, and May are more pronounced in temperate regions, particularly in the transition from winter to spring. These trends indicate the influence of seasonal factors on regional warming.

3.3. Seasonal trends in the tropical, temperate, and polar regions

In all seasons, the positive temperature trend increases progressively from the tropical regions towards the polar regions (*Figs. 5,6,* and *8, Table 3*). In the polar region, winter records the highest positive temperature trend with an increase of 0.018 °C. The months of February, January, March, and December show the highest positive temperature trends in the polar region, all of which are statistically significant. During the cold months, a larger percentage of the polar region experiences a significant temperature trend, while in the tropical region, the area with a significant temperature trend decreases during the cold months. Conversely, during the warm months, the tropical region shows a larger significant area with increasing temperature trends (*Fig. 11*). The temperate regions, on the other hand, exhibit the smallest significant area with temperature trends throughout the year (*Fig. 11*). Spring, summer, and autumn show the highest positive temperature trends in the polar region. In the temperate region, the highest temperature increases during the cold months occur in March, January, February, and December. However, in the tropical region, autumn records the largest temperature increase (*Table 3, Fig. 6*). For the tropical region, it is not possible to clearly rank the months with the highest temperature increases based on cold or warm seasons, as temperature changes in this region are influenced by various factors that do not align strictly with seasonal patterns.

Table 3. Seasonal temperature trend increase rates in the tropical, temperate, and polar regions (1940–2023)

Season	**Polar**	**Temperate**	**Tropical**
Winter	0.081	0.050	0.036
Spring	0.052	0.044	0.024
Summer	0.046	0.039	0.030
Autumn	0.045	0.041	0.037

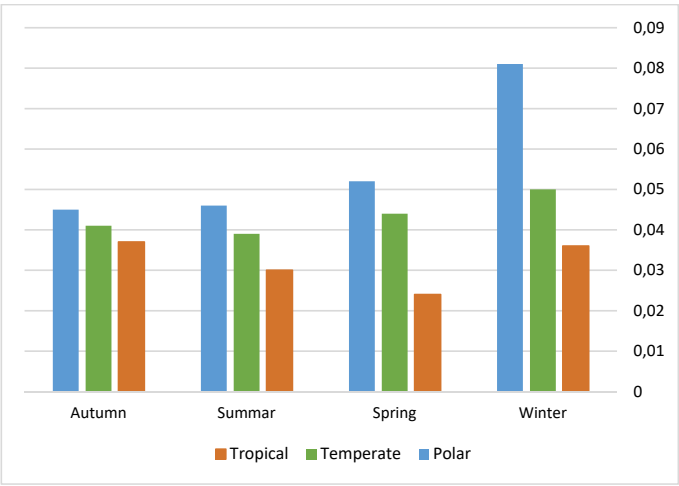

Fig. 6. Seasonal temperature increase rates in tropical, temperate, and polar regions (1940–2023).

3.4. Monthly trends in the tropical, temperate, and polar regions

The monthly temperature trends in tropical, temperate, and polar regions were analyzed separately. According to *Steiner et al*. (2020), the most intense warming occurs in the mid-to-high latitudes of the Northern Hemisphere, with the Arctic warming at twice the global average. However, recent research has shown that even tropical regions are undergoing changes (*Seidel et al*., 2008), although the smallest temperature variations occur in the tropical region (*Manabe et al*., 2011). Compared to the temperate and polar regions, the tropical region has the highest percentage of area with a positive trend and, consequently, the lowest percentage of areas with a negative trend (*Figs. 4–10*, *Tables 4* and *5*). Except for the months of April and October, the warming in the tropical region is lower than in other regions (*Fig. 5*, B, E, *Fig. 10*, B, E; *Fig 7* and *9, Tables 4-5*), which is consistent with previous findings. However, this study revealed that the lower warming trend in the tropical region is mainly confined to latitudes between 0 and 8 degrees north, where the rate of temperature increase is more uniform and lower compared to other regions. This does not apply to other tropical areas between 8 and 30 degrees north. Based on the rate of temperature increase, the tropical region can be divided into two parts: 0 to 8 degrees north and 8 to 30 degrees north. In all months except December, the warming trend in the Intertropical Convergence Zone (ITCZ) region (between 0 and 8 degrees north) is lower than in other tropical regions and other parts of the Northern Hemisphere (*Figs. 4,5,8,* and *10*). In this zone, the rate of temperature increase is consistent, ranging between 0.02 and

0.025 °C. North of 8 degrees, up to 30 degrees, the warming rate increases. The rate of warming in latitudes between 8 and 30 degrees is similar to that of temperate and polar regions (*Figs. 4, 5, 8, and 10*, D, E, F). For instance, in September, the warming rate between 8 and 30 degrees is higher than in the temperate and polar regions (*Fig. 10*, D). Additionally, in October, November, and May, warming hotspots in northern Africa show a greater increase compared to the temperate and polar regions (*Fig. 10*, E, F*; Fig. 5*, C).

Since air temperature is often described as an average (*Tamarin-Brodsky et al.*, 2019), temperature trends represent trends in average temperatures. The average temperature of the tropical region reflects on a combination of lower temperatures in the ITCZ and higher temperatures in latitudes between 8 and 30 degrees. This is why the warming trend in the tropical region is recorded as lower than in other regions. Among all the months of the year, the warming trend in the tropical region during October and April stands out from other months (*Table 4, Fig. 7*, B). In April, the tropical region experiences a higher warming trend compared to temperate regions and equal to that of the polar region (*Fig. 7,* B). In October, the warming trends in the tropical and temperate regions are equal to and higher than in the polar region. In December, temperatures between 0 and 3 degrees north remain around 0.02 °C, but beyond 4 degrees, the temperature increases (*Fig. 7*, B). This explains why the tropical region exhibits its highest warming trend in December compared to other months (*Table 4, Fig. 7*).

Table 4. Percentage of the area and the value of the increasing trend of the Northern Hemisphere in the three tropical, temperate, and polar regions during the statistical period of 1994-2023

Month	Percentage of area with positive trend in the tropics (%)	Rate of positive trend in the tropics	Percentage of area with positive trend in the temperate region (%)	Rate of positive trend in the temperate region	Percentage of area with positive trend in the polar region (%)	Rate of positive trend in the polar region
December	98.93	0.0138	90.30	0.0147	99.18	0.0230
January	95.31	0.0113	80.00	0.1950	91.66	0.0270
February	97.45	0.0110	87.17	0.0160	93.13	0.0310
March	94.89	0.0037	83.21	0.0198	90.67	0.0270
April	98.87	0.0129	93.57	0.0113	99.20	0.0129
May	97.38	0.0048	87.07	0.0136	89.99	0.0125
June	96.58	0.0100	88.08	0.0140	74.94	0.1520
July	97.61	0.0100	91.80	0.0130	92.60	0.0190
August	97.96	0.0103	91.06	0.0124	94.80	0.0123
September	98.28	0.0114	91.80	0.0130	93.80	0.0154
October	98.90	0.0138	84.57	0.0138	92.59	0.0120
November	99.79	0.0124	87.91	0.0145	98.68	0.1800

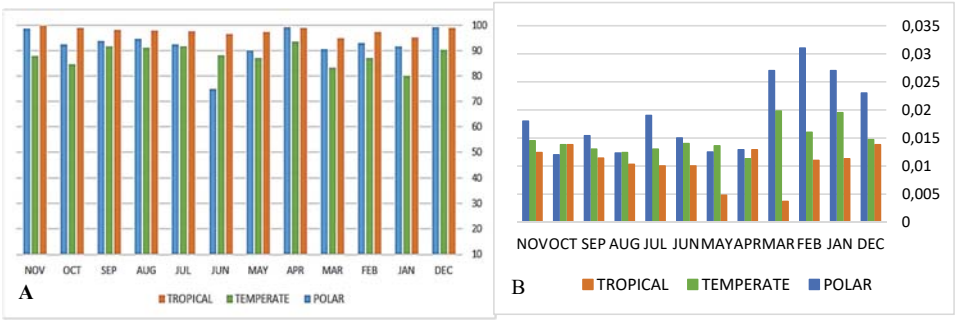

Fig. 7. A - percentage of area with increasing trends; B - magnitude of increasing trends in tropical, temperate, and polar regions (1994–2023).

The temperate region has the largest area with a decreasing trend compared to the tropical and polar regions (*Table 5, Fig. 9*, B). In January, the largest area with a decreasing trend was recorded in the temperate region, which contrasts with the pattern observed in other months (*Fig. 8*, B, E, *Table 5, Fig. 9,* A). This indicates that the area with a decreasing trend in the polar regions has diminished. In June, 25% of the polar region showed a decreasing trend, marking the highest area with a decreasing trend in the polar region compared to other months (*Fig. 8*, A, D). However, the greatest amount of trend reduction was recorded in February (*Table 5, Fig. 9*, A). The tropical region also experienced a decreasing trend, with the highest reduction occurring in June (*Table 5, Fig. 9*, B). The amount of decrease in the tropical, temperate, and polar regions varies across other months and cannot be clearly categorized based on warm or cold months (*Table 5, Fig. 9*).

Table 5. Percentage of the area and the amount of the decreasing trend of the Northern Hemisphere in the tropical, temperate and polar regions during the statistical period of 1994–2023

Month	Percentage of area with negative trend in the tropics (%)	Rate of decreasing trend in the tropics	Percentage of area with negative trend in the mid-latitudes (%)	Rate of decreasing trend in the mid-latitudes	Percentage of area with negative trend in the polar region (%)	Rate of decreasing trend in the polar region
December	1.06	-0.0051	9.86	-0.0037	0.081	-0.0091
January	4.68	-0.0046	19.99	-0.0050	8.230	-0.0059
February	2.54	-0.0030	12.82	-0.0130	6.860	-0.0128
March	5.10	-0.0119	16.78	-0.0083	9.320	-0.0076
April	1.12	-0.0026	6.42	-0.0033	0.700	-0.0015
May	2.62	-0.0010	12.92	-0.0045	10.000	-0.0025
June	3.41	-0.0092	11.91	-0.0049	25.050	-0.0076
July	2.38	-0.0048	8.19	-0.0055	7.370	-0.0054
August	2.03	-0.0061	8.93	-0.0034	5.160	-0.0050
September	1.79	-0.0047	8.19	-0.0055	6.150	-0.0060
October	1.07	-0.0051	15.42	-0.0087	7.400	-0.0040
November	0.20	-0.0018	12.08	-0.0037	1.310	-0.0210

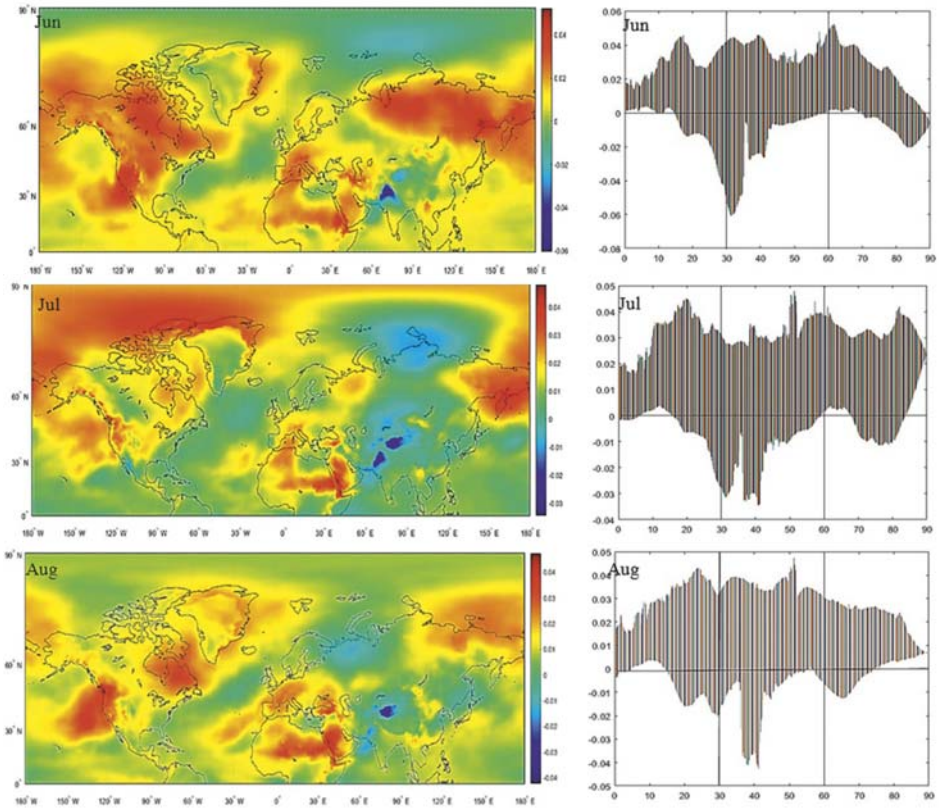

Fig. 8. The temperature trend of the summer months (June, July, August) of the Northern Hemisphere during the statistical period from 1940 to 2023.

Fig. 8 highlights the warming trends during summer months (June, July, August), where the northern temperate regions exhibit the strongest warming compared to tropical areas. This pattern suggests that summer warming is more regionally heterogeneous.

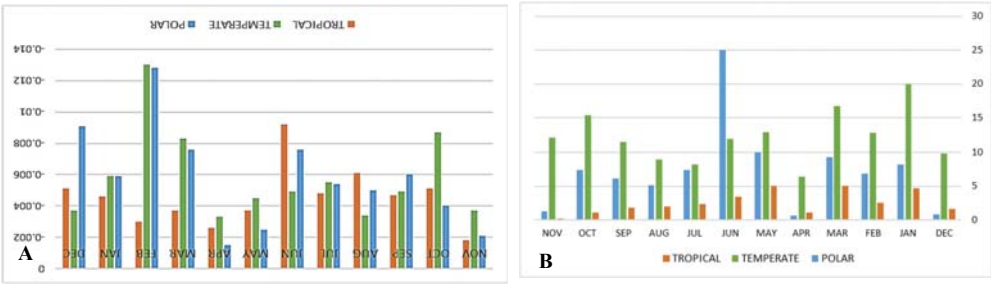

Fig. 9. A – percentage of the area of decreasing trend, B –magnitude of the decreasing trend in the tropical, temperate and polar regions of the Northern Hemisphere during the statistical period of 1994–2023.

3.5. Polar regions

The increasing temperature trend across the entire polar region is clearly evident. *Savita et al*. (2005) attributed the warming of recent decades in the polar region and North America to human activities and internal changes. Seasonal and monthly analyses of the polar region show that the temperature increase is more significant during the cold seasons (*Figs. 4–10, Tables 4* and *5*). However, regional differences in the temperature increase are notable. Although some studies have shown that the highest warming occurs in the high northern latitudes (e.g., *Steiner et al*., 2020), the temperature trend maps in this study indicate that the increase in temperature diminishes between 60 to 90 degrees north and south, with the warming trend decreasing from 60 to 90 degrees north. This finding does not align with *Steiner*'s (2020) results. The discrepancies between our findings and earlier studies, such as *Steiner et al*. (2020), can potentially be attributed to several factors. First, the temporal range of this study (1940–2023) is significantly broader than most previous studies, capturing longer-term climatic trends. Second, differences in datasets this study utilizes, ERA5 reanalysis data may introduce variability due to differing resolutions and calibration techniques. Third, physical changes such as the accelerated melting of the Arctic ice sheets and associated feedback mechanisms, which were less pronounced in earlier studies, could explain the observed divergence. These findings highlight the importance of integrating non-linear models and higher-resolution regional datasets in future research to resolve these contradictions.

Based on these findings, the polar region can be divided into two parts according to the degree of temperature increase, similarly to the tropical region. This division varies by month. In March (*Fig. 5*, A, D), September, October (*Fig. 10*, A, B, D, E), December (*Fig. 4*, A, D), August (*Fig. 8*, C, F), and January (*Fig. 4*, B, E), the temperature increase is greater between 60 to 80 degrees, while the warming decreases between 80 to 90 degrees. In May (*Fig. 5*, C, E), November

(*Fig. 10*, B, E), and April (*Fig. 5*, B, E), the warming is more pronounced between 60 to 75 degrees, while it decreases beyond 75 degrees north. October (*Fig. 10*, B, E) and June (*Fig. 8*, A, D) show the lowest temperature increase in the polar region. In June, from 60 to 90 degrees north, the temperature trend becomes negative, with temperatures dropping between 85 and 90 degrees north (*Fig. 8*, A, D). February exhibits the highest temperature increase in the polar region, with only a slight decrease between 85 to 90 degrees north (*Fig. 4*, B, E). In each of these two parts, regional variations are also notable. For example, Alaska, Siberia, Greenland, and the Arctic Ocean in the subpolar region (up to 75 degrees north) show greater temperature increases compared to latitudes above 75 degrees. This finding contradicts the results of *Stouffer et al.* (1989) and *Manabe et al.* (1991), who suggested that the warming in subpolar regions of the Arctic Ocean is generally minimal. Subpolar oceans have emerged as warming hotspots in the Northern Hemisphere, with higher temperatures than the more northern parts of the polar region. Additionally, cooling cores in the polar regions are located between 60 to 70 degrees north, particularly in southern Greenland, the North Atlantic, Iceland, the Norwegian Sea, and Greenland (again). There are also temperature trend differences between eastern and western parts of the polar region above 70 degrees north, particularly in March, May, June, and July. In May, June, and July, the eastern polar region even experiences a negative temperature trend (*Figs. 4, 5, 8, and 10*). The temperature increase also correlates with the latitude in Greenland, where the warming trend follows a south-to-north gradient. Southern Greenland has the lowest temperature, and as the latitude increases, the warming trend intensifies. *Manabe et al.* (2011) reported a 1 °C temperature decrease in southern Greenland. However, this study found that in October, the opposite occurred, with southern Greenland experiencing higher temperatures, and cooling cores were observed in northern Greenland (*Fig. 10*, B). Alaska and Siberia are warming hotspots in the polar regions. Alaska is a hotspot for increasing temperature trends in North America in every month except September. In September, southern Alaska exhibits a negative trend (*Fig. 10*, A). In December, the temperature increase in Alaska reaches 0.06 °C (*Fig. 4*, A), while in January, it decreases to 0.01 °C (*Fig. 4*, B). The temperature increase in eastern and northern Siberia is also significant. In most months, eastern Siberia serves as a warming core in Europe. During the autumn months, eastern Siberia experiences the highest temperature increase in Europe, reaching up to 0.05 °C (*Fig. 10*). In winter, the increase slows to 0.01 to 0.02 °C (*Fig. 4*). Only in January does eastern Siberia show a negative temperature trend, with a decrease of up to -0.01 °C. The Arctic region has experienced the most significant warming. However, as mentioned at the beginning of this section, this warming decreases as latitudes increase. The annual surface temperature in Alaska and Siberia has increased from 2 °C to 3 °C. Predictions suggest that by 2050, the Arctic region (north of 60 degrees) will warm by 1.1 °C, and by 2100, it could increase by

5.5 °C. The smallest temperature changes are expected in tropical latitudes, with annual variations projected between 0.1 to 3 °C (*Manabe et al*., 2011).

Continents and cold regions of the Northern Hemisphere were analyzed separately. Europe shows a higher warming trend compared to other continents in the Northern Hemisphere. The temperature trend in North Africa closely resembles that of Europe and North America. However, Asia exhibits a different pattern, with a lower warming trend than other continents in most months of the year. Asia shows a lower warming trend compared to Europe, North America, and North Africa (*Figs. 4, 5, 8,* and *10*). Throughout the year, Asia has cooling cores, especially in the tropical and temperate regions, particularly in Pakistan, the southeastern coast of Iran, the Himalayas, and northern, northwestern, and western China. Although studies by *Li* and *Zhang* (2021) for the period 1971–2013 and *Fang et al.* (2016) for the period 1960 to 2010, reported significant warming for most parts of China, and found that warm indices increased faster than cold ones, central China, eastern and northern Tibet, and western China, including the highlands of Xinjiang, have experienced cooling trends throughout the year, making them part of the cooling cores in the Northern Hemisphere. Warming cores in Asia, in all months except November, are mostly concentrated in the Middle East. In November, the warming trend in the Middle East weakens, and even Turkey and Iran experience a cooling trend (*Fig. 10*, C, F). The Arabian Peninsula, which is highly influenced by extreme temperatures (*Krishna,* 2015; *Salimi* and *Al-Ghamdi.,* 2020), and Turkey show a significant warming trend in the Middle East. The Arabian Peninsula, in particular, remains one of the warming cores in the Middle East and Asia throughout the year. Studies by *Paeth et al*. (2009) and *El Kenawy et al*. (2015) have also highlighted significant warming in North Africa and the Middle East.

In *Fig. 10*, autumn temperature trends reveal a gradual warming from tropical to polar regions. Notable variations include consistent warming in September and localized cooling in northern regions during November.

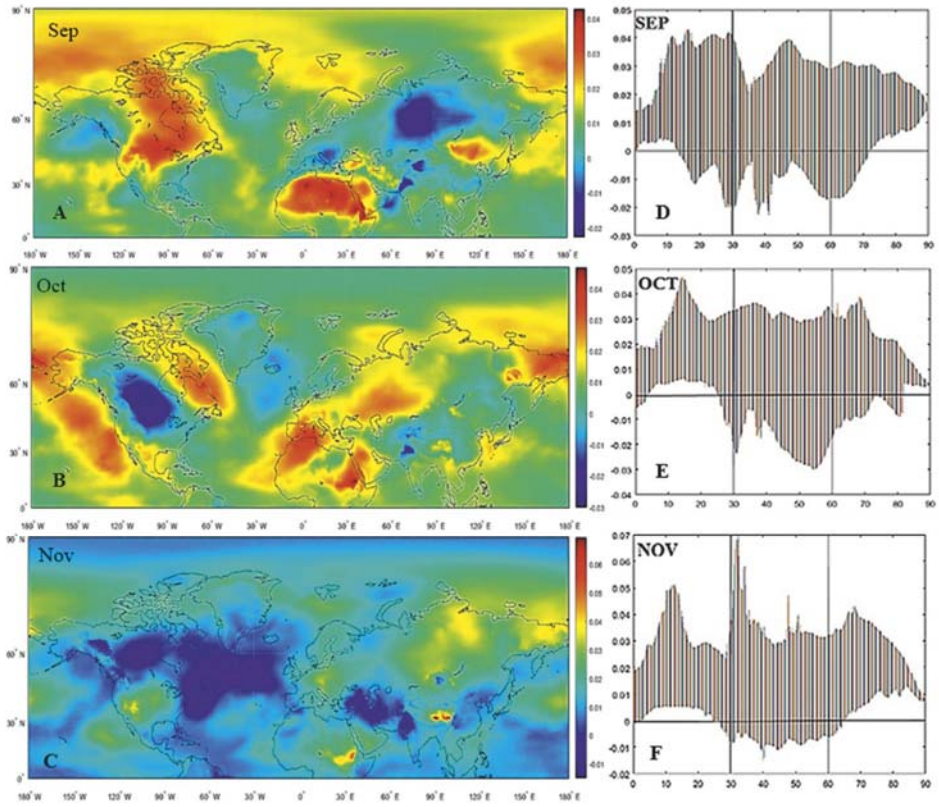

Fig. 10. the temperature trend of the months of September, October, and November in the Northern Hemisphere during the statistical period of 1940–2023.

The Tibetan Plateau, a key warming core in Asia, experiences a warming trend of 0.03 to 0.05 °C annually, with the highest trends (0.07 °C) in the eastern regions during the cold seasons (September to March) (*Figs. 4* and *10*). In contrast, the warming trend during the warm seasons drops to 0.01 °C in August. Over the past 119 years, the extent of cold regions in the Tibetan Plateau has decreased significantly (*Huang*, 2020). Similarly, studies by *Zhang* and *Zhou* (2009), *Zhang et al.* (2013), and *Li* and *Zhang* (2021) confirm these seasonal variations.

South Asia, including the Indian subcontinent, Bangladesh, and Myanmar, shows a weaker warming trend during winter (December to March), with a negative trend of -0.005 °C in February (*Fig. 4*, B). However, in months like August, September, and November, the warming trend intensifies, aligning with *Naveendrakumar et al*. (2019), who reported a linear temperature increase in South Asia.

Cold and high-altitude regions like the Atlas Mountains, Rockies, Alps, Himalayas, and Siberia also exhibit notable trends. The Rockies show warming on western slopes and cooling on eastern slopes during October, with slight cooling in December (*Fig. 4*, A). The Alps, as one of Europe's warming cores, exhibit consistent warming throughout the year, with impacts such as glacier retreat, reduced snow cover below 1300 m, and vegetation shifts (*Paul et al*., 2004; *Scherrer et al*., 2004). The Himalayas show warming from August to March and cooling from April to July, with western regions experiencing more significant cooling (*Figs. 5* and *8*). The Atlas Mountains, in contrast, display year-round warming, except in September, where trends drop to 0–0.005 °C (*Fig. 10*, A).

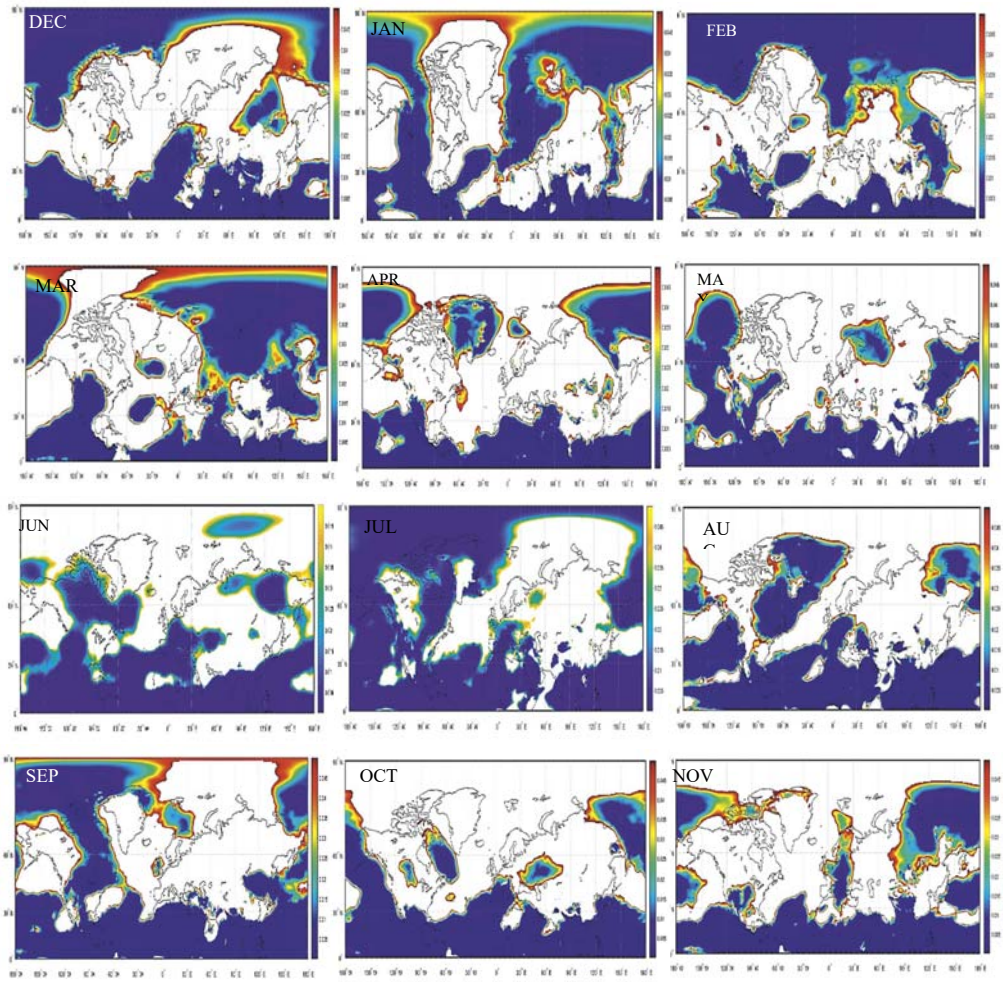

Fig. 11. The significant level of the temperature trend in the Northern Hemisphere during the statistical period of 1940–2023.

Fig. 11 provides a detailed visualization of the spatial and seasonal variability of temperature trends across the Northern Hemisphere during the statistical period of 1940–2023. The figure highlights significant warming in polar regions during winter, particularly in January and February, where trends exceed 0.02 °C per decade. Conversely, the summer months, such as June, exhibit localized areas of decreasing trends, most notably in the tropical and temperate zones. Temperate regions demonstrate marked variability, with pronounced warming during spring and autumn, reflecting the influence of transitional seasonal dynamics. Tropical regions, in contrast, show relatively stable trends with minimal seasonal fluctuations (*Fig. 11*).

4. Conclusion

This study analyzed monthly and seasonal temperature trends in the Northern Hemisphere from 1940 to 2023 using least squares regression at a 95% significance level. Trends were evaluated across the tropical, temperate, and polar regions to examine the intensity and spatial variability of warming and cooling patterns.

The findings revealed that increasing temperature trends dominate all months in the Northern Hemisphere, with evident regional and seasonal variability. The largest area with increasing trends was observed during autumn, while the highest temperature rise occurred in winter. In contrast, summer exhibited the smallest area with increasing trends and the lowest temperature rise. Notably, decreasing trends were most prominent in June, but their intensity did not align consistently with warm or cold months. Conversely, increasing trends were more pronounced in cold months than in warm months.

The analysis highlighted the importance of latitude in shaping warming trends. For instance, while the tropical region exhibited lower overall warming compared to the temperate and polar zones, significant variability was observed within the tropics. Latitudes 0–8°N showed uniform, lower warming, while latitudes 8–30°N exhibited higher warming rates, comparable to the temperate and polar regions. In September, warming in the 8–30°N range even exceeded that in the temperate and polar regions. This variability underscores the limitations of relying solely on average temperature data and emphasizes the need for temperature maps to capture regional nuances.

In the polar regions, the warming trend was most pronounced in winter but showed notable regional variability. The rate of warming diminished beyond the 60°N latitude, reflecting complex interactions between atmospheric circulation, sea ice albedo feedback, and oceanic heat transport. Similarly to the tropics, the polar region could be divided into two zones based on temperature trends, which varied across months.

Continental analysis showed that Europe experienced the highest warming trends, followed by North America and North Africa. Asia exhibited lower

warming trends overall, with cooling cores in regions such as Pakistan, southeastern Iran, the Himalayas, and northern China. Mountain ranges like the Atlas Mountains, Tibetan Plateau, Alps, Rockies, and Appalachians demonstrated year-round warming trends, with Alaska and Siberia forming major warming cores. However, the Himalayas differed, with a weaker warming trend and seasonal cooling from April to July. From August to March, the Himalayas experienced warming trends, highlighting their distinct climatic behavior compared to other mountain ranges.

Acknowledgements: This work is based upon research funded by Iran National Science Foundation (INSF) under project No.4031542.

References

Almazroui, M, 2020: Changes in temperature trends and extremes over Saudi Arabia for the period 1978–2019. *Adv. Meteorol 2020*(1), 8828521. https://doi.org/10.1155/2020/8828421

Al-Mutairi, M, Labban A, Abdeldym A, and *Abdel Basset H*, 2023: Trend Analysis and Fluctuations of Winter Temperature over Saudi Arabia. *Climate 11*(3), 67. https://doi.org/10.3390/cli11030067

Asakereh, H, 2011: Fundamentals of statistical climatology. Zanjan university publication, 222. (In Persian)

Chapman, W. L and *Walsh J. E*, 1993: Recent variation of sea ice and air temperature in high latitudes. *Bull. Amer. Meteor. Soc., 75*, 33–57. https://doi.org/10.1175/1520-0477(1993)074<0033:RVOSIA>2.0.CO;2

Choi G, Collins D, and *Ren G, 2*009: Changes in means and extreme events of temperature and precipitation in the Asia-Pacific network region, 1955–2007, *Int. J. Climatol*. *29*, 1906–1925. https://doi.org/10.1002/joc.1979

Christy J. R, Norris W. B. Spencer R. W, and *Hnilo J. J,* 2007: Tropospheric temperature change since 1979 from tropical radiosonde and satellite measurements. *J. Geophys Res: Atmospheres*, *112*(D6). https://doi.org/10.1029/2005JD006881

Chung Y.S and *Yoon M.B,* 2000: Interpretation of recent temperature and precipitation trends observed in Korea. *Theor. Appl. Climatol*. *67*, 171–180. https://doi.org/10.1007/s007040070006

Croitoru A.E, Holobace I.H, Lazar C, Moldovan F, and *Imbroavce A,* 2012: Air temperature trend and the impact on winter wheat phenology in Romania. *Climatic Change* 111, 393–410. https://doi.org/10.1007/s10584-011-0133-6

El Kenawy A, López-Moreno J I, McCabe M F, Brunsell N.A, and *Vicente-Serrano S.M,* 2015: Daily Temperature Changes and Variability in ENSEMBLES Regional Models Predictions: Evaluation and Intercomparison for the Ebro Valley (NE Iberia). Atmos. Res. Elsevier BV. http://doi.org/10.1016/j.atmosres.2014.12.007

Fang S, Qi Y, Han G, Li Q, and *Zhou G,* 2016: Changing trends and abrupt features of extreme temperature in mainland China from 1960 to 2010, *Atmosphere 7*(2), 22*;* https://doi.org/10.3390/atmos7020022

Feidas H, Makrogiannis T, and *Bora-Senta E,* 2005: Trend analysis of air temperature time series in Greece and their relationship with circulation using surface and satellite data: 1955–2001. *Theor. Appl Climatol 79*, 185–208. https://doi.org/10.1007/s00704-004-0064-5

Folland C.K, Karl T.P, Christy J.R, Clarke R.A, Gruza G.V, Jouzel J, Mann M.E, Oerlemans J, Salinger M.J, and *Wang S.W,* 2001: Observed climate variability and change. In Chapter 2 of Climate Change 2001; The Scientific Basis, Contribution of Working Group I to the Third Assessment Report of the Intergovernmental Panel on Climate Change (IPCC); *Houghton, J.T., Ding, Y., Griggs, .J., Noguer, M., van der Linden, P.J., Xiaoxu, D*., Eds.; Cambridge University Press: Cambridge, UK, 99–181.

Hansen J, Ruedy R, Sato M, and *Lo K* (2010) Global surface temperature change, *Rev. Geophys*. 48, RG4004-. https://doi.org/10.1029/2010RG000345

Huang Y, Zhang L, Li Y, Ren C, Pan T, Zhang W, and *Liu J,* 2023: Characteristics of the Northern Hemisphere cold regions changes from 1901 to 2019. *Sci. Reports 13*, 3879. https://doi.org/10.1038/s41598-023-30263-1

IPCC. 2007: Summary for policymakers. In Climate Change 2007: The Physical Science Basis.Contribution of Working Group I to the 5th Assessment Report of the Intergovernmental Panel on Climate Change (eds *S. Solomon, D. Qin, M. Manning, Z. Chen, M. Marquis, K. B. Averyt M. Tignor and H. L. Miller*). Cambridge, UK: Cambridge University Press.

IPCC. Climate Change 1995: The Science of Climate Change, *J. T. Houghton et al.,* Eds. Cambridge Univ. Press, Cambridge.

IPCC. Climate change, 2013: The Physical Science Basis. In Contribution of Working Group I to the Fifth Assessment Report of the Intergovernmental Panel on Climate Change; *Stocker, T.F., Qin, D., Plattner, G.K., Tignor, M., Allen, S.K., Boschung, J., Nauels, A., Xia, Y., Bex, V., Midgley, P.M*., Eds.; Cambridge University Press: Cambridge, UK; New York, NY, USA.

IPCC. Climate Change, 2014: Mitigation of Climate Change. In Contribution ofWorking Group III to the Fifth Assessment Report of the Intergovernmental Panel on Climate Change; *Edenhofer, O., Pichs-Madruga, R., Sokona, Y., Farahani, E., Kadner, S., Seyboth, K., Adler, A., Baum, I., Brunner, S., Eickemeier, P., et al*., Eds.; Cambridge University Press: Cambridge, UK; New York, NY, USA.

Jones PD and *Moberg A,* 2003: Hemispheric and large-scale surface air temperature variations: an extensive revision and an update to 2001. *J climate 16*(2):206–223.

Karl TR, Jones PD, Knight RW, Kukla G, Plummer N, Razuvayev V, Gallo KP, Lindseay J, Charlson RJ, and *Peterson TC,* 1993: Asymmetric trends of daily maximum and minimum temperature. *Papers Nat Resour 1*,185. https://doi.org/10.1175/1520-0477(1993)074<1007:ANPORG>2.0.CO;2

Karoly D.J and *Braganza K,* 2005: Attribution of recent temperature changes in the Australian region. *J. Climate 18*, 557–565. https://doi.org/10.1175/JCLI-3265.1

Krzyżewska A, Wereski S, and *Demczuk P,* 2020: Biometeorological conditions during an extreme heatwave event in Poland in August 2015. *Weather 75*(6), 183–189. https://doi.org/10.1002/wea.3497

Li L and *Zhang R,* 2021: Effect of upper-level air temperature changes over the Tibetan Plateau on the genesis frequency of Tibetan Plateau vortices at interannual timescales. *Climate Dynamics 57*(1), 341–352. https://doi.org/10.1007/s00382-021-05715-x

Lindsay, R.W and *Zhang L,* 2005: The thinning of Arctic sea ice, 1988–2003: Have we passed a tipping point? *J. Climat 18*, 4879–4894. https://doi.org/10.1175/JCLI3587.1

Lindzen, R.S and *Giannitsis C*, 2002: Reconciling observations of global temperature change. *Geophys. Res Letters*, *29*(12), 25-1. https://doi.org/10.1029/2001GL014074

Manabe, S and*, Stouffer R.J,* 1980: Sensitivity of a global climate model to an increase of CO2 concentration in the atmosphere. *J. Geophys. Res. 85*, 5529–5555. https://doi.org/10.1029/JC085iC10p05529

Manabe, S and*, Stouffer R.J,* 1979: A CO2-climate sensitivity study with a mathematical model of the global climate. *Nature 282*, 591–593. https://doi.org/10.1038/282491a0

Manabe S,Stouffer R,J, Spelman K, and *Bryan K,* 1991: Transient response of a coupled ocean–atmosphere model to gradual changes of atmosphericCO2. Part I: Annual mean response. *J. Climate 5*, 785–818. https://doi.org/10.1175/1520-0442(1991)004<0785:TROACO>2.0.CO;2

Manabe S., Ploshay J, and *Lau N. C,* 2011: Seasonal variation of surface temperature change during the last several decades. *J. Climate 25*, 3817–3821. https://doi.org/10.1175/JCLI-D-11-00129.1

Momeni, M, 2008: Statistical analysis using Spss software. New book publication, 35. (in Persian)

Naveendrakumar G, Vithanage M, Kwon HH, Chandrasekara SS, Iqbal MC, Pathmarajah S, Fernando WC, and *Obeysekera J,* 2019: South Asian perspective on temperature and rainfall extremes: a review, *Atmos. Res*. *225*, 110–120. https://doi.org/10.1016/j.atmosres.2019.03.021

Neter J, Wasserman W, and *Whitmore G.A,* 1988: Applied Statistics. Third Edition, Allyn and Bacon, Inc, 820–822.

Otterman J, Angell J.K, Ardizzone J, Atlas R, Schubert S, Starr D, and *Wu, M.L,* 2002: North-Atlantic surface winds examined as the source of winter warming in Europe. *Geophys. Res. Lett 29*, 18. https://doi.org/10.1029/2002GL015256

Paeth H, Born K, Girme, R, Podzun R, and *Jacob D,* 2009: Regional Climate Change in Tropical and Northern Africa due to Greenhouse Forcing and Land Use Changes. *J. Climate 22*, 115–132. https://doi.org/10.1175/2008JCLI2390.1

Paul F, Kääb A, Maisch M, Kellenberger T, and *Haeberli W,* 2004: Rapid disintegration of Alpine glaciers observed with satellite data. Geophys. *Res. Lett. 31*(21). https://doi.org/10.1029/2004GL020816

Quintana-Gomez R.A, 1999: Trends of maximum and minimum temperatures in Northern South America. *J. Climate 12*, 2105–2112. https://doi.org/10.1175/1520-0442(1999)012<2104:TOMAMT>2.0.CO;2

Reidmiller D.R, Avery C.W, Easterling D.R, Kunkel K.E, Lewis K.L.M, Maycock T.K, and *Stewart B.C,* 2018: Fourth national climate assessment, Volume II: Impacts, risks, and adaptation in the United States. Washington, DC, US Global Change Research Program.

Rosenzweig C, Karoly D, Vicarelli M, Neofotis P, Wu Q, Casassa G, Menzel A, Root T.L, Estrella N, Seguin B, and *Tryjanowski P,* 2008: Attributing physical and biological impacts to anthropogenic climate change, *Nature, 453*(7193), 353–357. https://doi.org/10.1038/nature06937

Salimi M and *Al-Ghamdi S.G,* 2020: Climate change impacts on critical urban infrastructure and urban resiliency strategies for the Middle East, *Sust. Cities Soc. 55,* 101958. https://doi.org/10.1016/j.scs.2019.101948

Salinger, M.J, 2005: Climate variability and change: past, present and future–an overview. *Climatic*

Savita A, Kjellsson J. J, Latif M, Nnamchi, H, and *Wahl, S*, 2025: Impact of multidecadal climate'modes variability on the Northern Hemisphere temperature trend in the recent decades (No. EGU25-11758). Copernicus Meetings. https://doi.org/10.5194/egusphere-egu24-11748

Scherrer SC, Appenzeller C, and *Laternser M,* 2004: Trends in Swiss Alpine snow days: The role of local- and large-scale climate variability. *Geophys Res Lett 31*, L13215. https://doi.org/10.1029/2004GL020255

Seidel D. J, Fu ., Randel W. J, and *Reichler, T.J*, 2008: Widening of the tropical belt in a changing climate. *Nat. Geosci. 1*, 21–25. https://doi.org/10.1038/ngeo.2007.38

Siddik. M and *Rahman. M,* 2014: Trend analysis of maximum, minimum, and average temperatures in Bangladesh: 1961–2008, *Theor Appl Climatol 116*(3–4). https://doi.org/10.1007/s00704-014-1135-x

Simmons A. J, Berrisford P, Dee D. P, Hersbach H, Hirahara S, and *Thépaut J.-N,* 2017: A reassessment of temperature variations and trends from global reanalyses and monthly surface climatological datasets, *Quart J Roy Meteorol Soc 153*(702), 101–119. https://doi.org/10.1002/qj.2949

Steiner AK, Ladstädter F, Randel WJ, Maycock AC, Fu Q, Claud C, Gleisner H, Haimberger L, Ho SP, Keckhut P, and *Leblanc T,* 2020: Observed temperature changes in the troposphere and stratosphere from 1979 to 2018. *J. Climate 33*(19):8165–8194. https://doi.org/10.1175/JCLI-D-19-0998.1

Stouffer R. J, Manabe S, and *Bryan K,* 1989: Interhemispheric asymmetry in climate response to a gradual increase of atmospheric CO2. *Nature 352*, 660–662.https://doi.org/10.1038/342660a0

Tamarin-Brodsky T, Hodges K, Hoskins B. J, and *Shepherd T.G,* 2019: A dynamical perspective on atmospheric temperature variability and its response to climate change. *J. Climate 32*, 1707–1725. https://doi.org/10.1175/JCLI-D-18-0462.1

Trewin L. V, 2016: Global observed long-term changes in temperature and precipitation extremes: a review of progress and limitations in IPCC assessments and beyond, *Weather Climate Extremes 11*, 5–16. https://doi.org/10.1016/j.wace.2015.10.007

Vinnikov K.Y, Groisman P.Y, and *Lugina K.M,* 1990: Empirical Data on Contemporary Global Climate Changes (Temperature and Precipitation). *J. Climate 3*, 662–677. https://doi.org/10.1175/1520-0442(1990)003<0662:EDOCGC>2.0.CO;2

Zhang D, Huang J, Guan X, Chen B, and *Zhang L,* 2013: Long-term trends of precipitable water and precipitation over the Tibetan Plateau derived from satellite and surface measurements. Journal of Quantitative Spectroscopy *Radiative Transfer 122,* 64–71. https://doi.org/10.1016/j.jqsrt.2012.11.028

Zhang RH and *Zhou SW,* 2009: Air temperature changes over the Tibetan Plateau and other regions in the same latitudes and the role of ozone depletion. *Acta Meteorol Sin 23*, 290–299.

DOI:10.28974/idojaras.2025.4.4

IDŐJÁRÁS

Quarterly Journal of the HungaroMet Hungarian Meteorological Service
Vol. 129, No. 4, October – December, 2025, pp. 443–464

Evaluation of bioclimatic conditions for tourism activities in the Podrinje-Valjevo Region (Serbia)

Jelena Milenković*and **Milica Lukić**

University of Belgrade - Faculty of Geography, Belgrade, Serbia

**Corresponding author E-mail:* jelenamilenkovic311@gmail.com

(Manuscript received in final form November 22, 2024)

Abstract— To better understand outdoor thermal comfort on both seasonal and monthly levels, the current trends and anomalies in the Podrinje-Valjevo Region (PVR) over the past 30 years (1991–2020) and their impact on tourist activities, two bioclimatic indices, the Universal Thermal Climate Index (UTCI) and the Tourism Climatic Index (TCI), were utilized for the temporal assessment of bioclimatic conditions in Loznica and Valjevo. The results show that spring and autumn are the most favorable seasons for outdoor tourism activities, with April, May, September, and October being particularly optimal. According to UTCI, November has also become more bioclimatically favorable due to a rise in average monthly UTCI values. Additionally, UTCI data reveal a notable upward trend in seasonal anomalies, especially during autumn and spring, with average seasonal UTCI values increasing. Although TCI indicates that summer is particularly ideal for tourist outdoor activities and tourists' thermal comfort, UTCI highlights that summer months can cause significant thermal discomfort due to moderate heat stress. The results obtained can serve to more effective tourism planning in the Podrinje-Valjevo Region in Serbia.

Key-words: Podrinje-Valjevo Region, Loznica, Valjevo, Universal Thermal Climate Index, Tourism Climatic Index

1. Introduction

Climate plays a crucial role in the development of tourism and is considered a significant "pull" factor in selecting tourist destinations (*Hu* and *Ritchie*, 1993; *Scott et al.*, 2016; *Dann*, 1981; *Lohmann* and *Kaim*, 1999). Climate can be viewed as both a direct and an indirect tourism value, influencing various aspects of human activity. When the climate of a location attracts tourists because it enables

certain activities, such as skiing, swimming, or heliotherapy, it serves as a direct tourism value. Conversely, climate also impacts the surrounding environment – such as vegetation, water bodies, and topography – which can enhance the region's appeal as a tourist destination, representing an indirect tourism value (*Stanković*, 2008). Additionally, unfavorable climatic conditions can restrict or inhibit tourism activities, highlighting the strong dependence of tourism on weather and climate conditions at the destination (*Grillakis et al.*, 2016). Since climate directly and indirectly influences tourism, impacting the development of various tourism types, tourist demand, and overall tourist satisfaction, the scientific community has begun to assess climate elements to determine favorable conditions for tourist activities. This assessment primarily relies on climate indices, which provide insights into how suitable a region's climate is for tourism activities.

Numerous studies in the scientific literature have been exploring climate tourism indices and the relationship between climate and tourism (*Besancenot et al.*, 1978; *Mieczkowski*, 1985; *de Freitas*, 1990; *Becker*, 1998; *Lise* and *Tol*, 2002; *Bigano et al.*, 2006). Understanding the effects of climate on specific tourist activities and predicting bioclimatic indicators can lead to more effective tourism planning at local, regional, and national levels (*de Freitas et al.*, 2008).

Bioclimate is a subfield of climatology that is particularly relevant to tourism. Bioclimatic evaluation of tourist sites offers significant potential and various advantages for planning tourism development. With over 100 bioclimatic indices available today, it is possible to describe the bioclimatic and microclimatic conditions of both outdoor and indoor environments, whether urban or rural, with great precision. In addressing climate change adaptation and mitigation, it is crucial to redefine the way we observe land use and incorporate new indicators that more comprehensively reflect the changing climatic conditions and outdoor thermal comfort for tourists. Some of those indicators should certainly be Universal Thermal Climate Index (UTCI) and Tourism Climatic Index (TCI).

The Universal Thermal Climate Index (UTCI) is one of the most frequently used indices in bioclimatic research worldwide and has found its significant application in contemporary tourism studies. *Błażejczyk et al.* (2020) have applied UTCI in the assessment of weather suitability for outdoor tourism in three different European regions (Ukraine, Poland, and Serbia). *Velea et al.* (2024) have conducted a study that addresses the characteristics of a climate service targeting tourists for selected urban destinations in Romania and Italy, with a particular focus on thermal stress information. *Pecelj et al.* (2018) have used UTCI in the geoecological assessment of the local environment for the purposes of recreational tourism. *Nam et al.* (2024) have investigated four European coastal regions in Germany, Spain, France, and Italy to support the planning and development of coastal areas and activities, in particular, beach tourism through a better understanding on the influence of heat stress on tourists, using UTCI. Furthermore, UTCI proved to be effective in the bioclimatic evaluation of rural

and mountain tourist regions, etc. (*Stojićević*, 2016; *Pecelj et al.*, 2020). The importance of UTCI in bioclimatic research is also indicated by the fact that this index is recognized and recommended by the World Meteorological Organization (WMO) (*Kolendowicz et al.*, 2018).

Another bioclimatic index that is strongly related to tourism is the Tourism Climatic Index (TCI). TCI assesses climatic factors that significantly impact both the quality of the tourist experience and tourists' physical comfort (*Mieczkowski*, 1985). This index has been successfully applied in a range of studies on climate and tourism (*Oğur* and *Baycan*, 2024; *Cao* and *Gao*, 2022; *Kovács* and *Unger*, 2014; *Lukić et al.*, 2021; *Masoudi*, 2021; *Scott et al.*, 2016; *Noome* and *Fitchett*, 2019; *Sobhani* and *Safarian Zengir*, 2020; *Mohmoud et al.*, 2019; *El-Masry et al.*, 2022; *Scott et al.*, 2004; *Amelung* and *Viner*, 2006; *Perch-Nielsen et al.*, 2010; *Rutty et al.*, 2020).

This paper aims to apply both UTCI and TCI to evaluate the climate conditions for tourism activities in the Podrinje-Valjevo Region (PVR) in western Serbia. Additionally, it aims to compare these two bioclimatic indices to determine which one offers a more comprehensive understanding of the relationship between climate and tourists' physical comfort throughout the year. Valjevo and Loznica, being the largest settlements in the region, were selected for this climate evaluation due to their availability of the necessary data to calculate these climatic indices.

2. Materials and methods

2.1. Study area

The Podrinje-Valjevo Region (PVR) is located in northwestern Serbia, on the southern border of the Pannonian Basin (*Fig. 1*). Spanning from the Drina River in the west to Ljig and Dičina rivers in the east, the PVR forms a distinct morphostructural unit that gradually slopes northward towards the Jadar-Kolubara basin. The PVR is characterized by relatively low-altitude mountains, with the majority of the terrain (88.6%) ranging between 200 and 800 meters. The extensive length and breadth of the mountain range (117 km), its pronounced topographical features, the proximity to the Drina River, and the submountainous climate in the south have all contributed to the region's climatic diversity and the development of microclimatic zones.

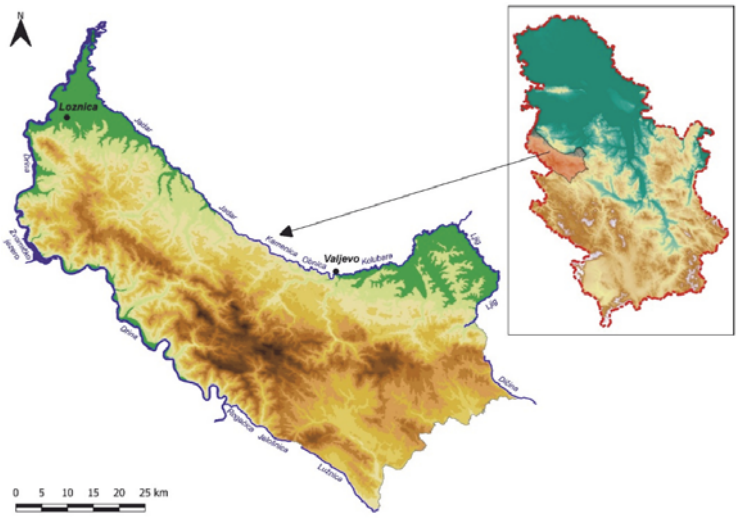

Fig 1. The Podrinje-Valjevo Region.

The PVR is situated within Serbia's humid continental climate zone, characterized by a continental precipitation regime (*Ćirković*, 1977). The region's proximity to the Pannonian Basin and its northern exposure contribute to its continental climate characteristics (*Simić*, 2016). Overall, the humid continental climate is marked by moderately warm summers and moderately cold winters, with relatively mild annual temperature variations (*Ćirković*, 1977; *Pjevač*, 1997; *Pjevač*, 2002). The transitional seasons are lengthy and typically lack extreme temperatures. Precipitation is heaviest at the end of spring and the beginning of summer, while it is least frequent at the start of autumn. In contrast, the subalpine climate found in mountainous areas above 800 meters is characterized by cooler, shorter summers, longer, harsher winters, and smaller annual temperature fluctuations (*Ćirković*, 1977).

In their study of Serbia's climate, *Ducić* and *Radovanović* (2005) classified the PVR as part of climatic subregion A-2. This subregion is defined by an average annual air temperature of approximately 9 °C and a temperature range of 20 °C throughout the year. The average air temperature in the hottest month of the mountains does not surpass 18.4 °C (*Ducić* and *Radovanović*, 2005).

2.2. Data description

The first phase of the research included the collection of meteorological data needed to conduct a bioclimatic analysis. The data set was taken from the Meteorological Yearbooks, for both meteorological stations (Valjevo 44°17'N, 19°55'E, 174 m, and Loznica 44°32'N, 19°14', 121 m), which are prepared and published by the Republic Hydrometeorological Service of Serbia (RHSS). Meteorological yearbooks are published annually, and on this occasion,

publications for the period 1991–2020 were used. To calculate UTCI, the mean monthly values of the following meteorological parameters were used: air temperature (t), relative humidity (f), wind speed at 10 m above the ground (v10m), and cloud cover/cloudiness (N). To determine the UTCI values, the software "Bio Klima 2.6 – Universal tool for bioclimatic and thermophysiological studies" was used. On the other side, to calculate TCI, the mean monthly values of seven climatic parameters were used: average daily maximum air temperature, average daily air temperature, average daily minimum air humidity, average daily air humidity, total precipitation, total insulation, and average wind speed.

2.3. Universal Thermal Climate Index (UTCI)

The Universal Thermal Climate Index (UTCI) is one of the most commonly used bioclimatic indices for determining outdoor thermal comfort in urban environments and is widely used in various fields: urban planning, tourism, ecology, public health, etc. (*Lukić et al.*, 2021). *Błazejczyk et al.* (2013) defined UTCI (°C) as: "the air temperature of the reference condition that causes the same model response as actual conditions". The UTCI was derived from the "Fiala multi-node model" (*Fiala et al.*, 2011; *Blazejczyk et al.*, 2011, 2013). The reference environment for this model was defined by the ISB Commission (International Society of Biometeorology) as: (i) condition of calm air, i.e., wind speed (v10m) 0.5 m/s at 10 m above the ground; (ii) a mean radiant temperature (Tmrt) equal to air temperature; (iii) Relative humidity (f) of 50% (capped at 20 hPa for air temperatures over 29 °C) (*Blazejczyk et al.*, 2011, 2013; *Bröde et al.*, 2013).

It is important to note that for the determination of UTCI, in addition to meteorological parameters, it is necessary to use physiological parameters in order to represent thermal comfort through the assessment of human energy balance, where the metabolic rate (M) has a crucial position (*Bröde et al.*, 2011a, 2011b, *Pecelj et al.*, 2020). Physiological parameters (metabolic rate and thermal properties of clothing) are taken as universal constants in the model due to the evaluation by means of regression equation (*Lukić et al.*, 2021; *Pecelj et al.*, 2020, 2021). This implies an outdoor activity where an average person walks at a speed of 4 km/h (1.1 m/s), resulting in a heat production of 135 W/m2 of metabolic energy and clothing insulation, which is self-adapting according to the environmental conditions (*Pecelj et al.*, 2021; *Havenith et al.*, 2011).

According to UTCI, there are 10 different categories of thermal stress (*Table 1*). The UTCI is calculated as follows: UTCI = f (t,f,v,tmrt), where: t = air temperature (°C), f = relative humidity (%), v = wind speed (m/s), tmrt = mean radiant temperature (°C).

Table 1. UTCI categories of thermal stress (*Blazejczyk et al.*, 2013)

UTCI (°C)	Stress Category
UTCI>46	Extreme heat stress
38<UTCI<46	Very strong heat stress
32<UTCI<38	Strong heat stress
26<UTCI<32	Moderate heat stress
9<UTCI<26	No thermal stress
0<UTCI<9	Slight cold stress
-13<UTCI<0	Moderate cold stress
-27<UTCI<-13	Strong cold stress
-40<UTCI<-27	Very strong cold stress
UTCI<-40	Extreme cold stress

2.4. Tourism Climatic Index (TCI)

The Tourism Climatic Index (TCI) is a bioclimatic indicator that assesses climatic elements most affecting the quality of the tourist experience and tourists' physical comfort (*Mieczkowski*, 1985). As a quantitative and statistical measure of tourist comfort, TCI primarily relies on temperature and relative humidity. However, the calculation of TCI also incorporates three additional climatic elements: insolation, precipitation, and wind speed.

The TCI values are calculated using the following formula:

$$TCI = 2 \times (4CID + CIA + 2P + 2S + W),$$

where CID is the daytime comfort index (obtained by combining the maximum daily temperature and the minimum daily relative air humidity); CIA is the daily comfort index (obtained by combining the average daily temperature and the average daily relative air humidity) (*Fig. 2*); P is the average precipitation (mm); S is the average daily insolation (hours per day), and W is the average wind speed (m/s).

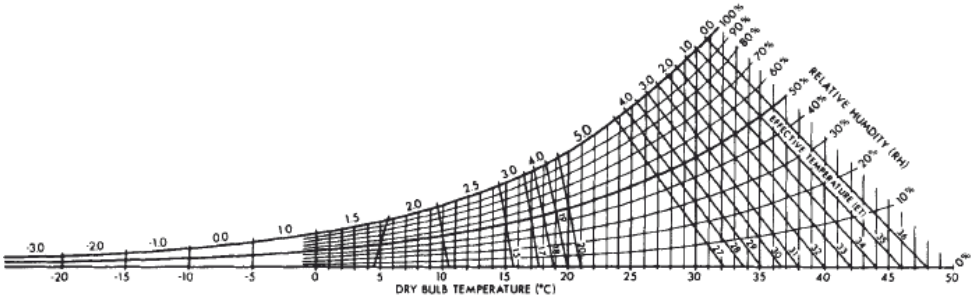

*Fig 2***.** Diagram of CID and CIA (*Mieczkowski*,1985).

Each parameter is scored between -3 (extremely unfavorable) and +5 (optimal) (*Table 2*). The total score is then multiplied by 2, allowing the maximum possible TCI score to be 100. TCI values are categorized as follows: ideal (90–100), excellent (80–89), very good (70–79), good (60–69), acceptable (50–59), possible (40–49), unfavorable (30–39), very unfavorable (20–29), extremely unfavorable (10–19), and impossible (<10) (*Table 3*) (*Mieczkowski*, 1985). It is important to emphasize that, despite being based on biometric literature and the available climate data of the time, the method used to evaluate these subindices and determine the final TCI values remains both descriptive and subjective.

Table 2. Matrix for assessing precipitation, insolation, and wind (*Mieczkowski*, 1985)

Points	P (mm)	S (h)	W (m/s)
5.0	≤14.9	>10	<0.8
4.5	15.0–29.9	9–10	0.8–1.5
4.0	30.0–49.9	8–9	1.6–2.5
3.5	50.0–59.9	7–8	2.6–3.3
3.0	60.0–74.9	6–7	3.4–5.4
2.5	75.0–89.9	5–6	5.5–6.7
2.0	90.0–104.9	4–5	6.8–7.9
1.5	105.9–119.9	3–4	-
1.0	120.0–134.9	2–3	8.0–10.7
0.5	135.0–149.9	1–2	-
0	150.0 or more	<1	>10.7
-0.5	-	-	-
-1.0	210.0–269.9	-	-
-1.5	-	-	-
-2.0	270.0–329.9	-	-

Table 3. Rating categories of TCI (*Mieczkowski,* 1985)

TCI	Category
90–100	ideal
80–89	excellent
70–79	very good
60–69	good
50–59	acceptable
40–49	marginal
30–39	unfavorable
20–29	very unfavorable
10–19	extremely unfavorable
<10	impossible

3. Results and discussion

The following text presents the results of a bioclimatic analysis of the PVR using two indices – UTCI and TCI – on both seasonal and monthly bases. This analysis aims to assess outdoor thermal comfort and tourists' physical comfort in the urban environments of Loznica and Valjevo over a 30-year period (1991–2020).

3.1. UTCI-based seasonal analysis of outdoor thermal comfort in Loznica and Valjevo

The conducted bioclimatic analysis of both urban environments (Loznica and Valjevo) showed a change in outdoor thermal comfort over 30 years (1991–2020). Climatic changes, longer and more frequent heat waves, and the increase in the average annual air temperature are reflected in the increase of UTCI annual and seasonal values – which may have a significant impact on tourist activities in the future.

Based on the data shown in *Table 4*, we can observe a continuous increase in the mean seasonal values of the UTCI during the last three decades. For instance, in Loznica, the average spring value of UTCI in the period 1991–2000 was 18.16 °C, in the period 2001–2010 it was 18.57 °C, and in the period 2011–2020, that value was 19.45 °C. The results for Valjevo show similar trends: during the first decade of research, the average spring UTCI value was 15.73 °C, during the second decade it was 16.7 °C, and during the third decade it reached 17.37 °C. Significant changes in terms of outdoor thermal comfort were also registered during the autumn season: the average autumn UTCI in Loznica for the period 1991–2000 was 18.34 °C, for the period 2001–2010 it was 18.49 °C, while during the period 2011–2020 it was 19.88 °C (the difference between the first and last decade of the researched period amounts to +1.54 °C). The fact that autumns in this part of Serbia are getting warmer, as well as that thermal discomfort is increasing, is also confirmed by the data for Valjevo: the average autumn value of UTCI in the period 1991–2000 was 17.08°C, and during the period 2011–2020, it was 18.62 °C (+1.54 °C). Significant changes were also registered during the summer season, both in Loznica and Valjevo, while they were slightly less pronounced during the winter.

Table 4. Average seasonal UTCI (°C) values in Loznica and Valjevo for the period 1991–2020, and average decade-long UTCI values for the 1st (1991–2000), 2nd (2001–2010), and 3rd decade (2011–2020).

Loznica	**Avg. UTCI winter**	**Avg. UTCI spring**	**Avg. UTCI summer**	**Avg. UTCI autumn**
1991–2000	7.39	18.16	28.71	18.34
2001–2010	5.73	18.57	28.61	18.49
2011–2020	8.10	19.45	29.63	19.88
Average for 1991–2020	7.07	18.72	28.98	18.90
Valjevo	**Avg. UTCI winter**	**Avg. UTCI spring**	**Avg. UTCI summer**	**Avg. UTCI autumn**
1991-2000	5.11	15.73	27.50	17.08
2001-2010	3.14	16.70	27.79	16.96
2011-2020	6.36	17.37	29.05	18.62
Average for 1991–2020	4.87	16.60	28.11	17.55

Fig. 3 shows the average seasonal UTCI in Loznica during the period 1991–2020 with trends. Based on the presented results, we can see that the most significant changes in bioclimatic conditions took place during the autumn months, considering that the average autumn UTCI values during the reference period achieved a positive trend of 0.069 °C/year. The maximum average autumn UTCI in Loznica was measured in 2019 (UTCI=21.13 °C). In the second place is the average spring UTCI, which achieved a positive trend, i.e., an increase in mean values at a rate of 0.062°C/year. The maximum average spring UTCI in Loznica was measured in 2018 (UTCI=21.54 °C). During the previous 30 years, the average summer UTCI increased at a rate of 0.038 °C/year, while the average winter values of the index increased at a rate of 0.028 °C/year. The maximum average summer UTCI was recorded in 2012 (31.45 °C), while the maximum average winter UTCI was recorded in 2014 (11.1 °C).

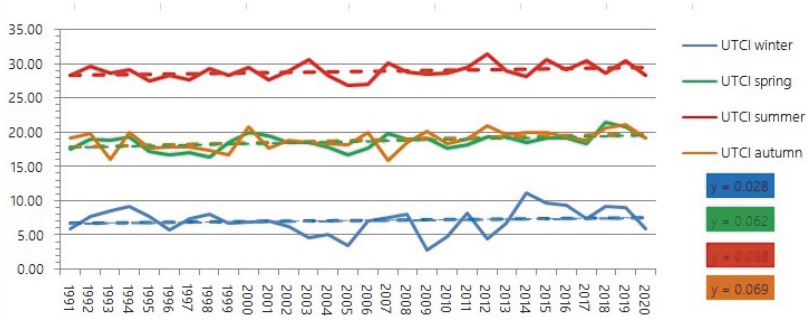

Fig. 3. Average seasonal UTCI during the period 1991–2020 in Loznica with trends.

To obtain a more detailed insight into the recorded changes in thermal comfort at the seasonal level in Loznica, the corresponding months were analyzed separately for each season. *Figs. 4.a* and *4.b*. show average monthly UTCI in the period 1991–2020 with trends for winter months (January, February, and December) and spring months (March, April, and May), while *Figs. 5.c.* and *5.d.* show average monthly UTCI with trends for summer months (June, July, and August) and autumn months (September, October, and November). Observing the obtained results, we can conclude that during all 12 months of the year, an increase in average monthly UTCI values was recorded, although the most noticeable changes were recorded during the autumn and spring months, especially November, March, and April. The average November UTCI value during the previous 30 years grew at a rate of as much as 0.145 °C/year. The average April UTCI values increased at a rate of 0.096 °C/year, while the average March UTCI values increased at a rate of 0.071 °C/year).

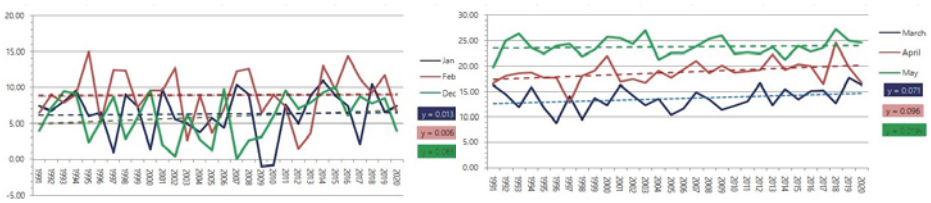

Fig. 4.a and *4.b.* Average monthly UTCI in the period 1991–2020 in Loznica with trends: winter months – January, February, December (left) and spring months – March, April, May (right).

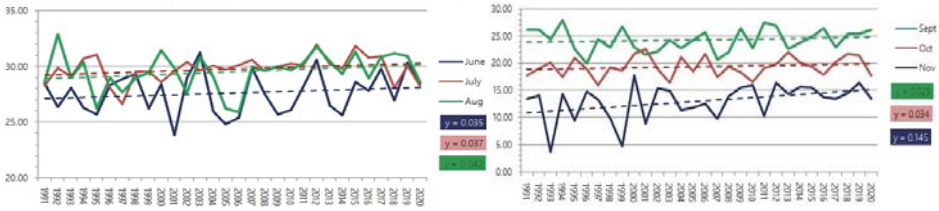

Fig. 5.c. and *5.d.* Average monthly UTCI in the period 1991–2020 in Loznica with trends: summer months – June, July, August (left) and autumn months – September, October, November (right).

Among the winter months, December especially stands out, where the average monthly UTCI values had a positive trend of 0.065 °C/year. The average February values of this index increased the slowest, at a rate of only 0.006 °C/year. The average January UTCI values had a positive trend of

0.013 °C/year. During the summer months, the rising trend of the average monthly UTCI values was relatively similar: for June it was 0.035 °C/year, for July it was 0.037°C/years and for August it was 0.042 °C/year.

Fig. 6 shows the average seasonal UTCI in Valjevo during the period 1991–2020 with trends. As in the case of Loznica, the most significant changes in the bioclimatic conditions of the local urban environment (Valjevo) were registered during autumn. The average autumn UTCI values during the past 30 years were increased at a rate of 0.076 °C/year. The maximum average autumn UTCI in Valjevo was recorded in 2019 (20.63 °C). The same growth rate of average seasonal values was reached by summer and spring UTCI with a positive trend of 0.073 °C/year. The maximum average summer UTCI in Valjevo was recorded in 2012 (30.81 °C), while the maximum average spring UTCI was recorded in 2018 (20.39 °C). The average winter UTCI has a positive growth trend of 0.063 °C/year. Its maximum seasonal value was measured in 2014 (9.21 °C).

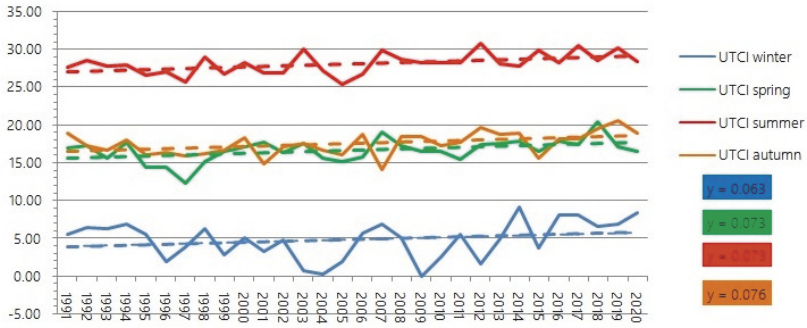

Fig. 6. Average seasonal UTCI during the period 1991–2020 in Valjevo with trends.

Figs. 7.a and *7.b.* show average monthly UTCI in Valjevo (1991–2020) with trends for winter months (January, February, and December) and spring months (March, April, and May), while *Figs. 8.c.* and *8.d.* show average monthly UTCI with trends for summer months (June, July, and August) and autumn months (September, Octobe,r and November). If we compare Valjevo and Loznica, we can conclude that more significant changes took place in Valjevo, where the average monthly values of the index grew at much higher rates. That difference is especially noticeable when we look at the summer months: for June the trend is 0.044 °C/year, for July it is 0.074 °C/year, and for August it is 0.103 °C/year. Considering the given values, we can expect more bioclimatically unfavorable summers in Valjevo, with more pronounced thermal stress that can have an impact

on public health, tourism, and recreation. Apart from the summer months, autumn is also getting warmer: the average September UTCI value has a rising trend of 0.054 °C/year, the average October UTCI value has a rising trend of 0.061 °C/year, while the average November UTCI has a rising trend of 0.112 °C/year. Among the spring months, April stands out, with a trend of growth in average monthly UTCI values at a rate of 0.128 °C/year. Among winter months, December stands out, with a trend of growth in average monthly UTCI values at a rate of 0.133 °C/year.

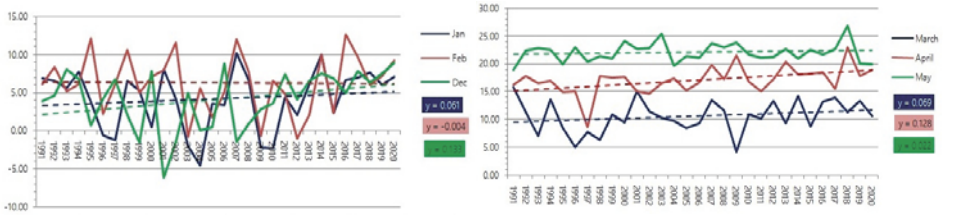

Fig. 7.a and *7.b.* Average monthly UTCI in the period 1991–2020 in Valjevo with trends: winter months – January, February, December (left) and spring months – March, April, May (right).

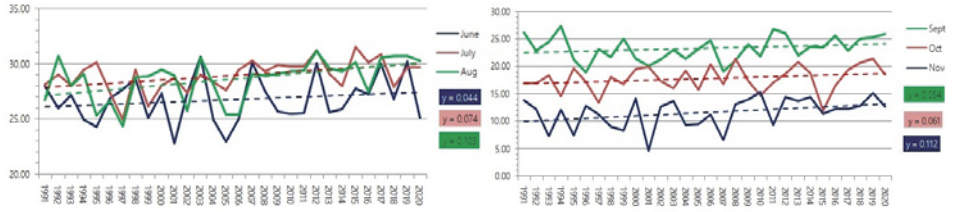

Fig. 8.c. and *8.d.* Average monthly UTCI in the period 1991–2020 in Loznica with trends: summer months – June, July, August (left) and autumn months – September, October, November (right)

The findings of this research are consistent with and further support the results of previous studies on climate, bioclimatic conditions, biometeorology, urban microclimates, and thermal comfort across Serbia. *Bajat et al.* (2014) analyzed the mean monthly air temperatures at 64 meteorological stations, including those in Loznica and Valjevo, over the period 1961–2010. Their research revealed a clear warming trend, particularly after 1989, with nearly all stations showing an increase in temperature ranging from 0.18 °C/decade to 3.63 °C/decade (or 0.36 °C/year). Similarly, *Unkašević* and *Tošić* (2013) analyzed daily minimum and maximum temperatures from 15 meteorological stations,

including Loznica, over the period 1949–2009. Their findings highlighted a pronounced warming trend in Serbia's climate, which became particularly evident after 2000. In addition to the rise in mean daily temperatures and extreme temperature values, they also observed an increase in the number of "summer drop", and "tropical days" and "tropical nights", while the number of "ice days" decreased (*Unkašević* and *Tošić*, 2013). In his doctoral dissertation, *Stojićević* (2016) examined the annual and seasonal variations of the bioclimatic index UTCI in western Serbia from 1979 to 2013. Since the Podrinje-Valjevo Region is part of western Serbia and this study covers the period after 2013, the results were compared with those of Stojićević. Both studies observed similar trends, confirming the rising temperatures and changing bioclimatic conditions in the region. *Stojićević* (2016) has showed that in the area of western Serbia, the mean annual values of the Physiological Equivalent Temperature (PET) index are growing at an average rate of 0.065 °C/year. During the summer months, the mean values of the PET index grew at a rate of 0.098 °C/year. In the area of western Serbia, the statistically significant trend of the PET index value during the spring months was 0.081 °C/year, and during the autumn it was 0.042 °C/year. If we look at the annual and seasonal variations of the UTCI bioclimatic index during the researched period, an average increase in the mean annual UTCI values by 0.052 °C/year was registered. Autumn values of the UTCI index also record a rising trend of 0.037 °C/year, spring values show 0.064 °C/year, while summer UTCI values show a growing trend of 0.057 °C/year. Similar findings were also noted in a study by *Lukić* and *Đurić* (2021), which focused on thermal discomfort during the summer months over a ten-year period (2009–2018) in the cities of Loznica (Serbia) and Bijeljina (BiH). Their results of daily and monthly UTCI values revealed an increase in the number of days with "moderate", "strong", and "very strong" heat stresses.

3.2. TCI analysis of tourists' physical comfort in Loznica and Valjevo

In the PVR, TCI was calculated for the climatological stations in Valjevo and Loznica over a 30-year period (1991–2020) and for each decade within this span (1991–2000, 2001–2010, 2011–2020). *Table 5* presents the climate indicators used for TCI calculations at these stations, along with their average monthly values for the 30-year period. The TCI calculations revealed which months are most and least favorable for outdoor sports and recreational activities.

The TCI values for the period from 1991 to 2020 range from "marginal" to "excellent", indicating that the climate of the PVR is generally favorable for outdoor tourism activities. According to TCI results, the winter months – December, January, and February – are the least favorable for outdoor tourism due to their low temperatures, high relative humidity, and reduced sunlight. However, despite being the least favorable according to TCI, these months also bring snowfall, creating ideal conditions for snow-based sports and recreational activities in the region's mountainous areas. This is one of the major shortcomings of TCI that is observed in various studies that have employed this index (*Matzarakis*, 2006).

Table 5. Average monthly values of climatic parameters for Valjevo and Loznica

Valjevo	**I**	**II**	**III**	**IV**	**V**	**VI**	**VII**	**VIII**	**IX**	**X**	**XI**	**XI**
T_{max}	5.8	8.4	13.2	18.4	22.8	26.5	28.7	29.0	23.9	18.8	12.9	6.5
T_{avg}	1.0	2.9	7.2	12.1	16.9	20.7	22.6	22.3	17.2	12.0	7.0	2.1
R_{min}	38.1	28.7	32.1	23.8	27.1	27.9	27.0	25.7	27.0	29.7	32.3	38.5
R_{avg}	83.2	77.3	70.4	68.3	70.0	69.3	67.0	67.7	73.8	78.6	80.8	83.9
P	49.0	49.1	58.2	58.5	87.6	102.8	76.5	66.3	64.9	65.3	54.2	60.1
S	2.4	3.5	4.8	6.1	7.2	8.3	9.5	8.9	6.6	5.0	3.2	2.1
W	1.1	1.4	1.8	1.7	1.5	1.5	1.5	1.5	1.4	1.2	1.2	1.2
Loznica	**I**	**II**	**III**	**IV**	**V**	**VI**	**VII**	**VIII**	**IX**	**X**	**XI**	**XI**
T_{max}	5.7	8.4	13.4	18.6	23.2	26.8	28.8	29.2	24.0	19.0	12.6	6.5
T_{avg}	1.4	3.2	7.5	12.4	17.1	20.9	22.5	22.2	17.2	12.3	7.3	2.5
R_{min}	41.2	31.2	23.7	25.1	27.9	31.4	29.9	28.5	28.5	31.3	34.0	41.7
R_{avg}	82.8	77.2	69.7	67.8	69.4	69.7	68.1	69.0	74.5	79.3	81.6	83.5
P	63.0	54.5	65.0	63.4	90.9	107.2	80.4	69.9	71.1	74.1	68.8	72.3
S	2.1	3.2	4.8	6.2	7.3	8.4	9.5	9.1	6.5	4.8	2.8	1.7
W	0.7	0.9	1.1	1.0	1.0	1.0	1.0	0.9	0.7	0.6	0.6	0.8

T_{max} – maximum daily air temperature (°C), T_{avg} – average daily air temperature (°C), R_{min} – minimum daily relative humidity (%), R_{avg} – average daily relative humidity (%),
P – total precipitation (mm), S – total daily insolation (h), W– average wind speed (m/s).
Source: Meteorological yearbook of RHSS (1991–2020).

March and November are characterized by "acceptable" conditions for tourist comfort for both urban environments, with TCI values ranging from 50 to 59. "Good" climate conditions for tourism begin in April at both climatological stations. May is considered "very good" for tourist activities both in Loznica and Valjevo. The summer months – June, July, and August, as well as October – provide "excellent" conditions for outdoor tourism, with TCI values ranging from 80 to 86 for both urban environments (*Table 6*, *Fig. 9*).

Table 6. TCI values for Loznica and Valjevo, presented by decade and as a 30-year average (1991–2020)

Loznica	I	II	III	IV	V	VI	VII	VIII	IX	X	XI	XII	x̄
1991-2000	45	53	55	66	82	82	86	88	81	71	48	41	66.5
2001-2010	45	47	53	68	81	81	87	85	78	65	52	40	65.1
2011-2020	45	44	55	74	71	83	85	85	84	73	52	45	66.3
1991–2020	45	48	54	69	78	82	86	86	81	69	50	42	66
Valjevo	**I**	**II**	**III**	**IV**	**V**	**VI**	**VII**	**VIII**	**IX**	**X**	**XI**	**XII**	**x̄**
1991-2000	48	52	56	61	81	81	87	87	80	62	53	44	66
2001-2010	48	50	52	63	82	81	86	84	75	60	51	42	64.5
2011-2020	46	47	54	71	70	85	84	87	85	74	55	46	67
1991–2020	47	49	54	65	78	82	85	86	80	65	53	44	65.8

Bioclimatic conditions for tourist activities: marginal (40–49), acceptable (50–59), good (60–69), very good (70–79), excellent (80–89). Source: independent data processing based on the data from Meteorological yearbook of RHSS (1991–2020).

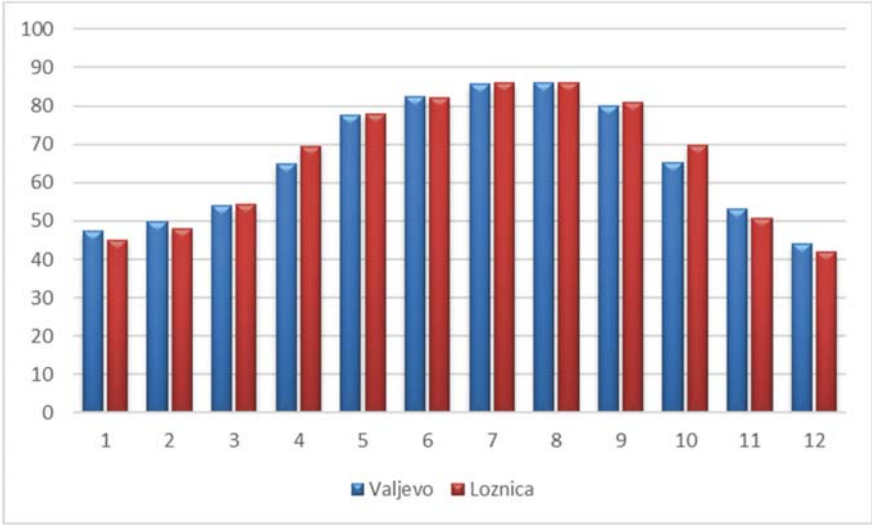

Fig. 9. TCI chart for the PVR (Valjevo and Loznica) over the 30-year period of 1991–2020.

High TCI values at the end of spring, during summer, and at the beginning of autumn are closely tied to the climatic conditions of these periods. During these periods, air temperatures rise, peaking in July and August. Conversely, relative humidity decreases starting in spring and hits its lowest in summer. Additionally, insolation is at its highest during this period. Interestingly, while May and June receive the most precipitation across all meteorological stations, TCI values for these months remain "very good" or "excellent". This is because the precipitation

during these months typically falls as brief showers, providing a refreshing effect and generally benefiting outdoor activities for tourists.

Table 6 also presents the TCI values for Loznica and Valjevo, broken down by three decades over the 30-year span from 1991 to 2020. The data for both climatological stations show that in the first decade (1991–2000), the TCI values were "excellent" from May to September. In the second decade (2001–2010), the TCI values for both climatological stations were "excellent" from May to August, "very good" in September, and "good" in April and October. However, this pattern has changed in the last decade (2011–2020), primarily due to the significant effects of climate change. The third decade reveals notable changes in TCI values for both climatological stations, with March and November rated as "good", April, May, and October as "very good", and the summer months as "excellent" for tourism and physical comfort.

3.3. Comparative analysis of the climate index results for the PVR

The application of the UTCI and TCI climate indices to the PVR has revealed some similar results. Both indices indicate that spring and autumn are the most favourable seasons for outdoor tourist activities. However, while TCI suggests that summer is particularly ideal for tourist activities and tourists' thermal comfort, UTCI indicates that summer months may induce moderate heat stress, leading to thermal discomfort for tourists.

The TCI index relies solely on climatic parameters and their mean monthly values, whereas the UTCI is a more complex bioclimatic index that incorporates both meteorological and physiological factors (such as metabolic rate and clothing thermal properties). Compared to other bioclimatic indices, the UTCI more effectively represents the temporal variability of thermal conditions, being more sensitive to outdoor factors like changes in air temperature, relative humidity, solar radiation, and wind speed (*Lukić et al*., 2021; *Pecelj et al.*, 2021; *Blazejczyk et al*., 2011). Moreover, the UTCI is particularly useful for detailed bioclimatic analysis based on daily and hourly meteorological data, offering a clearer picture of how bioclimatic conditions at a given location fluctuate throughout the day – from morning to evening and even at night. In contrast, the TCI provides a broader overview of the bioclimatic conditions in a specific area, without the ability to analyze the finer variability that the UTCI can reveal.

In most European countries, including Serbia, the summer season represents the peak of the tourist season. The TCI indicates that these months are generally the most favorable for outdoor tourist activities in the PVR. However, the effects of climate change have led to increasingly unfavorable bioclimatic conditions and extreme heat stress and thermal discomfort during July and August, as confirmed by the UTCI results. The thermal discomfort experienced in these peak summer months presents a health risk not only to vulnerable populations—such as the elderly, those with chronic health conditions, children, and pregnant women—but

also to the general public, including athletes and recreational tourists. This was particularly highlighted by *Obradović-Arsić* and *Gledović* (2012), who studied the effects of climate on public health. They found that while the human body can usually adapt to outdoor conditions, sudden and extreme weather changes, such as high temperatures and heatwaves, can disrupt thermoregulation. These disruptions may cause biochemical changes, resulting in both physical and psychological health issues. The severity of these effects varies depending on age, health status, and individual characteristics. Additionally, a study by *Giannopoulou et al.* (2014) on air temperature and humidity's influence on human thermal comfort during the summer found, that when thermal discomfort persists into the night, sleep becomes difficult, leading to fatigue the next day. In such prolonged discomfort, the body does not have the opportunity to recover, resulting in significant thermal stress that impacts even healthy individuals with high physical capabilities.

Given these considerations, from a bioclimatic standpoint, summer months are the least favorable for tourists' outdoor activities due to the highest likelihood of health risks related to heat stress and elevated temperatures (*Savić et al.*, 2018). With the expected increase in heat stress in the PVR, as shown by the rising trend in average August UTCI values – 0.103 °C/year (or 1.03 °C/dec) in Valjevo and 0.042 °C/year (or 0.42 °C/dec) in Loznica –, it is recommended that tourists avoid engaging in physical activities, including walking, between 9 AM and 6 PM during the summer months.

Considering the proximity of Banja Koviljača Spa, a key center for medical and health tourism, it is important for tourism development experts to examine the connection between weather conditions and the onset of specific health issues. To support this, it is recommended to refer to the study by the Belgrade Emergency Medical Institute and the Republic Hydrometeorological Service of Serbia (*Grupa autora*, 1988), which identified diseases affected by weather changes, referred to as meteorotropic diseases. These include various heart conditions, high blood pressure, strokes, respiratory infections, asthma, rheumatic diseases, and more. This is particularly relevant for the elderly, individuals with chronic health conditions, and children visiting the Specialized Rehabilitation Hospital in Banja Koviljača.

While TCI is a commonly used climate index for tourism and can indicate favorable periods for tourist activities, this study reveals that the tourism industry cannot rely solely on TCI results, especially during the summer months. This index does not effectively capture thermal comfort for tourists, especially as temperatures rise each year. Therefore, it is necessary to use newer bioclimatic indices, such as UTCI, for a more thorough assessment of a region's climate for tourism activities and associated thermal stress. However, neither TCI nor UTCI are reliable for assessing winter tourism conditions. Although UTCI values during winter months indicate the potential for optimal tourist thermal comfort, this also points to rising temperatures due to climate change. This trend poses a threat to winter sports

tourism, and if it continues, the PVR may be probably unable to support nature-based winter sports activities in the future. This will particularly affect the Maljen mountain and its Divčibare ski resort, a well-known winter sports destination in the PVR. The increasing winter temperatures are expected to raise the demand for artificial snowmaking, which could drive up ski pass prices and make it financially unfeasible for tourists (*Joksimović et al.,* 2020). Even with extensive artificial snow production, the rising winter temperatures could make it increasingly challenging to sustain winter sports tourism. As a result, there is a considerable risk that, in the future, Maljen could lose its Divčibare ski resort. Given these projections, the Maljen mountain and the entire Podrinje-Valjevo Region will need to explore alternative forms of tourism during the winter months in the coming years.

4. Conclusion

In this study, two climate indices (TCI and UTCI) were evaluated to assess tourism conditions in the Podrinje-Valjevo Region. Based on the conducted bioclimatic analysis, both climate indices have proved that the spring and autumn months are the most favorable for performing tourist activities, recreation, and being outdoors. However, while the results obtained from TCI assessment show that the summer months are the most favorable and "excellent" for outdoor activities, UTCI has proved otherwise, emphasizing the high potential of thermal discomfort for tourists due to moderate heat stress and high air temperatures. The disparity in results between the TCI and UTCI can be attributed to the fact that the TCI is based solely on climatic parameters and their mean monthly values, whereas the UTCI is a more complex bioclimatic index that takes into account both meteorological and physiological factors (such as metabolic rate and clothing thermal properties).

According to the UTCI results, the most favorable months for outdoor tourism activities are April, May, September, and October in both Loznica and Valjevo. Additionally, a notable increase in UTCI values was observed in November from 1991 to 2020. Specifically, the average November UTCI value in Loznica increased by 0.145 °C per year, while in Valjevo, it rose by 0.112 °C per year. The highest UTCI values, indicating the most severe heat stress, are recorded during the summer months, particularly July and August, posing potential health risks. This is of particular concern for tourists visiting the PVR during the summer, particularly vulnerable groups such as the elderly, those with chronic health conditions, children, and pregnant women. Therefore, it is recommended that tourists avoid physical activities, including walking, between 9 AM and 6 PM during the summer months.

With the recorded trends of increasing summer UTCI values in both examined urban environments, we can expect even more pronounced thermal discomfort in the future. The lowest monthly and seasonal UTCI values were

measured as expected during the winter months, when cold stress categories of thermal comfort were the most prevalent – which means that the winter months are also less favorable for tourist purposes from the bioclimatic viewpoint. However, since winter sports tourism is inherently dependent on snowfall and low temperatures, cold stress is expected and does not pose a significant barrier to winter sports activities in the PVR. Nevertheless, winters in western Serbia, i.e., Podrinje-Valjevo Region, are getting warmer, as it is shown by the increasing trends of the December's UTCI values (in Loznica 0.065 °C/year; in Valjevo 0.133 °C/year). This warming trend raises concerns about the future viability of nature-based winter sports in this region.

In a changing climate, the frequency of extreme weather events and heat waves is increasing. These global shifts are also affecting local environments (*Čegar et al.*, 2023; *Malinović-Milićević et al.*, 2015), influencing thermal comfort and bioclimatic conditions at tourist sites. *Nam et al.* (2024) emphasizes that understanding how climate change will influence thermal comfort is crucial for the tourism and hospitality sectors to identify risks and opportunities, and maintain competitiveness. While climate is just one factor influencing tourist behavior, it has a significant impact on the overall experience at a destination. By understanding the region's optimal climatic conditions and adjusting tourism offerings accordingly throughout the year, visitors satisfaction can be greatly enhanced. Some studies also suggest that tourists may begin to prefer travel during seasons with lower risks of heat stress (*Ebi et al.*, 2021; *Nam et al.*, 2024). Therefore, incorporating bioclimatic research into tourism planning is essential for the PVR. Since autumn and spring are the most favorable seasons for outdoor tourism in this region, it is recommended that local tourism stakeholders focus on diversifying tourism offerings during these periods. Key areas for development could include ecotourism, rural tourism, adventure tourism (such as kayaking, climbing, cave exploration), and cultural tourism, among others.

This study focused on assessing TCI and UTCI for tourism activities in Loznica and Valjevo, two urban areas in the Podrinje-Valjevo Region. These cities were chosen because they are the only ones in the region with available data necessary for applying bioclimate indices. However, the study does not cover the bioclimatic conditions of the entire region due to the absence of climatological stations in the mountainous areas of the PVR. This is a significant limitation of the paper, as it prevents a comprehensive understanding of the region's bioclimatic conditions and their impact on tourism activities. Future research will aim to include climate evaluations of these mountainous areas once data becomes available, and to investigate the correlation between tourist visits over the past 30 years and climate indices in the PVR.

Acknowledgements: The study was supported by the Ministry of Education, Science and Technological Development of the Republic of Serbia (Contract number 451/03/65/2024-03/200091).

References

Amelung, B., and *Viner, D.,* 2006: Mediterranean Tourism: Exploring the Future with the Tourism Climatic Index. *J. Sustain. Tourism 14*(4), 349–366. https://doi.org/10.2167/jost549.0

Bajat, B., Blagojević, D., Kilibarda, M., Luković, J., and *Tošić, I.,* 2014: Spatial analysis of the temperature trends in Serbia during the period 1961–2010. *Theor Appl Climatol*, 121, 289–301. https://doi.org/10.1007/s00704-014-1243-7

Becker, S., 1998: Beach Comfort Index – A New Approach to Evaluate the Thermal Conditions of Beach Holiday Resorts Using a South African Example. *GeoJournal 44*, 297–307. https://doi.org/10.1023/A:1006871805262

Besancenot, J., Mouiner, J., and *De Lavenne, F.*, 1978: Les conditions climatiques du tourisme littoral. *Norois 99*, 357–382.

Bigano, A., Hamilton, J.M. and *Tol, R.S.J.,* 2006: The Impact of Climate on Holiday Destination Choice. *Climatic Change 76*, 389–406. https://doi.org/10.1007/s10584-005-9015-0

Blazejczyk, K., Jendritzky, G., Bröde, P., Fiala, D., Havenith, G., Epstein, Y., Psikuta, A., and *Kampmann, B.*, 2013: An introduction to the Universal Thermal Climate Index (UTCI). *Geogr. Pol. 86*, 5–10. https://doi.org/GPol.2013.1

Blazejczyk, K., Epstein, Y., Jendritzky, G., Staiger, H., and *Tinz, B.*, 2011: Comparison of UTCI to selected thermal indices. *Int. J. Biometeorol. 56*, 515–535. https://doi.org/10.1007/s00484-011-0453-2

Blazejczyk, A., Pecelj, M., Skrynyk, O., Blazejczyk, K., and *Skrynyk, O.*, 2020: Weather suitability for outdoor tourism in three European regions in first decades of the twenty-first century. *Int. J. Biometeorol.*, Special issue: 1st European biometeorologists' meeting, https://doi.org/10.1007/s00484-020-01984-z

Bröde, P., Fiala, D., Blazejczyk, K., Holmér, I., Jendritzky, G., Kampmann, B., Tinz, B., and *Havenith, G.,* 2011a: Deriving the operational procedure for the Universal Thermal Climate Index (UTCI). *Int. J. Biometeorol. 56*, 481–494. https://doi.org/10.1007/s00484-011-0454-1

Bröde, P., Krüger, E., Rossi, F.A., and *Fiala, D.*, 2011b: Predicting urban outdoor thermal comfort by the Universal Thermal Climate Index UTCI - a case study in Southern Brazil. *Int. J. Biometeorol. 56*, 471–480. https://doi.org/10.1007/s00484-011-0452-3

Bröde, P., Blazejczyk, K., Fiala, D., Havenith, G., Holmér, I., Jendritzky, G., Kuklane, K., and *Kampmann, B.*, 2013: The Universal Thermal Climate Index UTCI Compared to Ergonomics Standards for Assessing the Thermal Environment. *Ind. Health 51*, 16–24. https://doi.org/10.2486/indhealth.2012-0098

Cao, K., and *Gao, J.*, 2022: Assessment of climatic conditions for tourism in Xinjiang, China. *Open Geosciences 14(1)*, 2022, 382–392. https://doi.org/10.1515/geo-2022-0362

Ćirković, Lj., 1977: Klimatske osobine Zapadne Srbije. *Zbornik radova Geografskog instituta „Jovan Cvijić" SANU 29*, 105–133.

Čegar, N., Durlević, U., Dobrić, M., and *Vukašinović, S.*, 2023: A statistical analysis of temperature and precipitation in Belgrade, Serbia (1961–2020). *Forum Geografic 22(1)*, 5–15. https://doi.org/10.5775/fg.2023.090.i

Dann, G. M., 1981: Tourist Motivation an Appraisal. *Annals of Tourism Research 8*, 187–219. https://doi.org/10.1016/0160-7383(81)90082-7

Ducić, V., and *Radovanović, M.*, 2005: *Klima Srbije*. Zavod za udžbenike, Beograd.

Ebi, K., Capon, A., Berry, P., Broderick, C., de Dear, R., Havenith, G., Honda, Y., Kovats R., Ma, W., and *Malik, A.*, 2021: Hot weather and heat extremes: health risks. *Heath and Health 398*, 10301, 698–708. https://doi.org/10.1016/S0140-6736(21)01208-3

El-Masry, E.A., El-Sayed, M.K., Awad, M.A., El-Sammak, A.A., and *El Sabarouti, M.A.*, 2022: Vulnerability of tourism to climate change on the Mediterranean coastal area of El Hammam–EL Alamein, Egypt. *Environ Dev Sustain 24*, 1145–1165. https://doi.org/10.1007/s10668-021-01488-9

Fiala, D., Havenith, G., Bröde, P., Kampmann, B., and *Jendritzky, G.*, 2011: UTCI-Fiala multi-node model of human heat transfer and temperature regulation. *Int. J. Biometeorol. 56*, 429–441. https://doi.org/10.1007/s00484-011-0424-7

de Freitas, C.R., 1990: Recreation Climate Assessment. *International J. Climatol. 10*, 89–103. https://doi.org/10.1002/joc.3370100110

de Freitas, C.R., Scott, D., and *McBoyle, G.*, 2008: A second generation climate index for tourism (CIT): specification and verification. *Int J Biometeorol 52(5)*, 399–407. https://doi.org/10.1007/s00484-007-0134-3

Giannopoulou, K., Livada, I., Santamouris, M., Saliari, M., Assimakopoulos, M., and *Caouris, Y.*, 2014: The influence of air temperature and humidity on human thermal comfort over the greater Athens area. *Journal Sustainable Cities and Society*, 10, 184–194. https://doi.org/10.1016/j.scs.2013.09.004

Grillakis, M.G., Koutroulis, A.G., Seiradakis, K.D., and *Tsanis, I.K.*, 2016: Implications of 2°C global warming in European summer tourism. *Clim. Serv. 1*, 30–38. https://doi.org/10.1016/j.cliser.2016.01.002

Grupa autora, 1988: Uticaj vremena na zdravlje ljudi – Studija Gradskog zavoda za hitnu i medicinsku pomoć Beograd i Republičkog hidrometeorološkog zavoda SR Srbije. Naučna knjiga, Beograd.

Havenith, G., Fiala, D., Blazejczyk, K., Richards, M., Bröde, P., Holmér, I., Rintamaki, H., Benshabat, Y., and *Jendritzky, G.*, 2011: The UTCI-clothing model. *Int. J. Biometeorol. 56*, 461–470. https://doi.org/10.1007/s00484-011-0451-4

Hu, Y. and *Ritchie, J.R.B.*, 1993: Measuring Destination Attractiveness: A Contextual Approach. *Journal of Travel Research 32*, 25–34. https://doi.org/10.1177/004728759303200204

Joksimović, M., Gajić, M., Vujadinović, S., Milenković, J., and *Malinić, V.,* 2020: Artificial Snowmaking: Winter Sports Between State-Owned Company Policy and Tourist Demand. *J. Hospital. Tourism Res. 45*, 1170–1187. https://doi.org/10.1177/1096348020957072

Kolendowicz, L., Półrolniczak, M., Szyga-Pluta, K., and *Bednorz, E.*, 2018: Human-biometeorological conditions in the southern Baltic coast based on the universal thermal climate index (UTCI). *Theor. Appl. Clim, 134*, 363–379. https://doi.org/10.1007/s00704-017-2279-2

Kovács, A., and *Unger, J.*, 2014: Modification of the Tourism Climatic Index to Central European climatic conditions – examples. *Időjárás 118(2)*, 147–166.

Lise, W., and *Tol, R.S.J.*, 2002: Impact of Climate on Tourist Demand. *Climatic Change 55*, 429–449. https://doi.org/10.1023/A:1020728021446

Lohmann, M., and *Kaim, E.,* 1999: Weather and holiday destination preferences image, attitude and experience. *The Tourist Review 54(2)*, 54–64. https://doi.org/10.1108/eb058303

Lukić, D., Petrović, M., Radovanović, M.M., Tretiakova, T.N., and *Syromiatnikova J.A.,* 2021: The Role of TCI and TCCI Indexes in Regional Tourism Planning. *European Journal of Geography 12(4)*, 006–015. https://doi.org/10.48088/ejg.d.luk.12.4.006.015

Lukić, M., Filipović, D., Pecelj, M., Crnogorac, Lj., Lukić, B., Divjak, L., Lukić, A., and *Vučićević A.,* 2021: Assessment of Outdoor Thermal Comfort in Serbia's Urban Environments during Different Seasons. *Atmosphere 12(8)*, 1084, https://doi.org/10.3390/atmos12081084

Lukić, M., and *Đurić, D.*, 2021: Comparative analysis of the outdoor thermal comfort in urban environments - case study of Bijeljina and Loznica. *Collection of papers „the 5th Serbian congress of geographers - Innovative approach and perspectives of the applied geography"*. University of Novi Sad, Faculty of Sciences, Department of geography, tourism and hotel management, Novi Sad, 361–370, ISBN 978-86-7031-589-1

Malinović-Milicević, S., Radovanović, M., Stanojević, G., and *Milovanović, B.*, 2015: Recent changes in Serbian climate extreme indices from 1961 to 2010. *Theor Appl Climatol 124*. https://doi.org/10.1007/s00704-015-1491-1

Masoudi, M., 2021: Estimation of the spatial climate comfort distribution using tourism climate index (TCI) and inverse distance weighting (IDW) (case study: Fars Province, Iran). *Arab J Geosci 14*, 363. https://doi.org/10.1007/s12517-021-06605-6

Matzarakis, A., 2006: Weather and Climate – Related Information for Tourism. *Tourism and Hospitality Planning & Development 3*, 99–115. https://doi.org/10.1080/14790530600938279

Mieczkowski, Z., 1985: The Tourism Climatic Index: A Method of Evaluating World Climates for Tourism. *The Canadian Geographer/Le Géographe canadien 29(3)*, 220–233.

Mohmoud, D., Gamal, G., and *Abou El Seoud, T.*, 2019: The Potential Impact of Climate Change on Hurghada City, Egypt, using Tourism Climate Index. *GeoJournal of Tourism and Geosites 25*, 496–508. https://doi.org/10.30892/gtg.25218-376

Nam, C., Lierhammer, L., Buntemeyer, L., Evadzi, P., Cabana, D., and *Celliers, L.*, 2024: Changes in universal thermal climate index from regional climate model projections over European beaches. *Climate Services 34*, 100447. https://doi.org/10.1016/j.cliser.2024.100447

Noome, K., and *Fitchett, J.M*., 2019: An assessment of the climatic suitability of Afriski Mountain Resort for outdoor tourism using the Tourism Climate Index (TCI). *J. Mt. Sci 16*, 2453–2469. https://doi.org/10.1007/s11629-019-5725-z

Obradović-Arsić, D., and *Gledović, Z*., 2012: *Medicinska geografija*. Univerzitet u Beogradu – Geografski fakultet, Beograd.

Oğur, A.A., and *Baycan, T.*, 2024: How to manage tourism development based on impacts of climate change in Turkiye. *Asia-Pacific Journal of Regional Science*, 1–24.

Pecelj, M.M., Lukić, M., Vučičević A, De Una-Alvarez, E., Esteves da Silva, C.G.J., Freinkin, I., Ciganović, S., and *Bogdanović, U.*, 2018: Geoecological evaluation of local surroundings for the purposes of recreational tourism. *Journal of Geografical Institute "Jovan Cvijic" SASA 68(2)*, 215–231. https://doi.org/10.2298/IJGI1802215P

Pecelj, M.M., Lukić, M.Z., Filipović, D.J., Protić, B., and *Bogdanović, U.M.*, 2020: Analysis of the Universal Thermal Climate Index during heat waves in Serbia. *Nat. Hazards Earth Syst. Sci. 20*, 2021–2036. https://doi.org/10.5194/nhess-20-2021-2020

Pecelj, M., Matzarakis, A., Vujadinović, M., Radovanović, M., Vagić, N., Đurić, D., and *Cvetković, M.,* 2021: Temporal Analysis of Urban-Suburban PET, mPET and UTCI Indices in Belgrade (Serbia). *Atmosphere 12*, 916. https://doi.org/10.3390/atmos12070916

Perch-Nielsen, S.L., Amelung, B. and *Knutti, R.*, 2010: Future climate resources for tourism in Europe based on the daily Tourism Climatic Index. *Climatic Change 103*, 363–381. https://doi.org/10.1007/s10584-009-9772-2

Pjevač, N., 1997: *Turistički potencijali Valjevskih planina*. Univerzitet u Beogradu – Geografski fakultet, Beograd, doktorska disertacija.

Pjevač, N., 2002: *Valjevske planine – mogućnosti razvoja turizma*. Zadužbina Andrejević, Beograd.

Polish Academy of Sciences, Institute of Geography and Spatial organization, Department of Geoecology and Climatology, 2010: BioKlima (Version 2.6), author: Prof. Krzysztof Błażejczyk, PhD. Retrieved from https://www.igipz.pan.pl/Bioklima-zgik.html

Republic Hydrometeorological Service of Serbia, 1991–2020: Meteorološki godišnjak - klimatološki podaci [Meteorological Yearbook - climatological data]. Retrieved from http://www.hidmet.gov.rs/latin/meteorologija/klimatologija_godisnjaci.php

Rutty, M., Scott, D., Matthews, L., Burrowes, R., Trotman, A., Mahon, R., and *Charles, A.,* 2020: An Inter-Comparison of the Holiday Climate Index (HCI:Beach) and the Tourism Climate Index (TCI) to Explain Canadian Tourism Arrivals to the Caribbean. *Atmosphere 11*, 412. https://doi.org/10.3390/atmos11040412

Savić, S., Marković, V.; Šećerov, I., Pavić, D., Arsenović, D., Milosevic, D., Dolinaj, D., Nagy, I., and *Pantelić, M.*, 2018: Heat wave risk assessment and mapping in urban areas: Case study for a midsized Central European city, Novi Sad (Serbia). *Nat. Hazards 91*, 891–911. https://doi.org/10.1007/s11069-017-3160-4

Scott, D., McBoyle, G., and *Schwartzentruber, M.*, 2004: Climate change and the distribution of climatic resources for tourism in North America. *Climate Research 27*, 105–117. doi:10.3354/cr027105

Scott, D., Rutty, M., Amelung, B., and *Tang, M.,* 2016: An Inter-Comparison of the Holiday Climate Index (HCI) and the Tourism Climate Index (TCI) in Europe. *Atmosphere 7*, 80. https://doi.org/10.3390/atmos7060080

Simić, S., 2016: *Vodni potencijal i hidrogeografska rejonizacija Valjevskih planina*. Univerzitet u Beogradu – Geografski fakultet, Beograd, doktorska disertacija.

Sobhani, B., and *Safarian Zengir, V.*, 2020: Evaluation and zoning of environmental climatic parameters for tourism feasibility in northwestern Iran, located on the western border of Turkey. *Model. Earth Syst. Environ 6*, 853–864. https://doi.org/10.1007/s40808-020-00712-1

Stanković, S., 2008: *Turistička geografija*. Zavod za udžbenike, Beograd.

Stojićević, G., 2016: *Bioklimatska slika Zapadne Srbije u funkciji turizma*. Univerzitet u Novom Sadu, Prirodno-matematički fakultet, Novi Sad, doktorska disertacija.

Unkašević, M., and *Tošić, I.*, 2013: Trends in temperature indices over Serbia: relationships to large-scale circulation patterns. *Int J Climatol 33*, 3152–3161. https://doi.org/10.1002/joc.3652

Velea, L., Chitu, Z., and *Bojariu, R.,* 2024: Thermal stress information as a tourism-oriented climate product: Performance analysis for selected urban destinations in Romania and Italy. *Heliyon 10*, e24682.

DOI:10.28974/idojaras.2025.4.5

IDŐJÁRÁS

Quarterly Journal of the HungaroMet Hungarian Meteorological Service
Vol. 129, No. 4, October – December, 2025, pp. 465–484

Recent insights into spatial and temporal changes of aridity in the region of southern and eastern Serbia

Milena Gocić [1,*], **Marko Ivanović** [2], **Nikola Milentijević** [2], **Jelena Živković** [1], and **Milan Miletić** [1]

[1] *University of Niš, Faculty of Science and Mathematics, Department of Geography, Niš, Serbia*

[2] *University of Priština in Kosovska Mitrovica, Faculty of Sciences and Mathematics, Department of Geography, Kosovska Mitrovica, Serbia*

**Corresponding author E-mail: milena.j.gocic@gmail.com*

(Manuscript received in final form October 29, 2024)

Abstract— This study investigated the spatial and temporal distribution of aridity indices to determine climatic conditions in regions of southern and eastern Serbia in the period 1961-2022. We used the mean monthly and annual air temperature and precipitation data obtained from nine meteorological stations in the study area. Three indices were used to quantify aridity: the de Martonne aridity index, the Emberger index and the Pinna combinative index. Calculations are carried out on an annual scale for all the indices mentioned. The results show large territorial differences in the de Martonne aridity index, which distinguishes between two climate types on an annual basis. The Emberger index is characterized by humid climate types for all meteorological stations in the area. The Pinna combinative index also indicates humid conditions in the entire area, although the annual values of the index vary considerably. There was no change in the trend of aridity in the study area during the period of investigation. The spatial distribution was determined via the inverse distance weighting interpolated method. The Mann-Kendall test indicated that the aridity trends at all the meteorological stations were not statistically significant.

Key-words: aridity indices, trends, spatial analysis, region of Serbia

1. Introduction

Climate change is not only a concern for future generations, but its impacts are also already evident. This change can lead to significant damage to natural and socioeconomic systems. According to the *IPCC* (2021) report, extreme heat

events have increased in almost all regions of the world since the 1950s. Extreme precipitation and droughts have become more frequent and severe in most land areas worldwide. The absence of precipitation can have significant impacts on sectors such as agriculture and forestry, making its analysis crucial for adaptation strategies in a changing climate.

Aridity presents a lack of moisture and a temporary decrease in precipitation in an area (*Maliva* and *Missimer,* 2012) or water availability (*Moral et al*., 2015). According to the *American Meteorological Society* (2019), "aridity is the degree to which the climate lacks effective moisture to support life". Increasing aridity is a physical hazard that negatively affects many ecosystems and economic sectors, including water management, agriculture, forestry, and tourism. This is because it can be a limiting factor for the growth and spread of plants (*Moral et al.,* 2015). A regional study of aridity, therefore, requires appropriate aridity indices, which can be defined as numerical indicators of the degree of aridity of the climate in a given location. Aridity indices have been applied at continental and subcontinental scales and are mostly related to the distributions of natural vegetation and crops. The critical values of the indices were derived from the observed vegetation boundaries. The parameters for which there is a mathematical relationship between precipitation (and/or humidity) and air temperature are referred as aridity indices. These indices are highly valuable for tracking the impacts of climate change on local water resources (*Maliva* and *Missimer*, 2012). The higher the aridity index values in a region are, the greater the variability in water resources (*Deniz et al.,* 2011; *Arora,* 2002). To quantify aridity, numerous climatic and aridity indices have been developed (*Stephen,* 2005). Indices can be calculated as the ratio between precipitation and potential evaporation, i.e., the aridity index (AI) (*Shoshany* and *Mozhaeva,* 2023; *Zomer et al.,* 2022), the Thornthwaite aridity index (*Thornthwaite,* 1948), or the ratio of precipitation to temperature, i.e., the De Martonne aridity index (I_{DM}) (*De Martonne,* 1926), Lang rain factor (*Lang,* 1915), Pinna combinative aridity index (I_P) (*Zambakas,* 1992), Emberger aridity index (I_E) (*Emberger,* 1930), Lobova aridity index (*Burić et al.,* 2018), etc. The aforementioned indices are based on different variables, which is why they provide different results in the assessment of aridity.

Beštáková et al. (2023) investigated the spatial distribution of arid and humid regions in Europe through the aridity index for the period 1950–2019, concluded that the area of the Balkan Peninsula was identified as arid. *Paniagua et al.* (2019) examined variations in aridity in the Iberian Peninsula from 1960–2017 via the De Martonne aridity index, Pinna combinative aridity index, and Erinç aridity indices. Despite the large spatial variability, they reported that the entire area is dominated by arid conditions, with aridity increasing significantly in future projections on the basis of trends in air temperature and precipitation projections. In Calabria, Italy, researchers used the de Martonne aridity index to identify areas susceptible to aridity (*Pellicone et al*., 2019). The findings indicated that coastal regions were arid, whereas the highest mountains were classified as humid. This

study highlights a significant correlation between the de Martonne aridity index results and the region's orography.

Numerous studies have investigated aridity and drought in various Balkan countries, including Croatia (*Ugarković* and *Ugarković,* 2013), Bosnia and Herzegovina (*Trbić et al.,* 2022), Montenegro (*Luković et al*., 2024), North Macedonia (*Aksoy et al.,* 2020), Greece (*Baltas,* 2007), Bulgaria (*Nikolova* and *Yanakiev,* 2020), and Serbia (*Djurdjević et al.,* 2024; *Amiri* and *Gocić,* 2023; *Gocić et al.,* 2025; *Milentijević et al.,* 2025). *Şarlak* and *Mahmood Agha* (2018) used the aridity indices of Lang rain factor, De Martonne, UNEP, and Erinç to estimate the spatiotemporal variation in aridity in Iraq. *Gebremedhin et al*. (2018) and *Moral et al.* (2016) used De Martonne, the combined Pinna, and FAO aridity index, to assess the spatial distributions of aridity in Ethiopia and Spain, respectively. Similarly, *Nikolova* and *Yanakiev* (2020) used the De Martonne and Emberger indices to investigate the spatial pattern of aridity in southern Bulgaria. All the above studies have used aridity indices for specific regions worldwide. Therefore, there is a need for a more comprehensive study to estimate, compare, and interpret the spatiotemporal trends of multiple aridity indices in the study area.

Based on various aridity indices, southern and eastern Serbia are characterized as humid according to the global aridity index (AI) distribution (*Zomer et al.,* 2022), semiarid according to the I_{DM} index, and semidry based on the I_P index (*Radaković et al.,* 2017).

This study employs three aridity indices: the De Martonne aridity index (I_{DM}), the Emberger index (I_E), and the Pinna combinative index (I_P). These indices were calculated via monthly and annual temperature and precipitation data from nine meteorological stations in southern and eastern Serbia, covering the period from 1961–2022.

The main objectives of this study include a detailed analysis of the spatial and temporal distributions of the abovementioned indices. The study provides a detailed analysis of selected aridity indices, examines trends in these indices, and assesses their statistical significance via the nonparametric Mann-Kendall test and Sen's slope analysis. Geographic information systems (GIS) are utilized for spatial modeling of precipitation, temperature, and aridity indices at various time scales through the inverse distance weighted (IDW) interpolation method. Understanding the spatiotemporal patterns of the aridity index is crucial for effective agricultural and water management in the region.

2. Data and methods

2.1. Study area

This research focuses on the NUT 2 unit of southern and eastern Serbia (*Fig. 1*), which covers 26,248 km², or 29.7% of Serbia's total area (*Miletić et al.,* 2017).

The region extends from the Danube in the north to the North Macedonian border in the south, and from the Velika Morava and Južna Morava valleys in the west to the Bulgarian border in the east. The investigated area includes the Dacian Basin (the extreme northeastern part of the research area) toward Romania, and farther south are the mountains of the Carpathian-Balkan massif with valleys between the mountains, where larger settlements are located. South of the river Nišava are the mountains of the Rhodope Serbian-Macedonian massif. The terrain is mountainous with various small-scale features. The area under investigation is located in the central part of Balkan Peninsula, so the continentality of the region is pronounced (*Fig. 1*). The territory of Serbia has a warm temperate–humid climate with warm summers of the Cfb type according to the Köppen climate classification. The maximum precipitation occurs at the beginning of summer and at the end of spring (*Milovanović et al.,* 2017a).

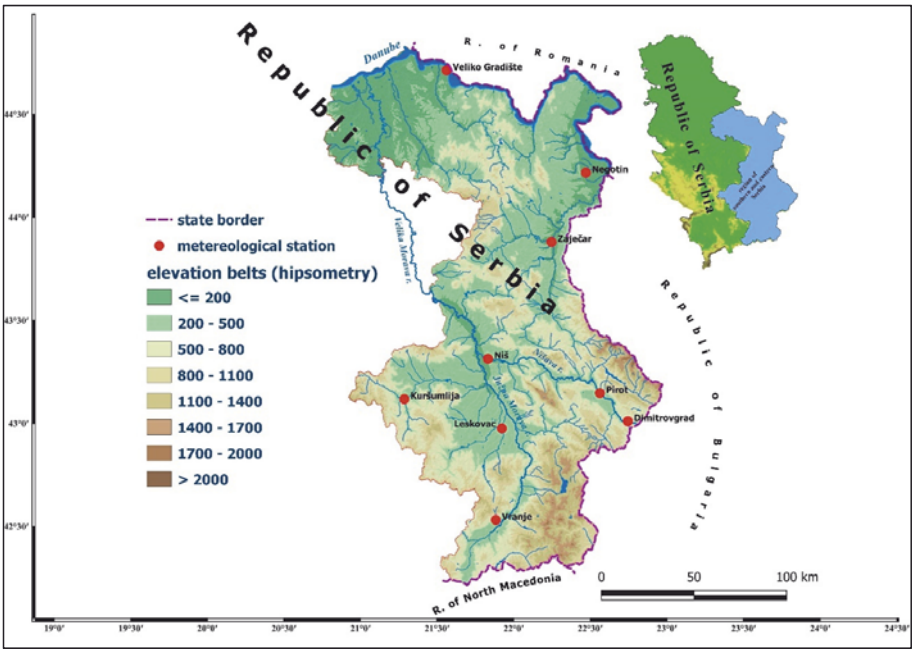

Fig. 1. The regions of southern and eastern Serbia with the locations of the meteorological stations.

To consider the climatic characteristics of the study area, we used the average monthly and annual values of air temperature and precipitation from nine meteorological stations (MS) for the period of 1961–2022 (*Table 1*). The data were retrieved from the Hydrometeorological Service of the Republic of Serbia

and can be found in meteorological yearbooks (*RHSS*, 2024). We have only analyzed meteorological stations that have data for the entire period.

Table 1. List of meteorological stations in the investigated area with coordinates, mean annual temperature (T), and precipitation

Meteorological Station (MS)	Latitude	Longitude	Altitude (m)	T (°C)	Precipitation (mm)
Dimitrovgrad	43º01'	22º45'	448	10.2	654.6
Kuršumlija	43º08'	21º16'	384	10.3	666.6
Leskovac	42º59'	21º57'	231	11.2	635.7
Negotin	44º14'	22º32'	42	11.9	637.8
Niš	43º20'	21º54'	202	12.0	602.3
Pirot	43º09'	22º35'	373	11.3	595.8
Veliko Gradište	44º45'	21º30'	80	11.4	666.7
Vranje	42º33'	21º55'	433	11.2	607.6
Zaječar	43º53'	22º17'	144	11.0	617.1

According to data in the yearbooks of RHSS, 2024

2.2. Methods

In our study, three aridity indices were used:

– The *de Martonne aridity index (I_{DM})* is a commonly used climate index for assessing aridity (*De Martonne,* 1926; *Croitoru et al.,* 2013). The index is defined by the following equation for annual (I_{DM}) values:

$$I_{DM} = \frac{P}{T+10} \ , \tag{1}$$

where P and T are the annual sums of precipitation (mm) and mean annual air temperature (°C), respectively. For monthly and seasonal I_{DM} values monthly and seasonal sums of precipitation and monthly and seasonal means of air temperature are used. The classification according to the I_{DM} is shown in *Table 2*.

Table 2. The De Martonne index (I_{DM}) classification

Climate	Values of I_{DM}
arid	I_{DM}<10
semiarid	10≤ I_{DM} <20
mediterranean	20≤ I_{DM} <24
semi humid	24≤ I_{DM} <28
humid	28≤ I_{DM} <35
very humid	35≤ I_{DM} <55
extremely humid	I_{DM} >55

– *The Emberger index (I_E)* is based on data from precipitation totals and average monthly air temperatures of the coldest and warmest months (*Emberger,* 1930). Emberger used this index to classify phytoclimatic regions. For this reason, some scientists have analyzed the distribution of vegetation according to the Emberger index (*Gavilán,* 2005; *Savo et al*., 2012). The Emberger index (I*E*) is calculated via the following formula:

$$I_E = \frac{100*P}{M^2-m^2}\ , \qquad (2)$$

where *P* is the annual sum of precipitation; *M* is the monthly average air temperature of the warmest month; and *m* is the average monthly air temperature of the coldest month. The climate types according to the Emberger index are given in *Table 3*.

Table 3. Climate types according to the Emberger index

Climate	Values I_E
arid	I_E < 30
semiarid	30 ≤ I_E ≤ 50
semi humid	51≤ I_E ≤ 90
humid	I_E > 90

– *The Pinna combinative index (I_P)* developed by Pinna (*Baltas,* 2007; *Zambakas,* 1992) defines the combinative or perennial index as:

$$Ip = 0.5 * (\frac{P}{Tg+10} + \frac{12*Pdm}{Tgdm}), \qquad (3)$$

where *P* represents the annual precipitation (mm); *Tg* represents the annual mean temperature (ºC); *Pdm* represents the precipitation of the driest month (mm); and *Tgdm* represents the temperature of the driest month (ºC). The Pinna combinative index classifications are presented in *Table 4*.

Table 4. Pinna Combinative Index classification (*Baltas*, 2007)

Climate	Values of I_P
dry	$I_P < 10$
semiarid/mediterranean	$10 \leq I_P < 20$
humid	$I_P > 55$

As the index is calculated for a longer period of time, it is successfully used to identify regions threatened by aridity and drought. The dry periods of a year can be distinguished, which is important for agricultural and irrigation activities (*Deniz et al*., 2011).

To determine the magnitude and significance of the trends in the aridity indices and climatic parameters, the nonparametric Mann-Kendall test method and the Sen method were used (*Mann*, 1945; *Helsel* and *Hirsch,* 2002). Trend estimates were made for the period of 1961–2022 on an annual basis.

The geostatistical method of inverse distance weighting (IDW) was used to enable a clear and efficient interpretation of the results. Compared with other interpolation methods (e.g., kriging), this method is easy to apply (*Mei et al.,* 2017) and is preferable to other interpolation methods (*Derdous et al*., 2020). This method was used for the spatial analysis of climate parameters at the annual level. QGIS was used for data processing.

3. Results and discussion

3.1. Temperature and precipitation in the study area

3.1.1. Temperature in the study area

To determine the values of the selected aridity indices, the average longterm air temperature values had to be calculated first. The average air temperature for the period from 1961–2022 was between 10.1 °C at MS Dimitrovgrad and 11.9 °C at MS Nis. Differences in air temperature values at the stations depend on the location of the meteorological station, shelter, or exposure to intrusions of air masses, and altitude, but the differences in values are insignificant (*Table 5*). The lowest monthly average air temperatures at all the stations were recorded in

January. The highest monthly average temperatures were recorded during July and August (MS Vranje). *Fig. 2* shows the spatial distribution of the mean annual temperature in the study area.

Table 5. Mean monthly and annual air temperature values at the meteorological stations for the period 1961–2022

MS	I	II	III	IV	V	VI	VII	VIII	IX	X	XI	XII	Ann.
Veliko Gradište	0.0	2.0	6.3	11.8	16.7	20.0	21.7	21.4	16.9	11.7	6.5	1.5	11.4
Vranje	-0.3	2.3	6.3	11.2	15.9	19.3	21.3	21.5	17.1	11.8	6.3	1.3	11.2
Dimitrovgrad	-0.9	1.2	5.1	10.2	14.8	18.2	20.1	19.8	15.6	10.6	5.6	0.9	10.1
Leskovac	-0.3	2.2	6.5	11.5	16.3	19.8	21.5	21.2	16.6	11.1	6.2	1.4	11.2
Zaječar	-0.7	1.4	5.6	11.2	16.3	19.8	21.9	21.3	16.5	10.6	5.5	0.9	10.9
Kuršumlija	-0.2	1.7	5.6	10.5	14.8	18.3	19.9	19.6	15.3	10.6	6.0	1.4	10.3
Negotin	-0.2	1.9	6.6	12.3	17.5	21.3	23.2	22.4	17.6	11.6	6.1	1.6	11.8
Niš	0.4	2.8	7.1	12.2	16.9	20.4	22.3	22.2	17.6	12.2	7.0	2.1	11.9
Pirot	-0.1	2.2	6.3	11.4	15.9	19.5	21.4	21.1	16.8	11.6	6.4	1.6	11.2

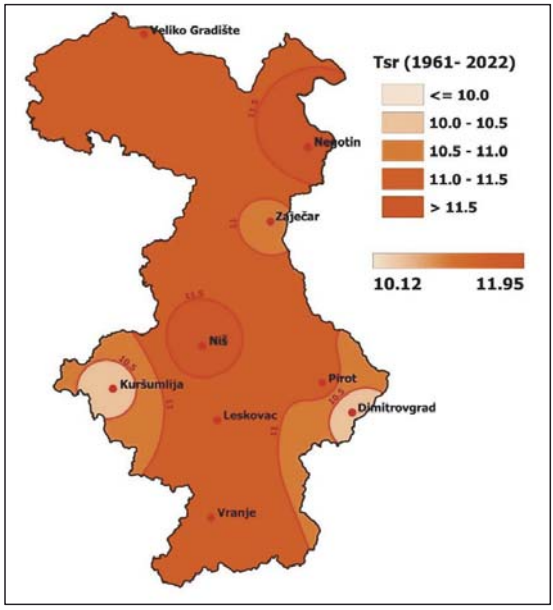

Fig. 2. Spatial distribution of mean annual temperatures in the study area for the period 1961–2022.

3.1.2. Precipitation in the study area

Precipitation was irregularly distributed in time and space in relation to the atmospheric processes and relief features. The mean annual precipitation values for the study period are shown in *Fig. 3*. The mean annual precipitation values for the study period were slightly greater than 600 mm (except for the Pirot MS), which is consistent with previous studies (*Milovanović et al*., 2017b; *Malinovic Milicevic et al*., 2015). The average amount of precipitation in the study area ranges from 595.8 (MS Pirot) to 666.7 mm (MS Veliko Gradište) (*Table 6*, *Fig. 3*). On a monthly basis, the highest precipitation amounts were recorded at the end of spring and the beginning of summer (May, June, July) and the lowest in the summer months (August) and winter (January), which is in line with previous studies (*Živanović et al*., 2024; *Milošević et al*., 2021; *Tošić,* 2004).The differences in the amount of precipitation are not large and depend largely on the location of the station, the orography of the surrounding area (MS Pirot, surrounded by mountains, although located in the basin, therefore receives less precipitation than the surrounding stations, e.g., MS Dimitrovgrad and MS Niš), and the proximity of the moisture source (MS Veliko Gradište near the Danube River). *Fig. 3* shows the spatial distribution of the mean annual precipitation in the study area.

Table 6. Mean monthly and annual precipitation totals at the meteorological stations for the period 1961–2022

MS	I	II	III	IV	V	VI	VII	VIII	IX	X	XI	XII	Ann.
Dimitrovgrad	45.4	41.0	48.2	53.8	75.1	78.7	63.2	48.7	47.5	50.1	55.0	48.0	654.6
Kuršumlija	46.3	44.3	51.7	54.6	69.5	66.8	62.0	49.0	50.8	51.7	60.6	59.2	666.6
Leskovac	47.1	43.4	50.6	56.7	63.5	67.4	47.8	44.5	49.2	48.8	59.8	56.8	635.7
Negotin	47.0	48.0	51.4	55.7	61.9	62.9	50.5	39.8	47.0	53.5	60.1	60.0	637.8
Niš	44.0	39.1	46.0	53.5	66.9	62.8	46.6	44.7	46.2	44.4	53.3	54.8	602.3
Pirot	40.7	36.5	42.2	49.3	67.8	77.5	49.9	44.3	44.7	45.0	51.2	46.5	595.8
Veliko Gradište	47.3	43.5	42.1	56.2	72.1	75.3	72.6	54.2	53.9	47.2	46.6	55.8	666.7
Vranje	42.6	41.4	43.5	51.9	61.3	64.3	48.6	40.0	48.1	53.3	59.9	52.7	607.6
Zaječar	43.0	41.2	46.8	52.4	74.6	66.2	57.4	41.5	41.5	46.9	51.8	53.8	617.1

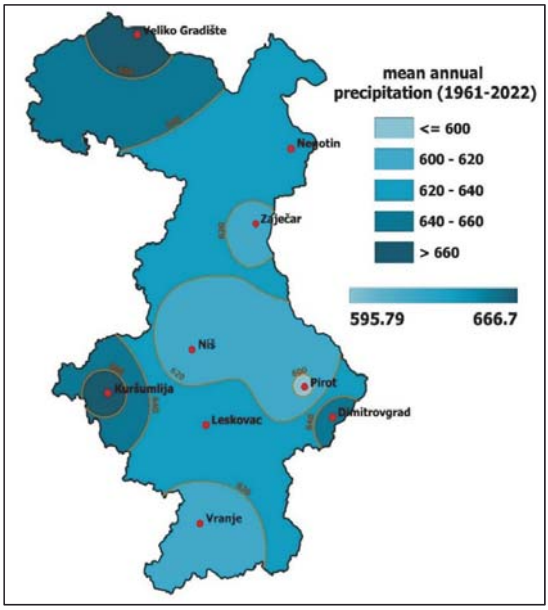

Fig. 3. Spatial distribution of mean annual precipitation in the study area for the period 1961–2022.

3.2. Aridity indices – annual values

The annual values of the three aridity indices were analyzed separately.

3.2.1. De Martonne aridity index

The distribution of the annual I_{DM} values for the period of 1961–2022 is shown in *Fig. 4*. Five out of seven climate types according to the de Martonne classification were found in the analyzed area. The semiarid climate is represented in only one year, 2000, which is characterized as extremely dry by many authors (*Radaković et al*., 2017; *Gocić* and *Trajković,* 2013). Mediterranean climate was represented in 6 years, semihumid climate in 11 years, humid climate in 38 years, and very humid climate in 6 years.

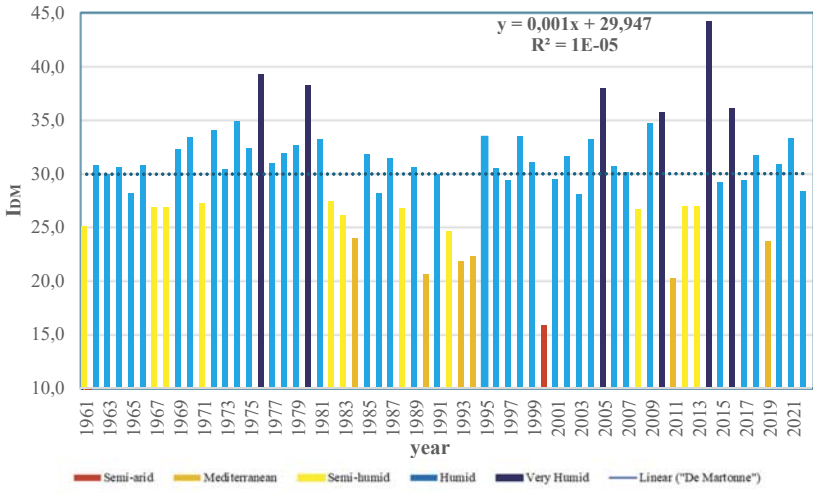

Fig. 4. Annual time series of I_{DM} for all meteorological stations for the period 1961–2022.

The maximum value of this index (44.2) was recorded at all stations in 2014. According to *Tošić et al.* (2017), the maximum value of the I_{DM} in 2014 was confirmed by the extreme annual precipitation, which was the highest for the period of 1961–2014 for all meteorological stations in Serbia. The minimum value of the index was recorded in 2000, with a value of 15.8. During the year 2000, most of Serbia experienced extremely dry conditions (*Tošić* and *Unkašević,* 2014). The spatial pattern of the annual I_{DM} is shown in *Fig. 5*. The average value of the index ranges from 27.4 (MS Niš) to 32.7 (MS Kuršumlija). Humid climate is represented at all the meteorological stations, with the exception of MS Niš, where semihumid climate prevailed during the study period, which was previously established in the work of *Radaković et al.* (2017). The lower I_{DM} values at MS Niš can be attributed to the city's size and higher air temperatures, which indicate the presence of an "urban heat island." This phenomenon has also been observed in other major Serbian cities, such as Belgrade and Novi Sad (*Milovanović et al.*, 2020; *Milošević et al.,* 2021).

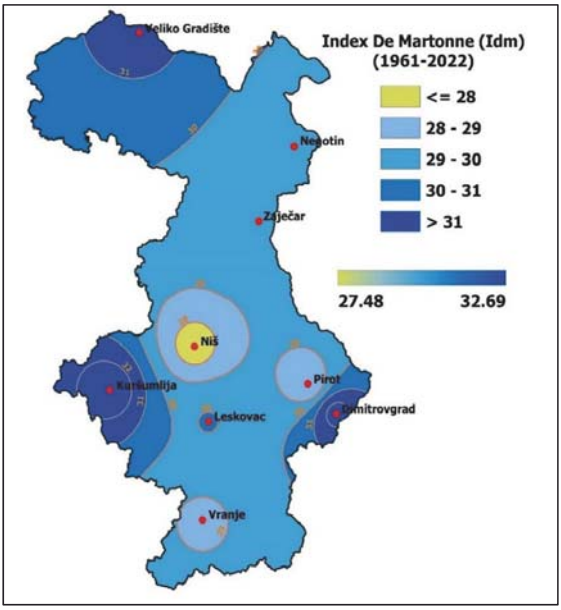

Fig. 5. Spatial distribution of I_{DM} for the period 1961–2022.

3.2.2. Emberger index (I_E)

The annual time series of I_E for all the meteorological stations for the period of 1961–2022 shows that humid climate was recorded in 58 years and semihumid climate was recorded in 4 years (*Fig. 6*). The highest values of I_E were measured in 1976 and 2014, with values of 208.3 and 201.2, respectively (which were described as extremely humid years in other studies due to extreme precipitation) (*Anđelković et al*., 2018; *Tošić et al*., 2017). The lowest value of I_E was measured in 2000 and was 58.9. The years with extremely high temperatures are 2007 (*Bajat et al*., 2015) and 2011 (*Živanović et al*., 2024), and the most extreme year is 2000, which is confirmed by the values of this index (the years belong to the semihumid climate), which is calculated on the basis of the values of temperature and precipitation.

The I_E value fluctuates between 113.8 (MS Negotin) and 167.1 (MS Kuršumlija) (*Fig. 7*). However, all the values are in the humid climate range (i.e., greater than 90).

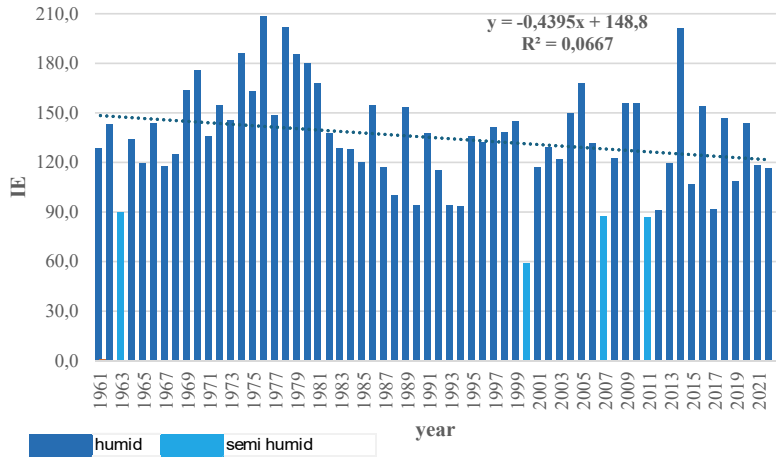

Fig. 6. Annual time series of I_E for all meteorological stations for the period 1961–2022.

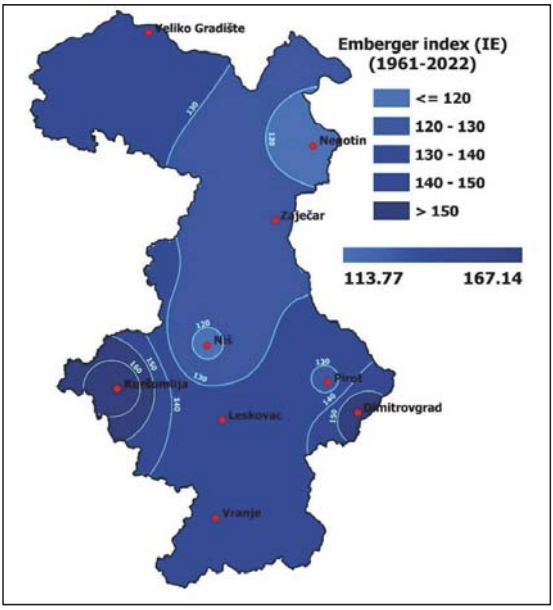

Fig. 7. Spatial distribution of I_E for the period 1961–2022.

3.2.3. Pinna combinative index (I_P)

The distribution of annual I_P values during the study period revealed that a humid climate predominated in the study area (48 years) (*Fig. 8*). The semiarid Mediterranean climate (13 years) is representative of arid climates only (2000). The data of this index are similar to those of the I_{DM} index, although they are calculated differently. The driest year according to this index is 2000 at all meteorological stations, with an average value of 9.4. The wettest year according to the Ip index was 2005, with an average value of 42.9 (*Fig. 8*), which was also demonstrated in the paper of *Radaković et al*. (2017). The results of the I_P index are consistent with the conclusions of *Nikolova* and *Yanakiev* (2020) for southwestern Bulgaria, which is territorially close to our study area.

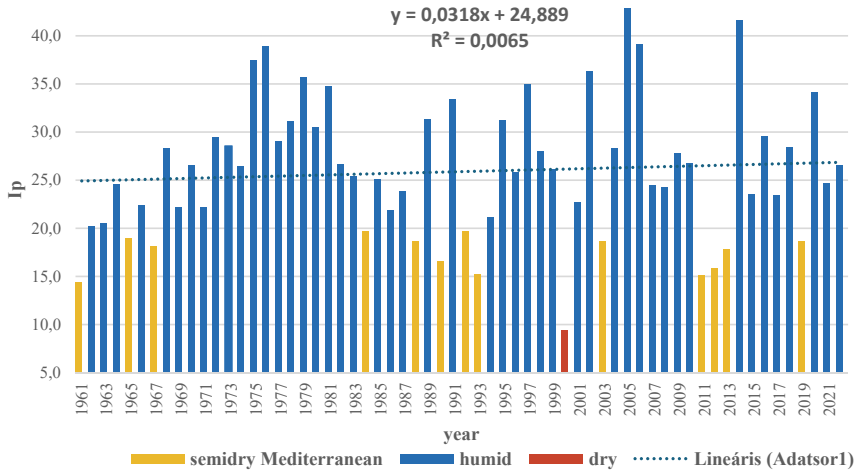

Fig. 8. Annual time series of I_P for all meteorological stations for the period 1961–2022.

Although the value of the I_P index indicates that the humid climate dominated the entire research area, slight differences were detected (*Fig. 9*). The average annual index values range from 22.2 (MS Vranje) to 30.2 (MS Kuršumlija).

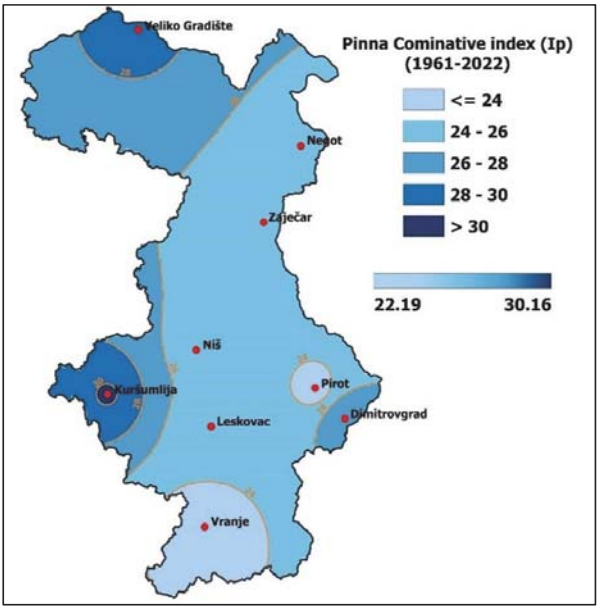

Fig. 9. Spatial distribution of I_P for the period 1961–2022.

All the three indices used show that some stations have relatively high humidity, namely, MS Kuršumlija, MS Dimitrovgrad, and MS Veliko Gradište. The reason for this is primarily the location of the stations in relation to the source of humidity (humid air masses coming to Serbia from the northwest and west) as well as the altitude of the stations (MS Dimitrovgrad and MS Kuršumlija). In the case of MS Veliko Gradište, the proximity of the Danube is the reason for the relatively high humidity. Therefore, lower air temperatures and greater amounts of precipitation were recorded. Although the values of all indices result from the relationship between temperature and precipitation, there are differences in the calculations.

3.3. Trend of aridity indices

The MK test revealed that when all the given values of the indices were considered, there was no significant change in the aridity trends over the last 62 years in the regions of southern and eastern Serbia.

The Mann-Kendall test was used to determine the statistical significance of the trend in the analyzed data for temperature, precipitation, and aridity indices. The Mann-Kendall test revealed a statistically significant positive trend for temperature (α=0.001) at all the meteorological stations in the study area (*Table 7*). Precipitation only shows a positive statistically significant trend for MS

Dimitrovgrad. A positive statistically significant trend was recorded for the I_{DM} at MS Kuršumlija and MS Leskovac at the α=0.05 significance level. The values of the Emberger index indicate a significant downward trend at the level of significance α=0.05 at the meteorological stations Negotin, Niš, Pirot, and Vranje.

The assessment of a statistically significant positive trend in temperature in southern and eastern Serbia is in line with the results at the global, European and local levels (*Twardosz et al*., 2021; *Mohorji et al*., 2017; *Rosmann et al.,* 2016). The positive/negative trends of the aridity indices depend on the choice of aridity index and the location of the area. An increase in aridity has been observed in Serbia and surrounding countries (*Radaković et al.,* 2017; *Gocić* and *Trajković,* 2014; *Vlădut* and *Licurici,* 2020; *Nikolova* and *Yanakiev,* 2020). Future scenarios predict an increase in the intensity of aridity in the central and eastern parts of the Balkan Peninsula (*Beštakova et al*., 2023; *Cheval et al.,* 2017; *Gao* and *Giorgi,* 2008), where the study area is located.

Table 7. Statistical summary of the mean annual temperature (T), mean annual precipitation (P), De Martonne aridity index (I_{DM}), Emberger index (I_E), Pinna combinative index (I_P) based on Mann–Kendall statistics and the magnitude of trends (β) calculated via Sen's slope estimator

MS	T			P			I_{DM}			I_E			I_P
	Z_{MK}	Ann Mean	β	Z_{MK}	Ann Mean	β	Z_{MK}	Ann Mean	β	Z_{MK}	Ann Mean	β	
Dimitrovgrad	**5.7*** **	11.4	9.09	**2.27**	654.6	609.18	1.06	32.36	32.61	-0.92	158.9	170.70	27.8
Kuršumlija	**6.5*** **	11.2	9.02	1.63	666.6	627.59	**1.93**	33.50	29.97	-0.51	167.1	172.40	30.2
Leskovac	**6.7*** **	10.1	10.13	1.51	635.7	628.70	**2.25**	30.10	27.66	-0.26	132.6	134.40	24.9
Negotin	**6.8*** **	11.2	10.32	-0.40	637.8	656.07	-1.38	29.24	31.95	**-2.25**	113.8	131.60	25.4
Niš	**5.9*** **	10.9	10.80	0.81	602.3	588.69	0.15	27.60	27.10	**-1.94**	117.7	126.30	25.5
Pirot	**6.2*** **	10.3	10.01	0.43	595.8	586.25	-1.03	27.93	29.77	**-3.10**	127.6	149.90	23.1
Veliko Gradište	**5.4*** **	11.8	10.31	0.17	666.7	669.86	0.03	31.44	30.67	-1.53	137.7	150.40	28.6
Vranje	**5.9*** **	11.9	10.09	0.99	607.6	562.86	-0.46	28.58	28.40	**-1.98**	134.7	144.00	22.2
Zaječar	**6.3*** **	11.2	9.84	0.37	617.1	588.75	-0.78	29.59	30.21	-1.56	124.6	129.60	25.4

Note: *** level of significance=0.001; bold values - level of significance=0.05

4. Conclusion

Based on the results of the spatial and temporal distribution of the aridity index in the analyzed area, we can conclude that there was no statistically significant trend of change. An increase in aridity and temperature is expected in the future, which will have a negative impact on agriculture, soil, and water resources. Climate change, increasingly characterized by long periods of drought combined with heavy rainfall and global warming, will make it increasingly difficult for humanity to adapt to natural and environmental conditions to ensure sufficient food and agricultural yields and the availability of clean and safe drinking water. The annual values of the De Martonne Index (I_{DM}) indicate humid climate, except for MS Niš, where the semihumid climate is dominant. The annual values of the I_{DM} index show a statistically significant positive trend at only two stations. The Emberger index and the Pinna Combinative index revealed that humid climate dominated throughout the entire research area. A comparison of the results of the I_{DM}, I_E and I_P indices revealed that the I_{DM} gives better results and more precisely defines the climate of the selected area. It can be concluded that the climate of the analyzed area shows a weak tendency to increase aridity (no significant trend) but may entail certain risks for the development of the agricultural sector and water supply.

Acknowledgments: The authors are grateful for the financial support of the Ministry of Science, Technological Development and Innovation of the Republic of Serbia (projects no. 451-03-65/2024-03/200124 and 451-03-65/2024-03/200123).

References

American Meteorological Society, 2019: Glossary of Meteorology. Available online: http://glossary.ametsoc.org/wiki/Aridity (accessed on 25 September 2019).

Amiri, M.A. and *Gocic M*., 2023: Analysis of temporal and spatial variations of drought over Serbia by investigating the applicability of precipitation-based drought indices. *Theor Appl Climatol 154*,2 61–274. https://doi.org/10.1007/s00704-023-04554-6

Aksoy, E., Arsov, S., Mincev, I., and *Fang C*., 2020: Agro-ecological atlas of the Republic of North Macedonia. Rome, FAO.

Anđelković, G., Jovanović, S., Manojlović, S., Samardžić, I., Živković, L., Šabić, D., Gatarić, D., and *Džinović, M.,* 2018: Extreme Precipitation Events in Serbia: Defining the Threshold Criteria for Emergency Preparedness. *Atmosphere 9*(5), 188. https://doi.org/10.3390/atmos9050188

Arora, V.K. 2002: The use of the aridity index to assess climate change effect on annual runoff. *J Hydrol 265*, 164–177.

Bajat, B., Blagojević, D., Kilibarda, M., et al., 2015: Spatial analysis of the temperature trends in Serbia during the period 1961–2010. *Theor Appl Climatol 121*, 289–301. https://doi.org/10.1007/s00704-014-1243-7

Baltas, E., 2007: Spatial distribution of climatic indices in northern Greece. *Meteorol Appl 14*, 69–78. https://doi.org/10.1002/met.7

Beštáková, Z., Strnad, F., Vargas Godoy, M.R., Singh, U., Markonis, Y., Hanel, M., Máca, P., and *Kyselý, J.,* 2023: Changes of the aridity index in Europe from 1950 to 2019. *Theor Appl Climatol 151*, 587–601. https://doi.org/10.1007/s00704-022-04266-3

Burić, D., Ivanović, R., and *Milenković, M.,* 2018: Indicators of specificity of climate: The example of Podgorica (Montenegro). *Journal of the Geographical Institute "Jovan Cvijic" SASA 68*, 399–403. https://doi.org/10.2298/IJGI180423009B

Cheval, S., Dumitrescu, A., and *Birsan, M.V*., 2017: Variability of the aridityin the South-Eastern Europe over 1961-2050. *Catena 151*,74–86. https://doi.org/10.1016/j.catena.2016.11.029

Croitoru, A.E., Piticar, A., Imbroane, A.M., and *Burada, D.C.,* 2013: Spatiotemporal distribution of aridity indices based on temperature and precipitation in the extra-Carpathian regions of Romania. *Theor Appl Climatol 112*, 597–607. https://doi.org/10.1007/s00704-012-0755-2

De Martonne, E., 1926: Une nouvelle fonction climatologique: L'Indece d'aridite. *La Meteorol 2*, 449–458.

Deniz, A., Toros, H., and *Incecik, S*., 2011: Spatial variations of climate indices in Turkey. *Int J Climatol 31*(3), 394–403. https://doi.org/10.1002/joc.2081

Derdous, O., Bouguerra,H.,Tachi, S.E., and *Bouamrane, A*., 2020: A monitoring of the spatial and temporal evolutions of aridity in northern Algeria. *Theor Appl Climatol 142*, 1191–1198. https://doi.org/10.1007/s00704-020-03339-5

Djurdjević, V., Stosic, B., Tošić, M., Lazić, I., Putniković, S., Stosic, T., and *Tošić, I*., 2024: Analysis of recent trends and spatiotemporal changes of droughts over Serbia using high-resolution gridded data. *Atmos Res 304*, 107376. https://doi.org/10.1016/j.atmosres.2024.107376

Emberger, L., 1930: La végétation de la région méditerranéenne: essai d'une classification des groupements végétaux. *Revue de Botanique, Librairie générale de l'enseignement 503*, 642–662. (In French)

Gao, X. and *Giorgi, F*., 2008: Increased aridity in the Mediterranean region under greenhouse gas forcing estimated from high resolution simulations with a regional climate model. *Glob Planet Change 62*(3-4),195–209. https://doi.org/10.1016/j.gloplacha.2008.02.002

Gavilán, R. G., 2005: The use of climatic parameters and indices in vegetation distribution. A case study in the Spanish Sistema Central. *Int J Biomteorol 50*, 111–120. https://doi.org/10.1007/s00484-005-0271-5

Gebremedhin, M.A., Kahsay, G.H., and *Fanta, H.G.,* 2018: Assessment of spatial distribution of aridity indices in Raya valley, northern Ethiopia. *Appl Water Sci 8*, 217. https://doi.org/10.1007/s13201-018-0868-6

Gocić, M. and *Trajković, S*., 2013: Spatiotemporal characteristics of drought in Serbia. *J Hydrol 510*, 110–123. https://doi.org/10.1016/j.jhydrol.2013.12.030

Gocić, M., Milentijević, N., Ivanović, M., Tošić, I., Živanović, S., Martić-Bursać, N. and *Stričević, Lj.,* 2025: Spatial and temporal variability of aridity indices in the region of Southern and Eastern Serbia. *Theor Appl Climatol 156*, 6. https://doi.org/10.1007/s00704-024-05233-w

Helsel, D,R. and *Hirsch, R,M.,* 2002: Statistical methods in water resources. In Book 4, Hydrologic analysis and interpretation, Chapter A3 (Techniques of water–resources investigations of the United States Geological Survey). https://doi.org/10.3133/tm4A3

IPCC, 2021: Summary for policymakers. In Climate Change 2021: The Physical Science Basis. Contribution of Working Group I to the Sixth Assessment Report of the Intergovernmental Panel on Climate Change. Eds.: *Masson-Delmotte, V., Zhai, P., Pirani, A., Connors, S.L., Péan, C., Berger, S., Caud, N., Chen, Y., Goldfarb, L., Gomis, M.I., Huang, M., Leitzell, K., Lonnoy, E., Matthews, J.B.R., Maycock, T.K., Waterfield, T., Yelekçi, O., Yu, R.* and *Zhou, B*., Cambridge, UK and New York, USA, Cambridge University Press, 3−32. Available at https://doi. org/10.1017/9781009157896.001

Lang, R., 1915: Versuch einer exakten Klassifikation der Boden in klimatischer und geologischer Hinsicht. *Internationale Mitteilungen für Bodenkunde 5,* 312.

Luković, J., Burić, D., Mihajlović, J., and *Pejović M.* 2024: Spatial and temporal variations of aridity-humidity indices in Montenegro. *Theor Appl Climatol 155:* 4553–4566. https://doi.org/10.1007/s00704-024-04893-y

Malinovic Milicevic, S., Radovanovic, M., Stanojevic, G., and *Milovanovic, B.,* 2015: Recent changes in Serbian extreme indices from 1961-2010. *Theor Appl Climatol 124*, 1089–1098. https://doi.org/10.1007/s00704-015-1491-1

Maliva, R. and *Missimer, T.,* 2012: Aridity and Drought. In: Arid Lands Water Evaluation and Management. *Environmental Science and Engineering* (Environmental Engineering), Springer, Berlin, 21-39. https://doi.org/10.1007/978-3-642-29104-3_2

Mann, H.B., 1945: Nonparametric tests against trend. *Econometrica 13*, 245–259.

Mei, G., Xu, L., and *Xu, N*., 2017: Accelerating adaptive inverse distance weighting interpolation algorithm on a graphics processing unit. *Royal Society open science 4,* 170436. http://dx.doi.org/10.1098/rsos.170436

Milentijević, N., Martić-Bursać, N., Gocić, M., Ivanović, M., Obradović Strålman, S., Pantelić, M., Milošević, D. and *Stričević, Lj.,* 2025: Spatio-Temporal Variability of Aridity and Humidity Indices in Bačka (Serbia). *Pure Appl Geophys 182*, 705-728. https://doi.org/10.1007/s00024-024-03628-4

Miletić, R., Miljanović, D., and *Vuković D*., 2017: Regional development, regional competitiveness, and regional cooperation in Serbia. In: (Ed *Radovanović, M.,*) Geography of Serbia. Serbian Academy of Sciences and Arts, Belgrade 811–870. (In Serbian)

Milošević, D., Savić, S,, Kresoja, M., Lužanin, Z., Šećerov, I., Arsenović, D., Dunjić, J., and *Matzarakis, A*., 2021: Analysis of air temperature dynamics in the "local climate zones" of Novi Sad (Serbia) based on long-term database from an urban meteorological network. *Int J Biometeorol* 1–14. https://doi.org/10.1007/s00484-020-02058-w

Milovanović, B., Radovanović, M., and *Schneider, C.,* 2020: Seasonal distribution of urban heat island intensity in Belgrade (Serbia). *Journal of the Geographical Institute "Jovan Cvijić" 70*(2): 163–170.

Milovanović, B., Ducić, V., Radovanović, M., and *Milivojević, M*., 2017a: Climate regionalization of Serbia according to Köppen climate classification. *Journal of the Geographical Institute "Jovan Cvijic"*, SASA *67*(2): 103–114. https://doi.org/10.2298/IJGI1702103M

Milovanović, B., Schuster, P., Radovanović, M., Vakanjac Ristić, V., and *Schneider, C.,* 2017b: Spatial and temporal variability of precipitation in Serbia for period 1961-2010. *Theor Appl Climatol 130*(1). https://doi.org/10.1007/s00704-017-2118-5

Mohorji, A.M., Şen, Z., and *Almazroui, M*., 2017: Trend Analyses Revision and Global Monthly Temperature Innovative Multi-Duration Analysis. *Earth Syst Environ 1*, 9. https://doi.org/10.1007/s41748-017-0014-x

Moral, F.J., Rebollo, F.J., Paniagua, L.L., García-Martín, A., and *Honorio, F.,* 2016: Spatial distribution and comparison of aridity indices in Extremadura, southwestern Spain. *Theor Appl Climatol 126*, 801–814. https://doi.org/10.1007/s00704-015-1615-7

Nikolova, N. and *Yanakiev, D*., 2020: Climate aridity in southern Bulgaria for the period 1961- 2015 *Forum geografic 19*(1), 10–17. https://doi.org/10.5775/fg.2020.010.i

Paniagua, L.L., García–Martín, A., Moral, F.J., and *Rebollo, F.J*., 2019: Aridity in the Iberian Peninsula (1960–2017): distribution, tendencies, and changes. *Theor Appl Climatol 138*, 811–830. https://doi.org/10.1007/s00704-019-02866-0

Pellicone, G., Caloiero, T., and *Guagliardi, I.,* 2019: The De Martonne aridity index in Calabria (Southern Italy). *Journal of Maps 15,* 788–796. https://doi.org/10.1080/17445647.2019.1673840

Radaković, M.G., Tošić, I., Bačević, N., Mladjan, D., Gavrilov, M.B., and *Marković, S.B*., 2017: The analysis of aridity in Central Serbia from 1949 to 2015. *Theor Appl Climatol 133*, 887–898. https://doi.org/10.1007/s00704-017-2220-8

Radulović, D.M., Vuković, D.B., Voronov, M.P., and *Simeunović I*., 2015: Statistical territorial units with purpose of measuring level of development of regions in Serbia. *Ëko-potencial 2*, 87–99.

Savo, V., De Zuliani, E., Perini, L., and *Ganeva, G*., 2012: Long-term changes in precipitation and temperature patterns and their possible impacts in vegetation (Tolfa-Certie Area, Central Italy). *Appl Ecol Environ Res 10*, 243–266.

Stephen, J., 2005: Aridity Indexes. In: (eds *Oliver, J.E*.) Encyclopedia of World Climatology. Encyclopedia of Earth Sciences Series. Springer, Dordrecht, 89–94. https://doi.org/10.1007/1-4020-3266-8_17

Rosmann, T., Dominguez, E., and *Chavarro, J.,* 2016: Comparing trends in hydrometeorological average and extreme data sets around the world at different time scales. *J Hydrol: Regional Studies 5*, 200–212. http://dx.doi.org/10.1016/j.ejrh.2015.12.061

RHSS, http://www.hidmet.gov.rs/ciril/meteorologija/klimatologija_godisnjaci.php (Retrieved September 19, 2024)

Şarlak., N. and *Mahmood Agha, O.M.,* 2018: Spatial and temporal variations of aridity indices in Iraq. *Theor Appl Climatol 133*, 89–99. https://doi.org/10.1007/s00704-017-2163-0

Shoshany, M. and *Mozhaeva S.,* 2023: Climate and aridity measures relationships with spectral vegetation indices across desert fringe shrublands in the South-Eastern Mediterranean Basin. *Environ Monitoring Assess 195*, 563. https://doi.org/10.1007/s10661-023-11082-3

Thornthwaite, C.W., 1948: An approach toward a rational classification of climate. *Geograph Rev 38*, 55–94.

Tošić, I., Unkašević, M., and *Putniković, S.,* 2017: Extreme daily precipitation:the case of Serbia in 2014. *Theor Appl Climatol* 128:785–794. https://doi.org/10.1007/s00704-016-1749-2

Tošić, I., and *Unkašević, M.,* 2014: Analysis of wet and dry periods in Serbia. *International Journal of Climatology 34*(5), 1357-1368. https://doi.org/10.1002/joc.3757

Tošić, I., 2004: Spatial and temporal variability of winter and summer precipitation over Serbia and Montenegro. *Theor Appl Climatol 77*, 47–56. https://doi.org/10.1007/s00704-003-0022-7

Trbic, G., Popov, T., Djurdjevic, V., Milunovic, I., Dejanovic, T., Gnjato, S., and *Ivanisevic, M*., 2022: Climate Change in Bosnia and Herzegovina According to Climate Scenario RCP8.5 and Possible Impact on Fruit Production. *Atmosphere 13(*1), 1. https://doi.org/10.3390/atmos13010001

Twardosz, R., Walanus, A., and *Guzik, I.,* 2021: Warming in Europe: Recent Trends in Annual and Seasonal temperatures. *Pure Appl Geophys 178*, 4021–4032. https://doi.org/10.1007/s00024-021-02860-6

Ugarković, D. and *Ugarković, K.,* 2013: Changes and trends of climate elements and indices in the region of Mediterranean Croatia. *Journal of Central European Agriculture 14*(1), 236-249. https://doi.org/10.5513/JCEA01/14.1.1189

Vlăduţ, A.Ş. and *Licurici, M.,* 2020: Aridity conditions within the region of Oltenia (Romania) from 1961 to 2015. *Theor Appl Climatol 140*, 589–602. https://doi.org/10.1007/s00704-020-03107-5

Zambakas, J., 1992: General Climatology. Department of Geology, National & Kapodistrian University of Athens: Athens, Greece.

Zomer, R.J., Xu, J., and *Trabucco, A.,* 2022: Version 3 of the Global Aridity Index and Potential Evapotranspiration Database. *Sci Data 9*, 409. https://doi.org/10.1038/s41597-022-01493-1

Živanović, S., Gocić, M., and *Tošić, I.,* 2024: Vulnerability of Central Serbian national parks to wildfires. *Időjárás 128*, 99–120. https://doi.org/10.28974/idojaras.2024.1.6

IDŐJÁRÁS

VOLUME 129 * 2025

BUDAPEST, HUNGARY

AUTHOR INDEX

TABLE OF CONTENTS

I. papers

SUBJECT INDEX

W

Y

Z

INSTRUCTIONS TO AUTHORS OF *IDŐJÁRÁS*

The purpose of the journal is to publish papers in any field of meteorology and atmosphere related scientific areas. These may be

- research papers on new results of scientific investigations,
- critical review articles summarizing the current state of art of a certain topic,
- short contributions dealing with a particular question.

Some issues contain "News" and "Book review", therefore, such contributions are also welcome. The papers must be in American English and should be checked by a native speaker if necessary.

Authors are requested to send their manuscripts to

Editor-in Chief of IDŐJÁRÁS
P.O. Box 38, H-1525 Budapest, Hungary
E-mail: journal.idojaras@met.hu

including all illustrations. MS Word format is preferred in electronic submission. Papers will then be reviewed normally by two independent referees, who remain unidentified for the author(s). The Editor-in-Chief will inform the author(s) whether or not the paper is acceptable for publication, and what modifications, if any, are necessary.

Please, follow the order given below when typing manuscripts.

Title page should consist of the title, the name(s) of the author(s), their affiliation(s) including full postal and e-mail address(es). In case of more than one author, the corresponding author must be identified.

Abstract: should contain the purpose, the applied data and methods as well as the basic conclusion(s) of the paper.

Key-words: must be included (from 5 to 10) to help to classify the topic.

Text: has to be typed in single spacing on an A4 size paper using 14 pt Times New Roman font if possible. Use of S.I. units are expected, and the use of negative exponent is preferred to fractional sign. Mathematical formulae are expected to be as simple as possible and numbered in parentheses at the right margin.

All publications cited in the text should be presented in the *list of references*, arranged in alphabetical order. For an article: name(s) of author(s) in Italics, year, title of article, name of journal, volume, number (the latter two in Italics) and pages. E.g., *Nathan, K.K.,* 1986: A note on the relationship between photo-synthetically active radiation and cloud amount. *Időjárás 90,* 10–13. For a book: name(s) of author(s), year, title of the book (all in Italics except the year), publisher and place of publication. E.g., *Junge, C.E.,* 1963: *Air Chemistry and Radioactivity*. Academic Press, New York and London. Reference in the text should contain the name(s) of the author(s) in Italics and year of publication. E.g., in the case of one author: *Miller* (1989); in the case of two authors: *Gamov* and *Cleveland* (1973); and if there are more than two authors: *Smith et al.* (1990). If the name of the author cannot be fitted into the text: *(Miller,* 1989); etc. When referring papers published in the same year by the same author, letters a, b, c, etc. should follow the year of publication. DOI numbers of references should be provided if applicable.

Tables should be marked by Arabic numbers and printed in separate sheets with their numbers and legends given below them. Avoid too lengthy or complicated tables, or tables duplicating results given in other form in the manuscript (e.g., graphs). *Figures* should also be marked with Arabic numbers and printed in black and white or color (under special arrangement) in separate sheets with their numbers and captions given below them. JPG, TIF, GIF, BMP or PNG formats should be used for electronic artwork submission.

More information for authors is available: journal.idojaras@met.hu

Published by the HungaroMet Hungarian Meteorological Service

Budapest, Hungary

ISSN 0324-6329 (Print)

ISSN 2677-187X (Online)